Università della Calabria

Dipartimento Farmaco-Biologico
(SSD: MED/46 SCIENZE TECNICHE DI MEDICINA DI LABORATORIO)

Dottorato di Ricerca in "Biochimica Cellulare ed Attività dei Farmaci in Oncologia" (XXV ciclo)

DAX-1 at the connection between Androgen Receptor and Aromatase: a novel mechanism in the inhibition of estrogen-dependent cancer cell proliferation

Docente Tutor

Prof.ssa Marilena LANZINO

Coordinatore

Prof. Diego SISCI

Dottoranda

Dott.ssa Pamela MARIS

Anno Accademico 2011-2012

Università della Calabria

Dipartimento Farmaco-Biologico
(SSD: MED/46 SCIENZE TECNICHE DI MEDICINA DI LABORATORIO)

Dottorato di Ricerca in "Biochimica Cellulare ed Attività dei Farmaci in Oncologia" (XXV ciclo)

DAX-1 at the connection between Androgen Receptor and Aromatase: a novel mechanism in the inhibition of estrogen-dependent cancer cell proliferation

Docente Tutor

Prof.ssa Marilena LANZINO

Dottoranda

Dott.ssa Pamela MARIS

Coordinatore

Prof. Diego SISCI

Anno Accademico 2011-2012

INDEX

Scientific Publications

- **1.** Casaburi I., Avena P., Lanzino M., Sisci D., Giordano F., Maris P., Catalano S., Morelli C. and Ando' S. Chenodeoxycholic acid through a TGR5-dependent CREB-signaling activation enhances Cyclin D1 expression and promotes human endometrial cancer cell proliferation. Cell Cycle. 2012 Jul 15;11(14):2699-710.

- **2.** Puoci F., Morelli C., Cirillo G., Curcio M, Parisi O. I., Maris P., Sisci D. and Picci N. Anticancer Activity of a Quercetin-based Polymer Towards HeLa Cancer Cells. Anticancer Res. 2012 Jul; 32(7):2843-7.

- **3.** Morelli C., Maris P., Sisci D., Perrotta E., Brunelli E., Perrotta I., Panno M.L., Tagarelli A., Versace C., Casula M.F., Testa F., Andò S., Nagya J.B. and Pasqua L. PEG-templated mesoporous silica nanoparticles exclusively target cancer cells. Nanoscale, 2011, 3, 3198.

- **4.** Morelli C., Lanzino M., Garofalo C., Maris P., Brunelli E., Casaburi I., Catalano S., Bruno R., Sisci D., Andò S. Akt2 inhibiton enables the forkhead transcription factor FoxO3a to have a repressive role in Estrogen Receptor Alpha transcriptional activity in breast cancer cells. Mol. Cell Biol. 2010 Feb;30(3):857-70.

SUMMARY

In situ estrogen production by aromatase is a critical determinant for breast cancer growth and progression. Clinical and in vitro studies indicate that androgens have a protective role in mammary carcinogenesis. Here we demonstrated, in breast cancer cell lines, that ligand-activated androgen receptor (AR) induces the expression of the orphan nuclear receptor DAX-1 by a direct binding to a newly identified Androgen-Response-Element within the DAX-1 proximal promoter. In turn, androgen-induced DAX-1 is recruited, in association with the corepressor N-CoR, within the SF-1/LRH-1 containing region of the aromatase promoter, thereby repressing aromatase expression and activity. The molecular mechanism underlining the androgen-dependent modulation of DAX-1 and aromatase expression is reproducible in R2C rat Leydig tumor cells, highly expressing aromatase. Indeed, in vivo studies conducted in testes tissues from Fisher rats, spontaneously developing Leydig cell neoplasma, reveal an inverse relationship between AR/DAX-1 and aromatase levels.

In elucidating a novel mechanism by which androgens, through DAX-1, inhibit aromatase expression, these findings reinforce the theory of androgen-opposing estrogen-action opening new avenues for therapeutic intervention in endocrine-related cancers.

INTRODUCTION

Sexual hormones, estrogens and androgens, determine biological response in a tissue- and gender-specific manner and play a pivotal role in endocrine-mediated tumorigenesis (1-5). Estrogens influence the pathological processes of several hormone-dependent cancers since they are thought to be the driving force for the formation of breast, endometrial, ovarian and testicular tumors (6,7). In breast, estrogen signaling plays a critical role in cell proliferation and tumor development (8), and estrogen receptor α (ER-α) positive tumors comprise ~ 70% of annually diagnosed breast cancer cases (9). Importantly, in addition to the estrogen supply from the ovary, biologically active estrogens, especially estradiol (E_2), are locally produced in an intracrine mechanism within the breast cancer tissues and exert their actions on carcinoma cells. The puzzling hint was the observation that breast cancer incidence is higher in post-menopausal women, when the production of ovarian estrogens has ceased. It is now known that, in post-menopausal women, estrogen levels in breast tissue are 10-50 times elevated than in blood and significantly higher in malignant than in non-malignant tissues (10).

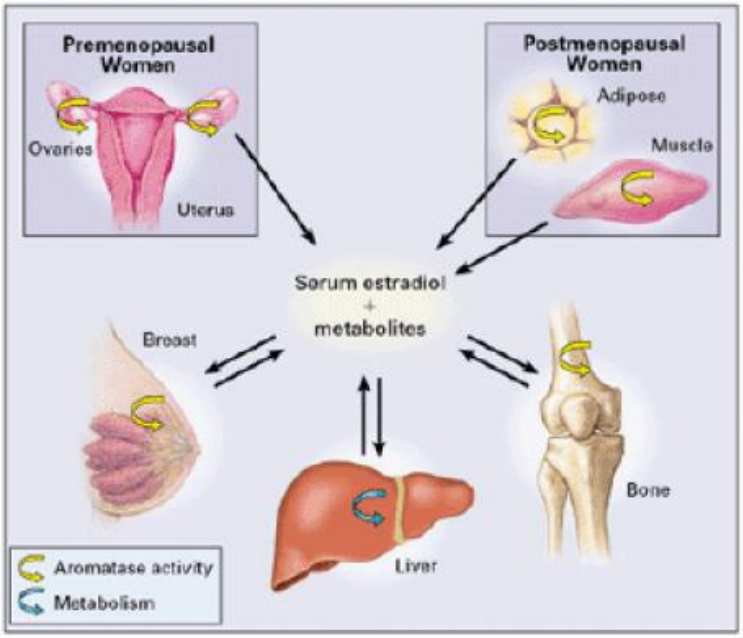

Figure 1. Schema illustrating sites of production of biologically active estrogens in pre- and post-menopausal women.

A series of enzymes are involved in this intra-tumoral or *in situ* production of estrogens in breast carcinoma tissues but aromatase, a member of the cytochrome P450 family, is a key enzyme of estrogen production through conversion from circulating adrenal androgens in estrogen-dependent postmenopausal breast cancer (11).

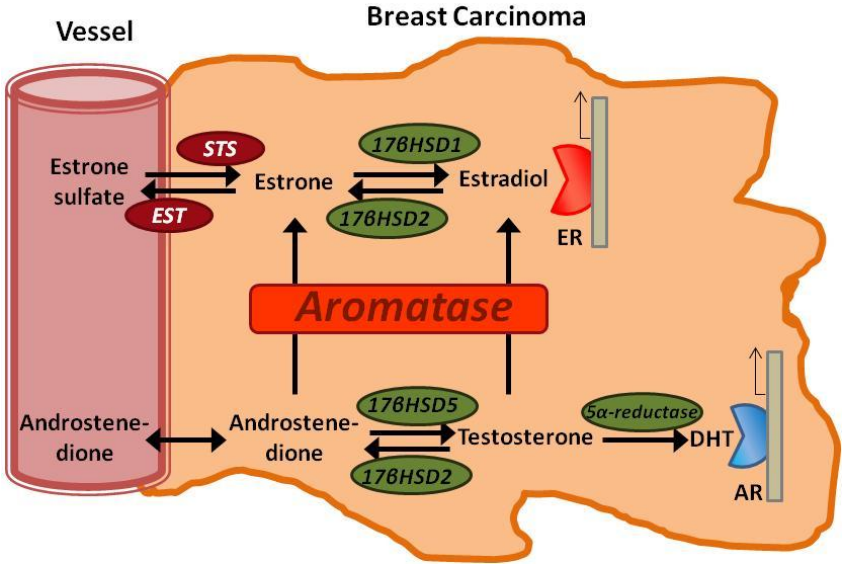

Figure 2. Scheme representing *in situ* production of sex steroids in human breast carcinoma tissues. High concentrations of circulating inactive steroids, such as estrone sulfate and androstenedione are precursor substrates of local production of estrogens and/or androgens in breast carcinomas. STS; steroid sulfatase, EST; estrogen sulfotrasferase, and 17βHSD; 17β-hydroxysteriod dehydrogenase.

Consequently, substantial efforts have been devoted to explore ways to block estrogen activity in breast cancer cells, underpinning the widespread use of antiestrogens and aromatase inhibitors in the adjuvant treatment of breast cancer (12,13).

The balance between ER-α and androgen receptor (AR) signalling has been proposed as a critical determinant of growth in the normal and malignant mammary epithelium, supporting the prevalent theory of androgens opposing estrogens in the mammary gland.

Studies on non-human primate or rodent support the notions that androgens inhibit mammary epithelial growth by reducing E2-dependend cell proliferation (14-16). Several lines of evidence sustain the idea of similar effects in humans: 1) androgens, such as dihydrotestosterone, oppose the E2-induced proliferation

and induce apoptosis in explant cultures from normal breast tissues, in an AR-dependent manner (17); 2) genotypically male individuals suffering from complete androgen insensitivity develop morphologically normal female breast during puberty (18); 3) girls with congenital adrenal hyperplasia and androgen excess do not undergo pubertal thelarche (19); 4) reduced or impaired AR signalling has been implicated in the development of hereditary male breast cancers (20); and 5) women who have AR alleles that encode for short polyglutamine tracts in the AR protein, resulting in a higher AR transcriptional activity (21), have a reduced risk of developing breast cancer (22). These observations suggest that androgens do play a role in the regulation of mammary gland development and imply that androgen signaling in the breast might protect against cancer development and progression.

A significant number of primary well differentiated breast tumors express AR (23) whose presence and functional activity appear to be related to positive prognostic factors, including ER positivity, smaller tumor size, low tumor grade, improved response to hormone therapy and longer patient survival (24-37). Interestingly, several events involved in breast cancer genesis or progression have been shown to alter AR expression or function, conferring a growth advantage to cancer cells. Indeed, a trend towards a loss of AR has been shown in BRCA1-mutated breast tumors (38-40) as well as in HER2-positive breast cancers, generally associated with a worse outcome (37,41).

These findings are consistent with cell-based assays indicating that, in ER/AR-positive breast tumor cell lines, AR activation by the agonist dihydrotestosterone decreases ER-α transcriptional activity (36,42) and inhibits basal as well as estrogen-dependent cell proliferation (43-48). These effects occur by an AR-mediated mechanism that negatively regulates the transcriptional activity of the *cyclin D1* gene promoter throughout the recruitment of a multiprotein repressor complex involving the participation of the orphan nuclear receptor DAX-1 (Dosage-sensitive sex reversal, Adrenal Hypoplasia Congenita (AHC) critical region on chromosome X, gene 1; NROB1) (47).

DAX-1 is an unusual orphan member of the nuclear receptor superfamily, lacking the classical zinc-finger DNA Binding Domain (49-52)

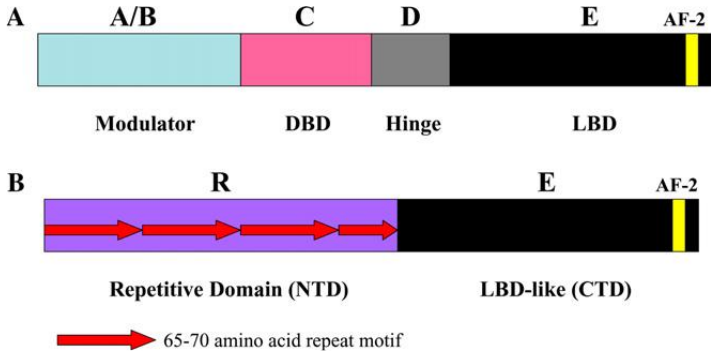

Figure 3. Comparison of functional domain structure of members of the nuclear receptor superfamily **(A)** with DAX-1 **(B)**.

Instead of directly binding to regulatory DNA sites, DAX-1 controls transcription mainly as a co-repressor by associating with nuclear receptors, (*e.g.,* AR, ER and progesterone receptor), or other transcription factors (*e.g.,* steroidogenic factor 1, SF-1 or Liver Receptor Homolog-1, LRH-1).

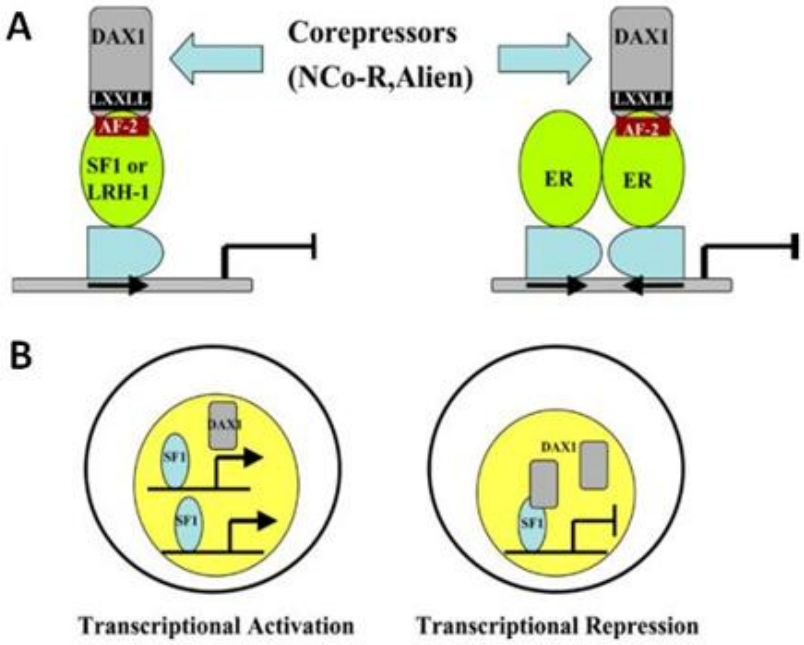

Figure 4. Mechanisms of DAX1-mediated repression of SF-1, ER, and LRH-1. **(A)** DAX1 binds the AF-2 domain of the nuclear receptors via its LXXLL motifs and recruits corepressor proteins to target gene promoters. **(B)** Effects of intracellular levels of DAX1 and SF-1 on transcriptional repression. Increased SF1 levels relative to DAX1 favor transcriptional activation (left), and increased levels of DAX1 relative to SF-1 favor transcriptional repression (right).

DAX-1 has a restricted expression pattern to tissues directly involved in steroid hormone production and reproductive function, such as adrenal cortex, Leydig and Sertoli cells in the testis and theca and granulosa cells in the ovary (53-55).

Within these tissues, DAX-1 acts as a global anti-steroidogenic factor by working in pair with SF-1/LRH-1 and repressing the expression of multiple enzymes involved in the steroidogenic pathway. Major steroidogenic targets include cytochrome P450 (e.g. CYP19 aromatase), cholesterol transporters (e.g., steroidogenic acute regulator protein, StAR) and hydroxysteroid dehydrogenase (53,55,56). DAX-1 expression has also been reported in several types of cancers. In adrenocortical tumours DAX-1 presence is inversely correlated to the level of steroid production (57,58). DAX-1 expression in breast (34,59), ovarian (60), endometrial (61) and prostate cancers (62) has been additionally described even though not narrowly investigated. Moreover, there are few studies on how DAX-1 expression is regulated.

Here we report the identification of a novel AR-mediated mechanism controlling the expression of DAX-1. Based on our model, ligand-activated AR may negatively regulate in situ estrogen production through an androgen receptor-dependent activation of DAX-1 gene transcription in estrogen-related cancer cell lines, providing new clues for a better comprehension of the mechanisms underlying the inhibitory role exerted by androgens on estrogen-dependent cancer cell proliferation.

MATERIAL AND METHODS

Cell cultures, animals and treatments

Breast cancer epithelial cell line MCF-7 (American Type Culture Collection, ATCC, UK) and human embryonic kidney cell line HEK-293 were grown in DMEM (Gibco, USA) supplemented with 5% and 10% fetal bovine serum (FBS; Gibco, USA) respectively. Human ductal breast epithelial tumor cell line T47D (Interlab Cell Line Collection, ICLC, Italy) was maintained in RPMI (Gibco) supplemented with 10% FBS. Rat Leydig tumor cells (R2C) were cultured in Ham's F-10 supplemented with 15% horse serum (HS; Gibco,) and 2.5% FBS. Before each experiment, cells were synchronized in phenol red-free serum free media (PRF-SFM) for 24h. All the experiments were performed in PRF-media containing 2,5% charcoal-treated FBS (PRF–CT). Male Fischer 344 rats (a generous gift of Sigma-Tau), 6 (FRN), (*n=3*) and 24 (FRT) (*n=4)* months of age, were used for studies. Twenty-four-month-old animals presented spontaneously developed Leydig cell tumors, which were absent in younger animals. Testes of all animals were surgically removed by qualified, specialized animal care staff in accordance with the Guide for Care and Use of Laboratory Animals (NIH) and used for experiments. The following agents were used for treatments: Mibolerone (Mb, Perkin Elmer, USA), Bicalutamide (Casodex; Santa Cruz Biotechnology, USA) and Hydroxyflutamide (OH-Fl; Sigma, Italy).

Cell proliferation assays

MCF-7 and R2C cells were seeded on 12-well plates at a density of 10^5 cells/well and grown overnight. The following day, cells were synchronized in PRF-SFM for 24h to avoid growth differences among cells. After 24h, cells were exposed to the desired concentration of Mb or left untreated. The effects of Mb on cell proliferation were measured at different time points following initial exposure to treatments by counting cells using a Burker's chamber, with cell viability determined by trypan blue dye exclusion or using the method of transcriptional and translational colorimetric assay (MTT) (47).

Plasmids, transfections and luciferase reporter assays

The following plasmids were used: pcDNA3-AR (AR) encoding full-length AR (63); CMV-P881 ($AR_{(Cys574\rightarrow Arg)}$) encoding the full-length AR carrying a mutation in the DNA-binding domain (DBD; Cys-574→Arg) (63); pGL3 vector containing human aromatase promoters II/1.3 ligated to a luciferase reporter gene (PII/1.3) (a gift from Dr. E. R. Simpson and Dr. C. D. Clyne, Prince Henry's Institute of Medical Research, Clayton, Australia); pGL3 vector containing rat aromatase promoter II ligated to a luciferase reporter gene (PII) and the pGL3 vector containing rat aromatase promoter II mutated in SF-1 binding site ligated to a luciferase reporter gene (mutPII) (a gift from Dr. M.J. McPhaul , Southwestern Medical Center, Dallas, USA); the vector-based pSiAR plasmid, coding for small interfering RNA targeting the 5'-untranslated region of AR mRNA, and the scrambled control construct pSiCon (64). The Renilla reniformis luciferase expression vector used was pRL-Tk (Promega, USA). The deletions of SF-1/LHR-1 sequence in the human aromatase promoter PII/1.3 were generated by PCR. The resulting plasmid encoding the aromatase promoter II and 1.3 containing the desired deletions was designated mutPII/1.3 The desired deletions of sequences were confirmed by nucleotide sequence analysis. The luciferase expression vector DAX-Luc-promoter (DAX-*Luc*), encoding the DAX-1 promoter, was generated by PCR on genomic DNA. The following primer pairs were used to amplify a 1336bp fragment spamming from position -1370 to -34 from the ATG of the DAX-1 gene: 5'-GAGGATGGGAGGGAGGGAAAAAGT-3' (forward) and 5'-AGGGCAGGGGAAAAGAGGAAACAT-3' (reverse). PCR primer pairs were selected analyzing the 5'-flanking region of DAX-1 gene. The PCR product was purified and the 1336bp fragment was inserted in the pCR 2.1 plasmid by using TOPO-TA cloning kit (Invitrogen, Milan, Italy) and sequenced. The fragment was cut with Kpn I and Xho I and cloned into the pGL3 basic vector (Promega, Italy). Cells were transfected using Fugene (Promega) according to the manufacturer's instructions. pRL-Tk was used to assess transfection efficiency. Luciferase activity was measured using Dual Luciferase Assay System (Promega), normalized to renilla luciferase activity. For western blotting (WB) assays, cells were plated on 60-mm dishes and transfected with an appropriate amount of various plasmids, as indicated in figure legends.

RNA extraction and reverse transcription-PCR assays

Total RNA was isolated using TRIzol reagent (Life Technologies, USA) according to the manufacturer's instructions and treated with DNase I (Ambion, USA). Two micrograms of total RNA were reverse transcribed with the High capacity cDNA Reverse Transcription Kit (Applied Biosystems, USA); cDNA was amplified by PCR to obtain products corresponding to cDNA fragments of DAX-1, P450 aromatase, GAPDH, or β-Actin. RT-PCR was performed using the DreamTaq DNA Polymerase (Fermentas, USA) and GeneAmp PCR System 9600 thermocycler (Perkin Elmer). Primers are listed in Table 1.

Western Blotting analysis

MCF-7 and R2C cells or total tissue of FRNT and FRTT were lysed in 500µl of 50mM Tris-HCl, 150 mM NaCl, 1% Nonidet P-40, 0.5% sodium deoxycholate, 2 mM sodium fluoride, 2mM EDTA, 0.1% SDS, containing a mixture of protease inhibitors (aprotinin, phenylmethylsulfonyl fluoride, and sodium orthovanadate) for protein extraction. Nuclear extracts were prepared as previously described (65), Western Blotting (WB) analysis was performed as previously described (66). The following monoclonal (m) and polyclonal (p) antibodies (Ab) were used: anti-AR mAb (4i299), anti-DAX-1 pAb (K-17), anti-Lamin-B pAb (C-20), anti-GAPDH pAb (FL-335), anti-β-Actin mAb (AC-15), (Santa Cruz Biotechnology), and anti-human cytochrome P450 aromatase mAb (Serotech, USA).

Immunofluorescence

MCF-7 and R2C cells were plated on coverslips, serum starved, and then treated or left untreated with Mb 10^{-8} M for the appropriated time. After incubation, cells were fixed with 4% paraformaldehyde and permeabilized with 0.2% Triton X-100, and nonspecific sites were blocked with bovine serum albumin (BSA, Santa Cruz Biotechnology) (3% for 30 min). The blocked samples were incubated O/N with a mixture of primary antibody recognizing DAX-1(K-17) pAb (Santa Cruz Biotechnology), washed with phosphate-buffered

saline (PBS) (Gibco), and incubated with a mixture of fluorescein-conjugated goat anti-rabbit IgG (Santa Cruz Biotechnology) secondary Abs. The cellular localization of the two proteins was examined under a Leica TCS SP2 confocal laser scanning microscope at X100 magnification.

DNA affinity precipitation assay

DNA affinity precipitation assay was performed as previously described (63). The DNA motif probes were prepared by annealing a biotinylated sense oligonucleotide (for DAX-1-ARE, 5'-[Bio]-CCAAATATCACATGTTCTCAC-3'; for DAX-1-mutatedARE, 5'-[Bio]- CCAAATGGAACATGGGATCAC-3') with the respective nonbiotinylated complementary oligonucleotide (for DAX-1-ARE, 5'-GTGAGAACATGTGATATTTGG-3'; for DAX-1-mutated ARE, 5'-GTGATCCCATGTTCCATTTGG-3').

Electrophoretic mobility shift assay

Nuclear protein extracts were prepared as previously described (67). The double-stranded oligonucleotides used as probes were end labeled with $[\gamma-^{32}P]$ATP and T4 polynucleotide kinase and purified using Sephadex G50 spin columns. The oligonucleotides used as probes and as cold competitors (Sigma Genosys, UK) were (nucleotide motifs of interest are underlined): probe: CCAAATATCACATGTTCTCAC-3'; mutated probe: 5'-CCAAATGGAACATGGGATCAC-3'. Nuclear extracts (20 μg) were incubated with 50000 cpm. of labeled probe, under conditions previously reported (67) The mixture was incubated at room temperature for 20 min in the presence or absence of the unlabelled competitor oligonucleotide. Mouse anti-AR monoclonal antibody (441) or normal mouse IgG (Santa Cruz Biotechnology) were included in some of the reaction mixtures with an additional 12h incubation at 4°C before addition of labelled probe. The entire reaction mixture was electrophoresed through a 6% polyacrylamide gel for 3 h at 150 V.

Aromatase activity assay

The aromatase activity in subconfluent R2C cell culture medium was measured by tritiated water-release assay using 0.5 Amol/L [1h-3H(N)]androst-4-ene-3,17-dione (DuPont NEN) as a substrate (75). Incubations were done at 37°C for 3h under a 95%:5% air/CO2 atmosphere.

Radioimmunoassay (RIA)

Before the experiments, R2C cells were maintained overnight in Ham/F-10 (medium only). The estradiol content of medium recovered from each well was determined against standards prepared in low-serum medium using a RIA kit (DSL 43100; Diagnostic System Laboratories) according to manufacturer's instructions.

Chromatin Immunoprecipitation

Chromatin Immunoprecipitation (ChIP) assay was performed as previously described (68). MCF-7, T47D, and R2C cells were grown in 100mm plates. Confluent cultures (90%) were shifted to SFM for 24 h and then treated with 10^{-8} M Mb for 2 h, or left untreated in 2,5% PRF–CT. Following treatment, the cells were washed twice with PBS and crosslinked with 1% formaldehyde at 37°C for 10 min. Next, the cells were washed twice with PBS at 4°C, collected and resuspended in 200 µl of lysis buffer (1% SDS, 10mM EDTA, 50mM Tris-HCl pH 8.1) and left on ice for 10 min. Then, the cells were sonicated four times for 10 s at 30% of maximal power (Fisher Sonic Dismembrator) and collected by centrifugation at 4°C for 10 min at 14.000 rpm. The supernatants were collected and diluted in 1.3 ml of IP buffer (0.01% SDS, 1.1% Triton X-100, 1.2mM EDTA, 16.7mM Tris-HCl pH 8.1, 16.7mM NaCl) followed by immunoclearing with 80 µl of sonicated salmon sperm DNA/protein A agarose (UBI) for 1 h at 4°C. The precleared chromatin was immunoprecipitated for 12 h with specific Abs: anti-AR mAb (441), anti-Polymerase II pAb (N-20), anti-DAX-1 pAb (K-17), and anti-N-CoR pAb (H-303) (Santa Cruz Biotechnology). Normal rabbit IgG and normal mouse IgG were used instead of primary Abs as negative controls. After this,

60μl of salmon sperm DNA/protein A agarose was added and precipitation was continued for 2 h at 4°C. After pelleting, precipitates were washed sequentially for 5 min with the following buffers: Wash A (0.1% SDS, 1% Triton X-100, 2mM EDTA, 20mM Tris-HCl pH 8.1, 150mM NaCl), Wash B (0.1% SDS, 1% Triton X-100, 2mM EDTA, 20mM Tris-HCl pH 8.1, 500mM NaCl), and Wash C (0.25M LiCl, 1% NP-40, 1% sodium deoxycholate, 1mM EDTA, 10mM Tris-HCl pH 8.1), and then twice with TE buffer (10mM Tris, 1mM EDTA). The immune complexes were eluted with elution buffer (1% SDS, 0.1M NaHCO3). The eluates were reverse crosslinked by heating at 65°C for 12 h and digested with proteinase K (0.5 mg/ml) at 45°C for 1 h. DNA was obtained by phenol and phenol/chloroform extractions. A 2 μl portion of 10 mg/ml of yeast tRNA was added to each sample and DNA was precipitated with EtOH for 12 h at 4°C and then resuspended in 20 μl of TE buffer. Immunoprecipitated DNA was analysed by RT-PCR by using 4 μl of each sample for RT-PCR. Primers are listed in Table 1.

RNA silencing

For AR gene silencing experiments, MCF-7 cells were transfected using the vector-based pSiAR plasmid or the scrambled control construct pSiCon (64), as described in the '*Plasmids, transfections and luciferase reporter assays*' paragraph. For DAX-1 gene silencing experiments, custom synthesized siRNA (Ambion, USA) annealed duplexes were used for effective depletion of DAX-1 mRNA. A scrambled siRNA (Ambion) that does not match with any human mRNA was used as a control for non-sequence-specific effects. Growing cells were switched to PRF-SFM for 24h, trypsinized and transfected in suspension with 80 pmol of siDAX-1 or 80 pmol of siScramble RNA in 60-mm dishes, using Lipofectamine 2000 (Life Technologies), following the manufactuer's instructions. Cells were incubated with the siRNA-Lipofectamine 2000 complex at 37°C for 6 h and then switched to fresh PRF-CT and treated or not with Mb before analysis.

Statistical analysis

All data were expressed as the mean±SD of at least three independent experiments. Statistical significances were tested using Student's t-test.

TABLE 1

Gene sequence	Primer sequence	Cycles	AT(°C)
DAX-1	5'-CGGGCCACGGCGCTTCTGTA-3'(forward)	30	63
	5'-TCCCGCCGCCTGGTGGTGAG-3'(reverse)		
Human P450 Aromatase	5'-CAAGGTTATTTTGATGCATGG-3'(forward)	30	58
	5'-TTCTAAGGTTTGCGCATGA-3';(reverse)		
Rat P450 Aromatase	5'-CAGCTATACTGAAGGAATCCACACTGT-3'(forward)	22	58
	5'-AATCGTTTCAAAAGTGTAACCAGGA-3'(reverse)		
GAPDH	5'-CCCACTCCTCCACCTTTGAC-3'(forward)	25	58
	5'-TGTTGCTGTAGCCAAATTCGT-3'(reverse)		
Rat β-Actin	5'-AGGCATCCTGACCCTGAAGTAC-3'(forward)	18	58
	5'-TCTTCATGAGGTAGTCTGTCAG-3'(reverse)		
DAX-1 ARE promoter	5'-AATGCAGGAACAGAAAACCAAATA-3' (forward)	33	62
	5'-GGCAGCGAGCAGGATGTAAAAGTG-3' (reverse)		
Human P450Aromatase Promoter	5'-TGATGGAAGGCTCTGAGAAG-3' (forward)	30	58
	5'-TAGCTCCTGTTGCTTCAGAGG-3' (reverse)		
Rat P450Aromatase promoter	5'-ATGCACGTCACTCTACCCACTCAA-3' (forward)	35	65
	5'-TAGCACGCAAAGCAGTAGTTTGGC-3' (reverse)		

Table 1. Gene and primers sequences

RESULTS

Ligand-activated AR increases DAX-1 expression in MCF-7 breast cancer cells.

DAX-1 has been detected in breast cancer cell tissues (59,69) and cell lines (70). Our first aim was to investigate DAX-1 levels and cellular compartmentalization in human MCF-7 breast cancer cell line following androgen administration. Experiments were carried out using the synthetic AR agonist Mibolerone (Mb) that was proved to be as effective as dihydrotestosterone (DHT) (47) in inhibiting MCF-7 cell proliferation (Fig. 5).

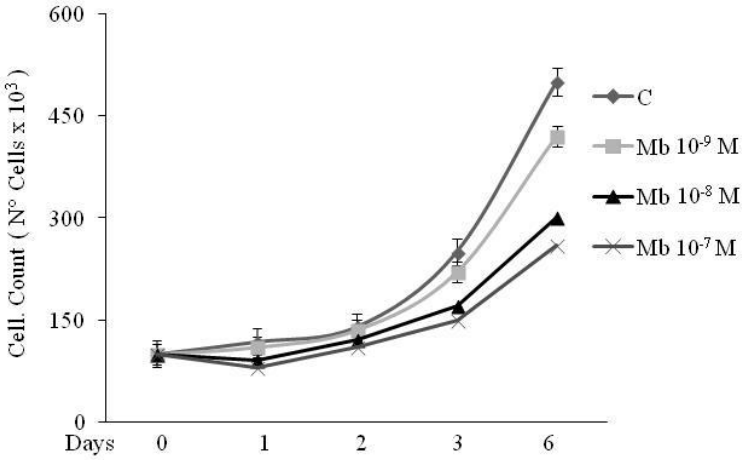

Figure 5. Serum starved MCF-7 cells were grown in PRF–CT in absence or presence of Mb as indicated. Cell proliferation was measured at 0, 1, 2, 3 and 6 days after initial exposure to Mb treatments by trypan blue dye exclusion test.

As shown in Fig.6, 24h Mb treatment increased both DAX-1 mRNA (Fig.6A, *left panel*) and protein cellular levels (Fig.6A, *right panel*). Immunofluorescence experiments, revealed that DAX-1 protein localizes in both cytoplasm and nucleus, even though a markedly stronger immunoreactivity could be observed in the nuclear compartment. Mb administration induced a significant increase of DAX-1 nuclear abundance (Fig. 6B). To ascertain whether activated AR could be involved in the positive regulation of DAX-1 levels a Short Hairpin plasmid was used to silence AR expression in MCF-7 cells. Western blotting analysis of

cytoplasmic and nuclear fractions further confirmed DAX-1 subcellular localization (Fig. 6C). Interestingly, reduction of the AR protein content resulted in the loss of the up-regulatory effect exerted by Mb on DAX-1 nuclear expression (Fig. 6C).

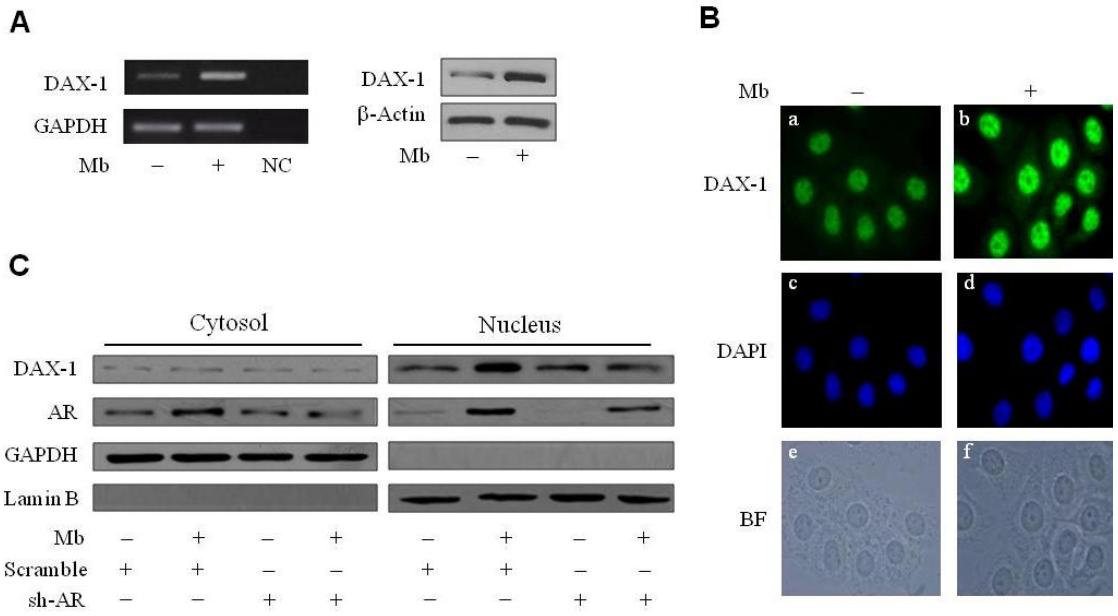

Figure 6. DAX-1 expression is modulated by ligand-activated AR in MCF-7 cells. **(A)** *Mb increases DAX-1 expression*. Cells were treated with 10^{-8} M Mb for 24h and DAX-1 mRNA (*left panel*) or protein content (*right panel*) were detected by RT–PCR or WB analyses, respectively. GAPDH mRNA, internal standard; NC, negative control. β-Actin protein, loading control. **(B)** *Subcellular localization of DAX-1*. DAX-1 (*a,b*), DAPI (c,*d*) immunofluorescence was detected in cells treated with 10^{-8} M Mb for 24h; BF, bright field (*e,f*); 100x optical magnification. **(C)** *AR silencing abrogates Mb-dependent DAX-1 modulation.* Cytoplasmic and nuclear proteins isolated from cells transfected with 0.5 μg pSiAR (sh-AR) or 0.5 μg pSiCon (scramble) and treated with 10^{-8} M Mb, were subjected to WB analysis. GAPDH and Lamin-B expression was assessed as control of protein loading and purity of lysate fractions. All the results are representative of three independent experiments.

Ligand-activated AR induces DAX-1 gene promoter activity

To determine whether the human DAX-1 gene is a target of the ligand-activated AR a 1.3kb (-1370/-34) sequence of the 5'-flanking region of the human DAX-1 gene was cloned, inserted into a reporter plasmid (DAX-1-Luc plasmid) and used to perform transient transfection experiments on MCF-7 cells. As shown in Fig. 7A, Mb administration induced a significant enhancement of DAX-1 promoter activity. This effect was reversed by the addition of the AR antagonist, Hydroxyflutamide (OH-Fl), indicating that it was mediated by AR activation. To confirm the involvement of ligand-activated AR in the modulation of DAX-1 gene

expression, we tested the ability of ectopic AR protein to trigger the activation of DAX-1 promoter in AR-negative HEK-293 cells. To this aim, HEK-293 cells were co-transfected with the DAX-1-Luc plasmid and increasing amounts of a full length AR-encoding plasmid. In the absence of exogenous AR expression, DAX-1 promoter activity was not influenced by Mb administration. Conversely, in the presence of ectopic AR, a dose-dependent increase in the basal DAX-1 transcriptional activity could be observed upon Mb treatment (Fig. 7B). Additionally, to explore if the ability of AR to induce the DAX-1 promoter is dependent on its transactivation properties, HEK-293 cells were transfected with increasing concentration of an expression plasmid encoding an AR carrying a mutation ($AR_{Cys574\rightarrow Arg}$) in the DNA binding domain (DBD), which renders the receptor unable to bind target DNA sequences (42,63). Interestingly, in these experimental conditions, no changes in DAX-1 promoter activity could be measured (Fig. 7B). These results clearly demonstrated that DAX1 promoter can be considered a valid target of AR and strongly suggest the existence, within the DAX-1 promoter, of putative androgen responsive region(s).

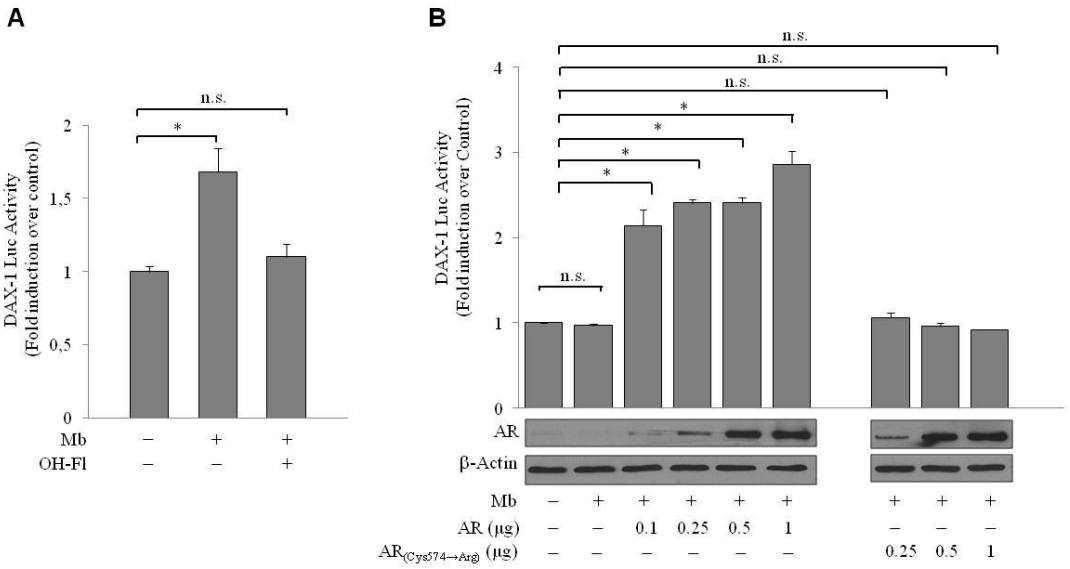

Figure 7. Mb-induced activation of DAX-1 gene promoter requires integrity of the AR DNA binding domain. **(A)** *Mb induces DAX-1 promoter activity***.** MCF-7 cells were transiently transfected with DAX-1-*Luc* plasmid (0.25 μg/well) and treated with 10^{-8} M Mb and/or 10^{-6}M OH-Fl, for 24h. **(B)** *DAX-1 promoter activation depends on a functional AR-DNA binding domain*. HEK-293 cells were co-transfected with DAX-1-Luc-plasmid (0.25 μg/well) plus increasing amounts (μg) of pcDNA3-AR (AR) or CMVP881 ($AR_{Cys-574\rightarrow Arg}$) as indicated, and treated with Mb 10^{-8}M for 24h. Linear relation between transfected AR plasmid and expressed AR protein quantity was evaluated by WB analysis; β-Actin protein, loading control. *, P<0.01; n.s., non significant.

Identification of a functional Androgen Responsive Element (ARE) within the DAX-1 promoter

Sequence analysis revealed that the DAX-1 promoter contains a putative androgen response element (ARE) located at position -1074bp upstream of the translation starting codon (Fig. 8A, *upper panel*) which is homolougus to the AREs found in the promoters of several androgen responsive genes (71) (Fig. 8A, *lower panel*).

To test the hypothesis that AR can effectively bind to this putative ARE motif (DAX-1-ARE), a DNA affinity precipitation assay (DAPA) was performed by using a double-stranded oligonucleotide containing the core ARE sequence and 10-11 bp of flanking sequence on either side. Endogenous AR was found associated with the putative consensus oligonucleotide following Mb administration only, while AR binding was unnoticeable in nuclear cell lysates from untreated cells. The use of biotinylated mutant oligonucleotide, abolished AR binding, indicating that the in vitro DNA-AR protein binding is sequence specific (Fig. 8B).

To better demonstrate the specificity of the putative ARE site, an electrophoretic mobility shift assay (EMSA) was performed using the identified ARE motif as a DNA probe. Factors present in MCF-7 nuclear extracts and ARE probe formed a protein-DNA complex (Fig. 8C, *lane 1*) which was strongly enhanced by Mb treatment (Fig. 8C, *lane 2*). The specificity of the protein-DNA association was demonstrated by its disappearance when 100-fold molar excess of unlabeled wild-type probe was added to the reaction as competitor (Fig. 8C, *lane 3*) or when a mutated labeled probe was used (Fig. 8C, *lane 4*). Coadministration of the anti-androgen bicalutamide (casodex) markedly decreased the Mb-induced DNA binding complex indicating the involvement of the AR (Fig. 8C, *lane 5*). Moreover, the DNA-protein complex formation was reduced (immunodepletion) in the presence of a specific anti-AR monoclonal antibody, indicating that this antibody recognizes AR epitopes that interact or interfere with AR association to ARE (Fig. 8C, *lane 6*) and further confirming the presence of AR in the protein-DNA complex. As expected, protein-DNA complex formation was unaffected by normal rabbit IgG (Fig. 8C, *lane 7*).

Chromatin immunoprecipitation (ChIP) analysis was next used to determine whether endogenous AR protein localizes to the native DAX-1 promoter in AR-positive MCF-7 and T47D breast cancer cells. AR occupancy of the DAX-1-ARE containing region of DAX-1 promoter was induced in a ligand-dependent manner, since AR recruitment was enhanced by Mb administration. The ability of AR to transactivate the DAX-1 gene is evidenced by the dynamic of RNA Pol II recruitment onto the DAX-1 promoter, that appears to be enhanced upon Mb treatment. Non-specific IgG antibody failed to precipitate any protein-DNA complexes (Fig. 8C).

Overall, these findings clearly demonstrated that activated AR can bind to the ARE motif within the DAX-1 proximal promoter in human breast cancer cells.

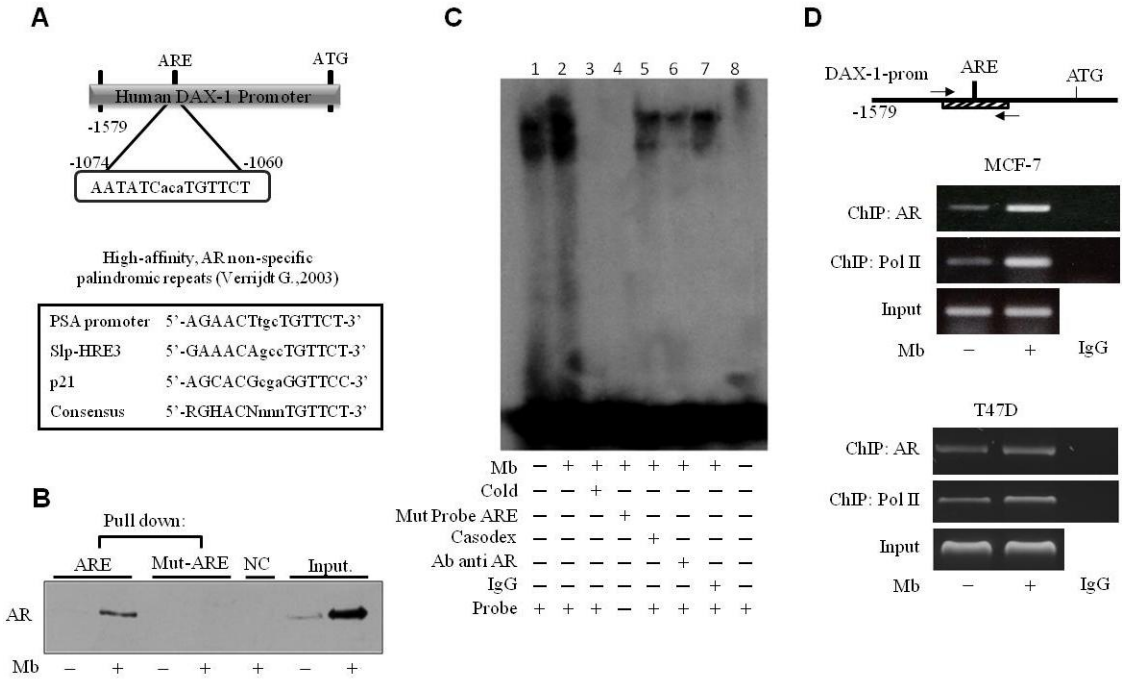

Figure 8. Activated AR binds to the ARE site within the DAX-1 promoter. **A**) Schematic representation of the putative ARE site within the DAX-1 promoter (*upper panel*). List of known ARE sequences (*lower panel*). **(B)** *Detection of AR/ARE binding*. Nuclear extracts from MCF-7 cells treated with 10^{-8} M Mb were incubated with either wt- (ARE) or mutated (mut-ARE) biotinylated oligonucleotide and subjected to DAPA assay. The unbound fraction was loaded as negative control (NC); cell nuclear extracts were used as positive control (Input). **(C)** *Evaluation of AR/ARE binding specificity*. Nuclear extracts from MCF-7 cells untreated (lane 1) or treated with 10^{-8} M Mb (lane 2-7) were incubated with a specific labelled probe. 100-fold molar excess of unlabeled probe (lane 3); labeled mutated probe (lane 4); addition of 10^{-5} M Casodex (lane 5); pre-incubation with anti-AR antibody (lane 6) or IgG (lane 7); probe alone (lane 8). **(D)** *AR recruitment onto the DAX-1 promoter.* Sheared chromatin from MCF-7 or T47D cells treated with 10^{-8} M Mb for 2h, was precipitated using anti-AR or anti-RNA Pol II antibodies. IgG, control samples. The investigated sequence was detected by PCR using specific primers. DNA Inputs were amplified as loading controls. All the results are representative of three independent experiments.

Androgen treatment inhibits aromatase expression through a DAX-1-mediated mechanism in breast cancer cells.

To comprehend the biological significance of the androgen-dependent up-regulation of DAX-1 expression, we explored the possibility that it might impact on in situ estrogen production since the aromatase gene *CYP19* has been shown to represent a physiologic target gene for DAX-1 (56). To this aim the expression of P450 aromatase upon androgen treatment was examined in MCF-7 cells. Mb administration decreased the cellular content of the enzyme at both mRNA and protein levels (Fig. 9A).

To provide evidence of the participation of DAX-1 in the androgen-dependent modulation of aromatase expression, DAX-1 gene was silenced by siRNA technology as evidenced in Fig. 9B. Interestingly, DAX-1 gene silencing was able to reverse the down-regulatory effect induced by Mb administration on aromatase mRNA and protein levels (Fig. 9C), clearly demonstrating the involvement of DAX-1 in this process.

Previous studies, demonstrated that DAX-1 is able to repress SF-1/LRH-1-mediated transactivation of several steroidogenic genes, including P450 aromatase (56,72,73), by acting as an adaptor molecule and recruiting the steroid receptor corepressor N-CoR (72). Accordingly, the occurrence of a similar mechanism in our experimental system upon androgen treatment has been also investigated. To this aim, the ability of Mb to regulate aromatase gene transcriptional activity through the PII-1.3 proximal promoter was evaluated firstly by transient transfection-based reporter gene assays in MCF-7 cells. As shown in Fig. 9D, a significant reduction of promoter transcriptional activity was observed upon Mb administration. On the contrary, no significant changes could be observed in MCF-7-cells transfected with a PII-1.3 reporter plasmid bearing a SF-1/LRH-1 mutated binding site, underlying the importance of this motif in the regulation of aromatase expression by androgens in MCF-7 breast cancer cells.

Then, the ability of DAX-1 to associate to the SF-1/LRH-1 containing region of the PII-1.3 aromatase proximal promoter upon androgen treatment was examined by ChIP assay. DAX-1 occupancy of the SF-1/LRH-1 site containing sequence of the PII-1.3 promoter was induced in a ligand-dependent manner,

since DAX-1 recruitment was enhanced by Mb administration. Similarly, recruitment of the corepressor N-CoR was significantly increased following Mb treatment (Fig. 9E).

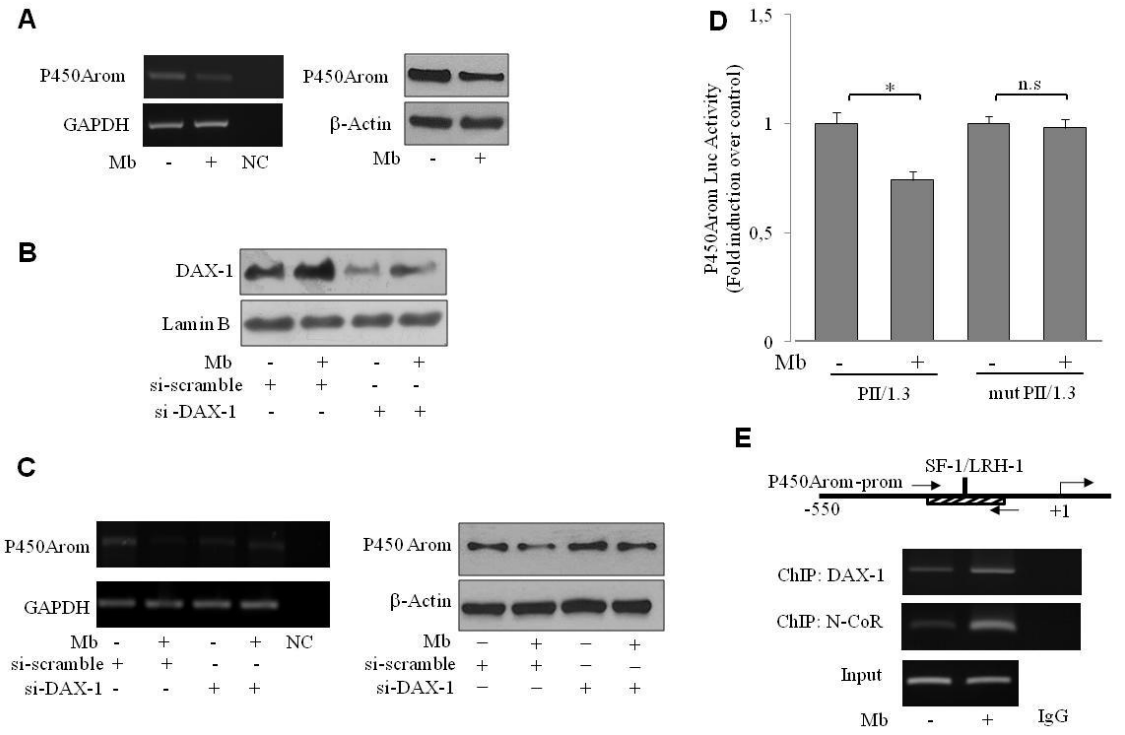

Figure 9. Mibolerone through DAX-1 inhibits P450aromatase expression and promoter activity in MCF-7 cells**. (A)** *Mb decreases aromatase expression*. Cells were treated with 10^{-8} M Mb for 48h and aromatase mRNA (*left panel*) or protein content (*right panel*) were detected by RT–PCR or WB analyses, respectively. GAPDH mRNA, internal standard; NC, negative control. β-Actin protein, loading control. **(B)** *DAX-1 gene knock-down*. Nuclear extracts from cells transfected with siDAX-1 or scrambled control siRNA (si-scramble) and treated with 10^{-8} M Mb for 48h were subjected to WB analysis. Lamin B expression was assessed as protein loading control. **(C)** *Aromatase expression in DAX-1-silenced cells*. Cells were treated as above described and aromatase mRNA (*left panel*) or protein content (*right panel*) were detected by RT–PCR or WB analyses, respectively. GAPDH mRNA, internal standard; NC, negative control. β-Actin protein, loading control. All the results are representative of three independent experiments. **(D)** *Mb modulates aromatase promoter activity*. Cells were transiently transfected with wt- PII/1.3- or a SF-1/LRH-1 mutant PII/1.3- (mut PII/1.3) aromatase promoter reporter plasmids (0.25 µg/well) and treated with 10^{-8} M Mb for 24h. *, $P<0.05$; n.s., nonsignificant. **(E) "***In vivo" DAX-1 recruitment onto the P450-aromatase promoter.* Sheared chromatin from MCF-7 cells treated with 10^{-8} M Mb for 2h, was precipitated using anti-DAX-1 or anti-N-CoR Abs. IgG, control samples. The investigated sequence was detected by PCR using specific primers. DNA Inputs were amplified as loading controls.

Androgens, by inducing DAX-1 expression, inhibit P450 aromatase in estrogen-dependent Leydig tumor cells, R2C

To investigated whether androgens might also play a role in the modulation of estrogen-dependent Leydig cell tumor growth, we used a rat Leydig tumor cell line R2C, characterized by a very low DAX-1 expression (74) but high aromatase content and activity responsible for high in situ estrogen production

which controls cell proliferation (75,76). The role of androgens on Leydig tumor cell proliferation was evaluated, firstly, by measuring the response of R2C cells to increasing concentrations of Mb for 6 days. As shown in Fig. 10A (*left panel*), Mb treatment significantly decreased R2C cell proliferation in a dose-dependent manner. The inhibitory effect of 10^{-8} M Mb was further confirmed, showing that it began 3 days after androgen administration and persisted thereafter (Fig. 10A, *right panel*).

Then, we aimed to evaluate, even in Leydigioma tumor cells, the existence of an androgen-dependent mechanism able to regulate DAX-1 cellular levels, as previously described in MCF-7 breast cancer cells. 72h Mb treatment induced an up-regulation of DAX-1 protein content (Fig. 10B). In addition, immunofluorescence analysis showed that immunoreactivity for DAX-1 was detected in both cytoplasm and nucleus of untreated R2C cells and strongly enhanced in the nuclear compartment upon Mb administration (Fig. 10C).

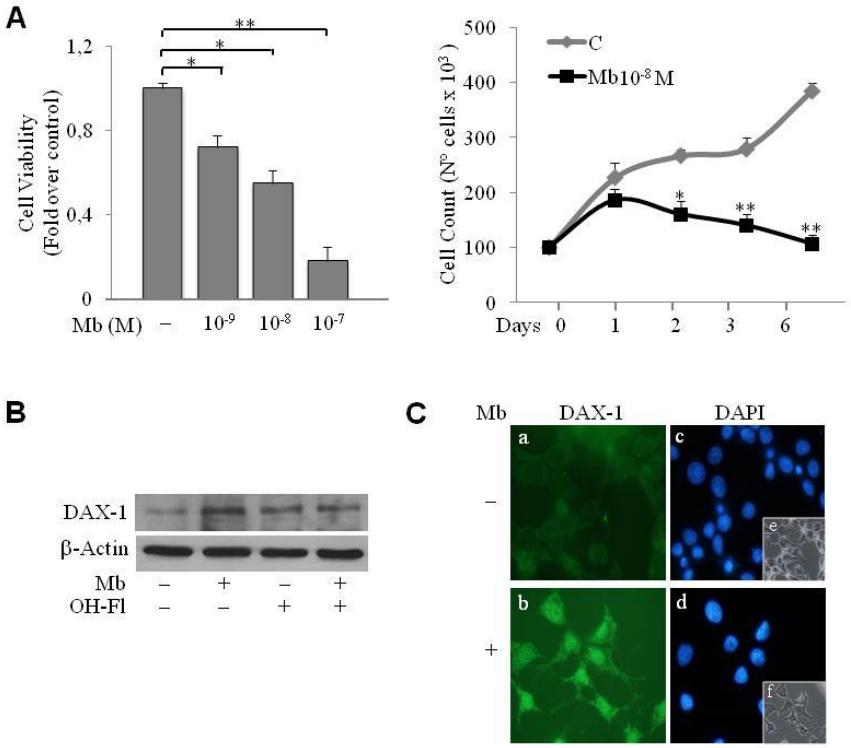

Figure 10. Androgen-dependent modulation of DAX-1 in R2C cells. **(A)** *Cell proliferation inhibition by Mb*. MTT assay (*left panel*) or cell counting by trypan blue exclusion test (*right panel*) were performed on cells treated for 6 days with Mb as indicated. *, P<0,05; **, P<0,01. **(B)** *Mb up-regulates DAX-1 expression*. Nuclear extracts from cells treated with 10^{-8} M Mb and/or 10^{-6} M OH-Fl were subjected to WB analysis to detect DAX-1 protein expression. β-Actin protein, loading control. **(C)** *Subcellular localization of DAX-1*. DAX-1 (*a, b*), DAPI (*c, d*) immunofluorescence was detected in cells treated with 10^{-8} M Mb for 24h; small squares, bright field (*e, f*); x1000 optical magnification. Results are representative of three independent experiments.

On the other hand, Mb treatment determined a decrease of aromatase mRNA and protein levels, which was completely abrogated by contemporary administration of the androgen antagonist Hydroxiflutamide (Fig. 11A).
Reduction of aromatase enzyme levels in R2C cells upon Mb treatment was paralleled by decreased aromatase enzymatic activity and estradiol production (Fig. 11B and C).

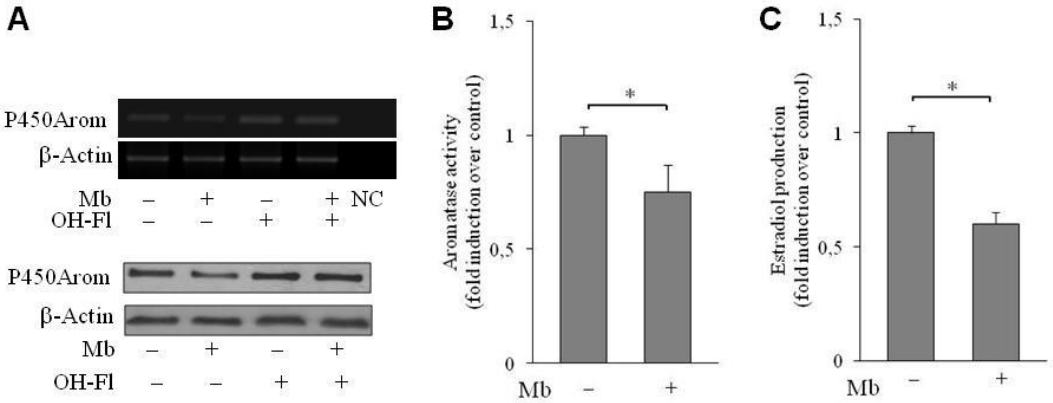

Figure 11. Androgen-dependent modulation of P450 aromatase in R2C cells **(A)** *Modulation of aromatase expression by Mb*. Cells were treated with 10^{-8} M Mb and/or 10^{-6} M OH-Fl and aromatase mRNA (*upper panel*) or protein content (*lower panel*) were detected by RT–PCR or WB analyses, respectively. β-Actin mRNA, internal standard; NC, negative control. β-Actin protein, loading control. Results are representative of three independent experiments. *Modulation of aromatase activity* **(B)** *and estradiol production* **(C)** *by Mb*. Aromatase activity and Estradiol production were assessed as described in materials and methods. The values represent the mean ± S.D. of three different experiments each performed with triplicate samples. (*, $p < 0.01$; **, $p < 0,05$).

To determine whether Mb treatment might negatively influence PII aromatase promoter transcriptional activity, transient transfection experiments were performed in R2C cells. As shown in Fig. 12A, Mb administration was able to determine a significant reduction of promoter activity. Disruption of the SF-1 binding site within the PII aromatase promoter resulted in the loss of the inhibitory effect exerted by Mb, evidencing that regulation by androngens requires the SF-1 motif. Additionally, ChIP assays indicated that DAX-1 accumulated at the SF-1 motif containing region of the PII aromatase promoter upon Mb treatment concomitantly with an equivalent increase in the occupancy of the corepressor N-CoR (Fig. 12B). These results underline the contribution of DAX-1 in the negative androgen-dependent modulation of aromatase gene.

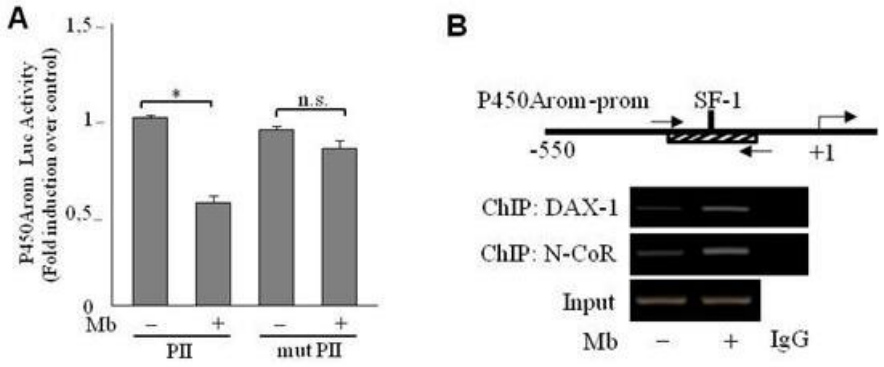

Figure 12. Androgen-dependent modulation of P450 aromatase promoter in R2C cells **(A)** *Mb modulates aromatase promoter activity.* Cells were transiently transfected with wt- PII- or a SF-1 mutant PII- (mut PII) aromatase promoter reporter plasmids and treated with 10^{-8} M Mb for 24h. *, P<0.05; n.s., nonsignificant. **(B) "***In vivo" DAX-1 recruitment onto the P450 aromatase promoter*. Sheared chromatin from MCF-7 cells treated with 10^{-8} M Mb for 2h, was precipitated using anti-DAX-1 or anti-N-CoR antibodies. IgG, control samples. The investigated sequence was detected by PCR using specific primers. DNA Inputs were amplified as loading controls. Results are representative of three independent experiments.

AR/DAX-1/Aromatase expression pattern in male Fisher rats

To evaluate the biological significance of the up-regulation of DAX-1 and the inhibition of aromatase levels exerted by ligand-activated AR, the expression pattern of DAX-1, aromatase and AR was investigated in male Fisher rats. To this aim immunoblotting analysis was performed on testes tissues from younger (Fisher Rats Normal Testes: FRNT) and older (Fisher Rats Tumor Testes: FRTT) Fisher rats. The latter group have a high incidence of spontaneously developing Leydig cell tumors. Worthily, as shown in Fig. 13, DAX-1 protein was highly expressed in FRNT but scarcely detectable in FRTT. A similar expression pattern was displayed by AR. On the contrary, a strongly increased aromatase immunoreactivity could be observed in FRTT compared to younger FRNT.

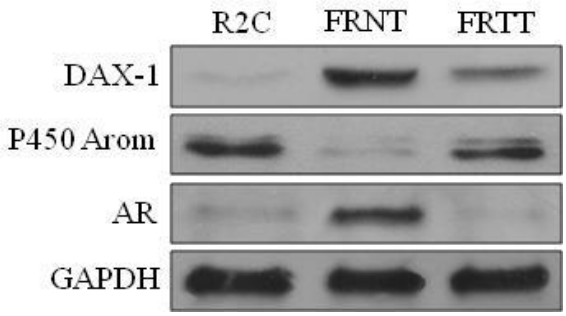

Figure 13. Expression analysis of AR, DAX-1 and P450 aromatase in Fisher rats**.** Total proteins extracted from R2C cells or from tissues of normal (FRNT) or tumoral (FRTT) Fisher rat testes were subjected to WB analysis to detect DAX-1, P450aromatase and AR expression levels. GAPDH levels were assessed as loading control. Single representative result.

DISCUSSION

In human hormone sensitive neoplasms such as breast and Leydig cell tumors, estrogens can be *de novo* produced (7,76-78), indicating an essential role of the androgen peripheral aromatization by P450 aromatase. Accordingly, aromatase inhibitors are currently established as the gold standard for the treatment for ER-positive breast cancers but resistance to the therapy still remains to be solved by other modes of suppression of intra-tumoral estrogen production (11). Hence, analysis of the modulation of intratumoral aromatase appears to be crucial not only for a better comprehension of the development and the biological behaviour of estrogen-dependent carcinomas, but also in the clinical management of cancer patients, since aromatase suppression by new agents may provide improvement in tumor endocrine therapy. Here we demonstrate a novel androgen receptor-mediated mechanism leading to the activation of the DAX-1 gene transcription which in turn negatively impacts on aromatase expression and activity in two distinct estrogen-related neoplasms, such as breast cancer and testicular Leydig cell tumor.

Orphan nuclear receptor DAX-1 has key roles in the development and the maintenance of reproductive function and hormone biosynthesis in mammals (53,79-82). However DAX-1 functions and regulation in sex steroid-dependent neoplasms, in which *in situ* steroid production and metabolism holds a crucial role, need to be further clarified. In node-negative breast cancer, DAX-1 expression correlates with positivity for ER, PR and AR, smaller tumor size (23,24,83) and excellent survival (84). Nevertheless, although several studies established DAX-1 as a crucial regulator of steroidogenesis, the precise molecular mechanism behind DAX-1 transcriptional control and/or its relationship to aromatase expression and activity in breast cancer cells still remains largely unknown. Our study identifies DAX-1 as an androgen-responsive gene, whose expression is positively modulated by ligand-activated AR. Indeed, in MCF-7 breast cancer cells, DAX-1 expression is up-regulated by Mb administration as evidenced by enhancement of its mRNA and protein levels, and increase of its promoter activity. These results are supported by previous observations in rat Sertoli cells indicating that DAX-1 expression is

regulated during spermatogenesis and peaks during the androgen-sensitive phase of the spermatogenic cycle (85). Activated AR has a fundamental role in the up-regulation of DAX-1 cellular levels since in AR-negative HEK-293 cells, induction of DAX-1 promoter activity can be evidenced only in the presence of exogenous AR expression and strictly depends on the integrity of the AR DNA binding domain, suggesting the existence, in the DAX-1 promoter, of putative androgen responsive region(s) which mediate androgen response. In the current study we identified an androgen response element (*DAX-1*-ARE: 5'-AATATCacaTGTTCT-3') located between -1074bp to -1060bp upstream of the DAX-1 gene translation initiation codon which displays the conventional inverted repeats of the 5'-TGTTCT-3' monomer-binding element found in the promoters of several androgen-responsive genes (71) such as prostate specific antigen (86), p21 (87) and *slp*-HRE3 (88). This DAX-1-ARE is functional, as demonstrated by transactivation studies, and capable to bind efficiently the AR, in a ligand-dependent manner. Furthermore, the *in vivo* interaction between AR and the DAX-1 promoter is supported by ChIP analysis showing that AR occupancy of the DAX-1-ARE containing promoter region is concomitant with an increase in RNA Pol II recruitment, consistent with the enhanced DAX-*1* transcriptional activity. Thus, activated AR may directly regulate or modulate the expression of DAX-1 and hence it may lie upstream of DAX-1 in a regulatory cascade directing steroid hormones biosynthesis in various steroidogenic tissues. Indeed, DAX-1 plays significant roles in the regulation of steroidogenesis through a variety of mechanisms of transcriptional repression and interaction with many other factors. Interestingly, studies on Dax-1 deficient mice, displaying an increased aromatase expression, indicate that *Cyp19* is a physiologic target for DAX-1 in Leydig cells (56). Consistent with these observations, we found that androgen-dependent up-regulation of DAX-1 significantly impacts on aromatase content in breast cancer cells as demonstrated by the evidence that silencing DAX-1 gene completely reversed the down-regulatory effect exerted by androgens on aromatase expression. Transcriptional control by DAX-1 occurs through its recruitment on the SF-1/LRH-1 binding site within the PII/1.3 aromatase proximal promoter in association with the transcriptional co-repressor N-CoR, leading to inhibition of aromatase gene transcription. The importance of our results is highlighted by

recent studies demonstrating that biologically active DHT is locally produced in breast carcinoma tissues (89) and increased by aromatase inhibitors treatment (90). Interestingly, intratumoral DHT levels are positively associated with AR and 5-α-reductase-1 expression but inversely correlated with tumor size, Ki-67 and aromatase expression (89). Thus in AR-positive breast carcinomas the use of aromatase inhibitors may be more effective by accumulation of the local DHT concentration which in turn, acting in an autocrine short loop through DAX-1, might further contribute to reduce aromatase levels (5). Therefore the molecular mechanism we identified might contribute to explain the negative influence of androgens on breast cancer cell proliferation, and well correlates with previous findings in endometrial carcinoma, where loss or decreased DAX-1 expression results in increased intratumoral steroids production and enhanced estrogen-dependent proliferation of cancer cells (61).

Estrogen dependence is also a feature of testicular tumors: excessive estrogen exposure has been shown to alter Leydig cell function, leading to hyperplasia, hypertrophy and Leydig cell adenomas (7,91). The above described androgen-dependent modulation of DAX-1 and aromatase expression, appears to be a more general mechanism since it can also be evidenced in R2C rat Leydig tumor cells in which growth and progression are strongly estrogen-dependent and consequent to a high aromatase expression (76). In the present study we demonstrated that androgen treatment in R2C cells decreases cell proliferation, enhances DAX-1 expression and reduces aromatase cellular levels. According to our findings, DAX-1 disrupted mouse model displays defective spermatogenesis and Leydig cell hyperplasia, possible due to aromatase up-regulation (56). The molecular mechanism responsible for the androgen-dependent inhibition of aromatase expression in R2C cells is transcriptional as well, involving the recruitment of DAX-1 within the SF-1 site containing region of the PII aromatase proximal promoter in association with N-CoR. Direct confirmation of the biological relevance of our findings comes from results obtained in testes tissues from younger (FRNT) and older (FRTT) Fisher rats. The latter group develops spontaneously Leydig cell neoplasma (92,93), a phenomenon not observed in young animals. Indeed, immunoblotting analysis reveals an inverse relationship between DAX-1 and aromatase expression. Specifically, FRNT are characterized by high levels of DAX-1 protein and very

low levels of aromatase enzyme. On the contrary, Leydig tumor development in FRTT is associated with an opposite expression pattern showing a barely detectable DAX-1 protein and a strongly increased aromatase immunoreactivity. Interestingly, DAX-1 expression pattern is paralleled by a similar mode of expression of the AR.

Collectively, our model for AR-mediated repression of aromatase in estrogen-related cancers (Fig. 14) proposes that ligand-activated AR directly binds to the DAX-1 promoter resulting in increased DAX-1 gene expression. In turn, DAX-1 represses aromatase through its recruitment within the SF-1/LRH-1 containing region of the aromatase promoter, causing reduced *in situ* estrogen production and inhibition of cell proliferation.

Our study identifies DAX-1 as an androgen target gene and provides new insights into the AR/DAX-1/aromatase interplay. Thus, targeting DAX-1 and AR signalling may represent an exploitable pharmacological tool in estrogen-related cancers, opening new avenues for therapeutic intervention.

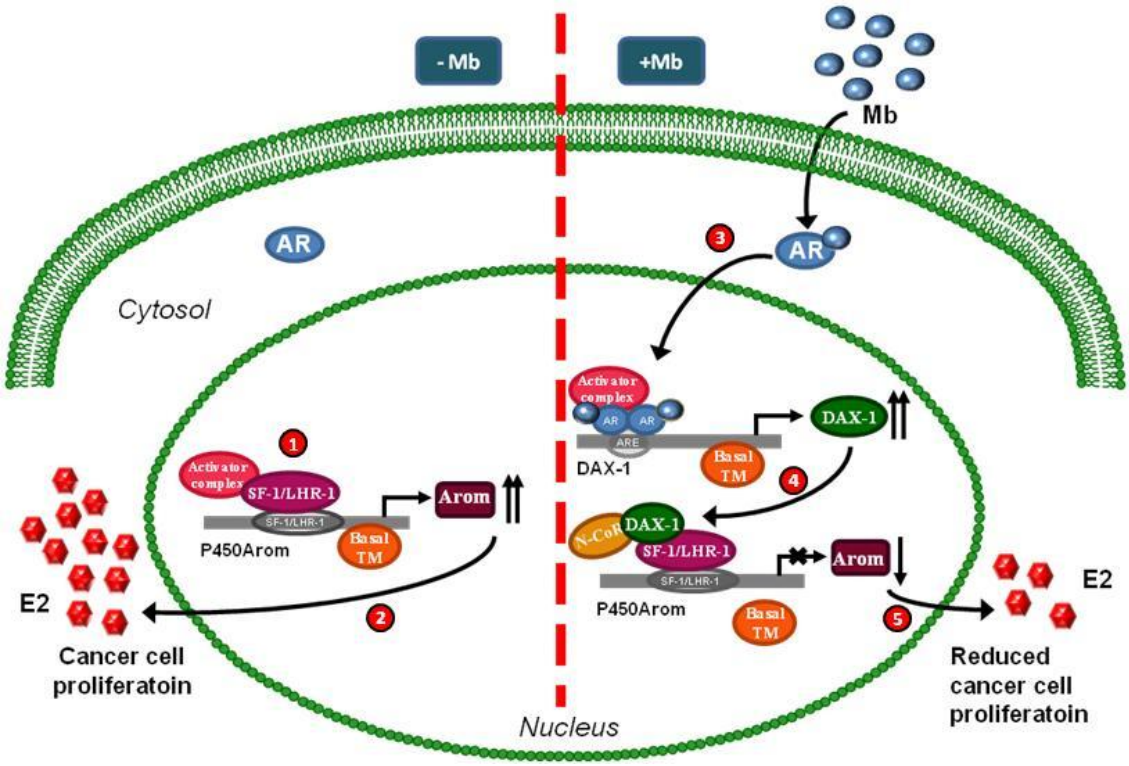

Figure 14. Proposed model for AR/DAX-1/Aromatase interplay in estrogen-related cancer cells. **(1)** In the absence of androgens, P450 *aromatase* is regulated by several factors sustaining gene transcription and aromatase protein expression leading to **(2)** enhanced *in situ* estrogen (E2) production responsible for cancer cell proliferation. In the presence of androgens, ligand-activated AR **(3)** binds to a specific ARE within the DAX-1 promoter gene triggering its activation. In turn, increased DAX-1 protein **(4)** is recruited onto the P450 aromatase proximal promoter and represses SF-1/LHR-1-mediated transcription, reducing locally produced estrogens thus affecting cancer cell proliferation **(5)**.

REFERENCES

1. Pasqualini, J.R. and Chetrite, G.S. (2005) Recent insight on the control of enzymes involved in estrogen formation and transformation in human breast cancer. *The Journal of steroid biochemistry and molecular biology*, **93**, 221-236.
2. Sasano, H., Nagasaki, S., Miki, Y. and Suzuki, T. (2009) New developments in intracrinology of human breast cancer: estrogen sulfatase and sulfotransferase. *Annals of the New York Academy of Sciences*, **1155**, 76-79.
3. Lopez-Otin, C. and Diamandis, E.P. (1998) Breast and prostate cancer: an analysis of common epidemiological, genetic, and biochemical features. *Endocrine reviews*, **19**, 365-396.
4. Nakamura, Y., Suzuki, T., Nakabayashi, M., Endoh, M., Sakamoto, K., Mikami, Y., Moriya, T., Ito, A., Takahashi, S., Yamada, S. *et al.* (2005) In situ androgen producing enzymes in human prostate cancer. *Endocrine-related cancer*, **12**, 101-107.
5. Takagi, K., Miki, Y., Nagasaki, S., Hirakawa, H., Onodera, Y., Akahira, J., Ishida, T., Watanabe, M., Kimijima, I., Hayashi, S. *et al.* (2010) Increased intratumoral androgens in human breast carcinoma following aromatase inhibitor exemestane treatment. *Endocrine-related cancer*, **17**, 415-430.
6. Chen, G.G., Zeng, Q. and Tse, G.M. (2008) Estrogen and its receptors in cancer. *Medicinal research reviews*, **28**, 954-974.
7. Fowler, K.A., Gill, K., Kirma, N., Dillehay, D.L. and Tekmal, R.R. (2000) Overexpression of aromatase leads to development of testicular leydig cell tumors : an in vivo model for hormone-mediated TesticularCancer. *Am J Pathol*, **156**, 347-353.
8. Henderson, I.C. and Canellos, G.P. (1980) Cancer of the breast: the past decade (first of two parts). *The New England journal of medicine*, **302**, 17-30.
9. Jemal, A., Siegel, R., Ward, E., Hao, Y., Xu, J. and Thun, M.J. (2009) Cancer statistics, 2009. *CA: a cancer journal for clinicians*, **59**, 225-249.
10. Yager, J.D. and Davidson, N.E. (2006) Estrogen carcinogenesis in breast cancer. *The New England journal of medicine*, **354**, 270-282.
11. Sasano, H., Miki, Y., Nagasaki, S. and Suzuki, T. (2009) In situ estrogen production and its regulation in human breast carcinoma: from endocrinology to intracrinology. *Pathology international*, **59**, 777-789.
12. Jordan, V.C. and Brodie, A.M. (2007) Development and evolution of therapies targeted to the estrogen receptor for the treatment and prevention of breast cancer. *Steroids*, **72**, 7-25.
13. Forbes, J.F., Cuzick, J., Buzdar, A., Howell, A., Tobias, J.S. and Baum, M. (2008) Effect of anastrozole and tamoxifen as adjuvant treatment for early-stage breast cancer: 100-month analysis of the ATAC trial. *The lancet oncology*, **9**, 45-53.
14. Zhou, J., Ng, S., Adesanya-Famuiya, O., Anderson, K. and Bondy, C.A. (2000) Testosterone inhibits estrogen-induced mammary epithelial proliferation and suppresses estrogen receptor expression. *FASEB journal : official publication of the Federation of American Societies for Experimental Biology*, **14**, 1725-1730.

15. Dimitrakakis, C., Zhou, J., Wang, J., Belanger, A., LaBrie, F., Cheng, C., Powell, D. and Bondy, C. (2003) A physiologic role for testosterone in limiting estrogenic stimulation of the breast. *Menopause*, **10**, 292-298.
16. Yeh, S., Hu, Y.C., Wang, P.H., Xie, C., Xu, Q., Tsai, M.Y., Dong, Z., Wang, R.S., Lee, T.H. and Chang, C. (2003) Abnormal mammary gland development and growth retardation in female mice and MCF7 breast cancer cells lacking androgen receptor. *The Journal of experimental medicine*, **198**, 1899-1908.
17. Eigeliene, N., Elo, T., Linhala, M., Hurme, S., Erkkola, R. and Harkonen, P. (2012) Androgens inhibit the stimulatory action of 17beta-estradiol on normal human breast tissue in explant cultures. *The Journal of clinical endocrinology and metabolism*, **97**, E1116-1127.
18. Quigley, C.A., De Bellis, A., Marschke, K.B., el-Awady, M.K., Wilson, E.M. and French, F.S. (1995) Androgen receptor defects: historical, clinical, and molecular perspectives. *Endocrine reviews*, **16**, 271-321.
19. New, M.I. (2004) An update of congenital adrenal hyperplasia. *Annals of the New York Academy of Sciences*, **1038**, 14-43.
20. Lobaccaro, J.M., Lumbroso, S., Belon, C., Galtier-Dereure, F., Bringer, J., Lesimple, T., Heron, J.F., Pujol, H. and Sultan, C. (1993) Male breast cancer and the androgen receptor gene. *Nature genetics*, **5**, 109-110.
21. Chamberlain, N.L., Driver, E.D. and Miesfeld, R.L. (1994) The length and location of CAG trinucleotide repeats in the androgen receptor N-terminal domain affect transactivation function. *Nucleic acids research*, **22**, 3181-3186.
22. Giguere, Y., Dewailly, E., Brisson, J., Ayotte, P., Laflamme, N., Demers, A., Forest, V.I., Dodin, S., Robert, J. and Rousseau, F. (2001) Short polyglutamine tracts in the androgen receptor are protective against breast cancer in the general population. *Cancer research*, **61**, 5869-5874.
23. Park, S., Koo, J., Park, H.S., Kim, J.H., Choi, S.Y., Lee, J.H., Park, B.W. and Lee, K.S. (2010) Expression of androgen receptors in primary breast cancer. *Annals of oncology : official journal of the European Society for Medical Oncology / ESMO*, **21**, 488-492.
24. Moinfar, F., Okcu, M., Tsybrovskyy, O., Regitnig, P., Lax, S.F., Weybora, W., Ratschek, M., Tavassoli, F.A. and Denk, H. (2003) Androgen receptors frequently are expressed in breast carcinomas: potential relevance to new therapeutic strategies. *Cancer*, **98**, 703-711.
25. Agoff, S.N., Swanson, P.E., Linden, H., Hawes, S.E. and Lawton, T.J. (2003) Androgen receptor expression in estrogen receptor-negative breast cancer. Immunohistochemical, clinical, and prognostic associations. *Am J Clin Pathol*, **120**, 725-731.
26. Soreide, J.A., Lea, O.A., Varhaug, J.E., Skarstein, A. and Kvinnsland, S. (1992) Androgen receptors in operable breast cancer: relation to other steroid hormone receptors, correlations to prognostic factors and predictive value for effect of adjuvant tamoxifen treatment. *European journal of surgical oncology : the journal of the European Society of Surgical Oncology and the British Association of Surgical Oncology*, **18**, 112-118.
27. Kimura, N., Mizokami, A., Oonuma, T., Sasano, H. and Nagura, H. (1993) Immunocytochemical localization of androgen receptor with polyclonal

antibody in paraffin-embedded human tissues. *The journal of histochemistry and cytochemistry : official journal of the Histochemistry Society*, **41**, 671-678.

28. Sauter, E.R., Lininger, J., Magklara, A., Hewett, J.E. and Diamandis, E.P. (2004) Association of kallikrein expression in nipple aspirate fluid with breast cancer risk. *International journal of cancer. Journal international du cancer*, **108**, 588-591.
29. Sauter, E.R., Tichansky, D.S., Chervoneva, I. and Diamandis, E.P. (2002) Circulating testosterone and prostate-specific antigen in nipple aspirate fluid and tissue are associated with breast cancer. *Environmental health perspectives*, **110**, 241-246.
30. Schippinger, W., Regitnig, P., Dandachi, N., Wernecke, K.D., Bauernhofer, T., Samonigg, H. and Moinfar, F. (2006) Evaluation of the prognostic significance of androgen receptor expression in metastatic breast cancer. *Virchows Archiv : an international journal of pathology*, **449**, 24-30.
31. Rakha, E.A., El-Sayed, M.E., Green, A.R., Lee, A.H., Robertson, J.F. and Ellis, I.O. (2007) Prognostic markers in triple-negative breast cancer. *Cancer*, **109**, 25-32.
32. Castellano, I., Allia, E., Accortanzo, V., Vandone, A.M., Chiusa, L., Arisio, R., Durando, A., Donadio, M., Bussolati, G., Coates, A.S. *et al.* (2010) Androgen receptor expression is a significant prognostic factor in estrogen receptor positive breast cancers. *Breast cancer research and treatment*, **124**, 607-617.
33. Park, I.H., Ro, J., Park, S., Lim, H.S., Lee, K.S., Kang, H.S., Jung, S.Y. and Lee, S. (2012) Lack of any association between functionally significant CYP2D6 polymorphisms and clinical outcomes in early breast cancer patients receiving adjuvant tamoxifen treatment. *Breast cancer research and treatment*, **131**, 455-461.
34. Chae, B.J., Lee, A., Bae, J.S., Song, B.J. and Jung, S.S. (2011) Expression of nuclear receptor DAX-1 and androgen receptor in human breast cancer. *Journal of surgical oncology*, **103**, 768-772.
35. Yu, Q., Niu, Y., Liu, N., Zhang, J.Z., Liu, T.J., Zhang, R.J., Wang, S.L., Ding, X.M. and Xiao, X.Q. (2011) Expression of androgen receptor in breast cancer and its significance as a prognostic factor. *Annals of oncology : official journal of the European Society for Medical Oncology / ESMO*, **22**, 1288-1294.
36. Peters, A.A., Buchanan, G., Ricciardelli, C., Bianco-Miotto, T., Centenera, M.M., Harris, J.M., Jindal, S., Segara, D., Jia, L., Moore, N.L. *et al.* (2009) Androgen receptor inhibits estrogen receptor-alpha activity and is prognostic in breast cancer. *Cancer research*, **69**, 6131-6140.
37. Lin Fde, M., Pincerato, K.M., Bacchi, C.E., Baracat, E.C. and Carvalho, F.M. (2012) Coordinated expression of oestrogen and androgen receptors in HER2-positive breast carcinomas: impact on proliferative activity. *Journal of clinical pathology*, **65**, 64-68.
38. Berns, E.M., Dirkzwager-Kiel, M.J., Kuenen-Boumeester, V., Timmermans, M., Verhoog, L.C., van den Ouweland, A.M., Meijer-Heijboer, H., Klijn, J.G. and van der Kwast, T.H. (2003) Androgen pathway dysregulation in BRCA1-mutated breast tumors. *Breast cancer research and treatment*, **79**, 121-127.
39. Haiman, C.A., Brown, M., Hankinson, S.E., Spiegelman, D., Colditz, G.A., Willett, W.C., Kantoff, P.W. and Hunter, D.J. (2002) The androgen receptor CAG repeat

polymorphism and risk of breast cancer in the Nurses' Health Study. *Cancer research*, **62**, 1045-1049.

40. Kollara, A., Kahn, H.J., Marks, A. and Brown, T.J. (2001) Loss of androgen receptor associated protein 70 (ARA70) expression in a subset of HER2-positive breast cancers. *Breast cancer research and treatment*, **67**, 245-253.
41. Ogawa, Y., Hai, E., Matsumoto, K., Ikeda, K., Tokunaga, S., Nagahara, H., Sakurai, K., Inoue, T. and Nishiguchi, Y. (2008) Androgen receptor expression in breast cancer: relationship with clinicopathological factors and biomarkers. *International journal of clinical oncology / Japan Society of Clinical Oncology*, **13**, 431-435.
42. Lanzino, M., De Amicis, F., McPhaul, M.J., Marsico, S., Panno, M.L. and Ando, S. (2005) Endogenous coactivator ARA70 interacts with estrogen receptor alpha (ERalpha) and modulates the functional ERalpha/androgen receptor interplay in MCF-7 cells. *J Biol Chem*, **280**, 20421-20430.
43. Ando, S., De Amicis, F., Rago, V., Carpino, A., Maggiolini, M., Panno, M.L. and Lanzino, M. (2002) Breast cancer: from estrogen to androgen receptor. *Molecular and cellular endocrinology*, **193**, 121-128.
44. de Launoit, Y., Dauvois, S., Dufour, M., Simard, J. and Labrie, F. (1991) Inhibition of cell cycle kinetics and proliferation by the androgen 5 alpha-dihydrotestosterone and antiestrogen N,n-butyl-N-methyl-11-[16' alpha-chloro-3',17 beta-dihydroxy-estra-1',3',5'-(10')triene-7' alpha-yl] undecanamide in human breast cancer ZR-75-1 cells. *Cancer research*, **51**, 2797-2802.
45. Lapointe, J. and Labrie, C. (2001) Role of the cyclin-dependent kinase inhibitor p27(Kip1) in androgen-induced inhibition of CAMA-1 breast cancer cell proliferation. *Endocrinology*, **142**, 4331-4338.
46. Greeve, M.A., Allan, R.K., Harvey, J.M. and Bentel, J.M. (2004) Inhibition of MCF-7 breast cancer cell proliferation by 5alpha-dihydrotestosterone; a role for p21(Cip1/Waf1). *Journal of molecular endocrinology*, **32**, 793-810.
47. Lanzino, M., Sisci, D., Morelli, C., Garofalo, C., Catalano, S., Casaburi, I., Capparelli, C., Giordano, C., Giordano, F., Maggiolini, M. *et al.* (2010) Inhibition of cyclin D1 expression by androgen receptor in breast cancer cells--identification of a novel androgen response element. *Nucleic acids research*, **38**, 5351-5365.
48. Poulin, R., Baker, D. and Labrie, F. (1988) Androgens inhibit basal and estrogen-induced cell proliferation in the ZR-75-1 human breast cancer cell line. *Breast cancer research and treatment*, **12**, 213-225.
49. Bardoni, B., Zanaria, E., Guioli, S., Floridia, G., Worley, K.C., Tonini, G., Ferrante, E., Chiumello, G., McCabe, E.R., Fraccaro, M. *et al.* (1994) A dosage sensitive locus at chromosome Xp21 is involved in male to female sex reversal. *Nature genetics*, **7**, 497-501.
50. Iyer, A.K., McCabe, E.R. (2004) Molecular mechanisms of DAX1 action. *Molecular Genetics and Metabolism,* **83,** 60–73.
51. Swain, A., Zanaria, E., Hacker, A., Lovell-Badge, R. and Camerino, G. (1996) Mouse Dax1 expression is consistent with a role in sex determination as well as in adrenal and hypothalamus function. *Nature genetics*, **12**, 404-409.
52. Zanaria, E., Muscatelli, F., Bardoni, B., Strom, T.M., Guioli, S., Guo, W., Lalli, E., Moser, C., Walker, A.P., McCabe, E.R. *et al.* (1994) An unusual member of the

nuclear hormone receptor superfamily responsible for X-linked adrenal hypoplasia congenita. *Nature*, **372**, 635-641.

53. Zazopoulos, E., Lalli, E., Stocco, D.M. and Sassone-Corsi, P. (1997) DNA binding and transcriptional repression by DAX-1 blocks steroidogenesis. *Nature*, **390**, 311-315.
54. Guo, W., Burris, T.P. and McCabe, E.R. (1995) Expression of DAX-1, the gene responsible for X-linked adrenal hypoplasia congenita and hypogonadotropic hypogonadism, in the hypothalamic-pituitary-adrenal/gonadal axis. *Biochemical and molecular medicine*, **56**, 8-13.
55. Lalli, E. and Sassone-Corsi, P. (2003) DAX-1, an unusual orphan receptor at the crossroads of steroidogenic function and sexual differentiation. *Mol Endocrinol*, **17**, 1445-1453.
56. Wang, Z.J., Jeffs, B., Ito, M., Achermann, J.C., Yu, R.N., Hales, D.B. and Jameson, J.L. (2001) Aromatase (Cyp19) expression is up-regulated by targeted disruption of Dax1. *Proc Natl Acad Sci U S A*, **98**, 7988-7993.
57. Reincke, M., Beuschlein, F., Lalli, E., Arlt, W., Vay, S., Sassone-Corsi, P. and Allolio, B. (1998) DAX-1 expression in human adrenocortical neoplasms: implications for steroidogenesis. *The Journal of clinical endocrinology and metabolism*, **83**, 2597-2600.
58. Shibata, H., Ikeda, Y., Mukai, T., Morohashi, K., Kurihara, I., Ando, T., Suzuki, T., Kobayashi, S., Murai, M., Saito, I. *et al.* (2001) Expression profiles of COUP-TF, DAX-1, and SF-1 in the human adrenal gland and adrenocortical tumors: possible implications in steroidogenesis. *Molecular genetics and metabolism*, **74**, 206-216.
59. Conde, I., Alfaro, J.M., Fraile, B., Ruiz, A., Paniagua, R. and Arenas, M.I. (2004) DAX-1 expression in human breast cancer: comparison with estrogen receptors ER-alpha, ER-beta and androgen receptor status. *Breast cancer research : BCR*, **6**, R140-148.
60. Abd-Elaziz, M., Akahira, J., Moriya, T., Suzuki, T., Yaegashi, N. and Sasano, H. (2003) Nuclear receptor DAX-1 in human common epithelial ovarian carcinoma: an independent prognostic factor of clinical outcome. *Cancer science*, **94**, 980-985.
61. Saito, S., Ito, K., Suzuki, T., Utsunomiya, H., Akahira, J., Sugihashi, Y., Niikura, H., Okamura, K., Yaegashi, N. and Sasano, H. (2005) Orphan nuclear receptor DAX-1 in human endometrium and its disorders. *Cancer science*, **96**, 645-652.
62. Nakamura, Y., Suzuki, T., Arai, Y. and Sasano, H. (2009) Nuclear receptor DAX1 in human prostate cancer: a novel independent biological modulator. *Endocrine journal*, **56**, 39-44.
63. Zoppi, S., Marcelli, M., Deslypere, J.P., Griffin, J.E., Wilson, J.D. and McPhaul, M.J. (1992) Amino acid substitutions in the DNA-binding domain of the human androgen receptor are a frequent cause of receptor-binding positive androgen resistance. *Mol Endocrinol*, **6**, 409-415.
64. Recchia, A.G., Musti, A.M., Lanzino, M., Panno, M.L., Turano, E., Zumpano, R., Belfiore, A., Ando, S. and Maggiolini, M. (2009) A cross-talk between the androgen receptor and the epidermal growth factor receptor leads to p38MAPK-dependent activation of mTOR and cyclinD1 expression in prostate

and lung cancer cells. *The international journal of biochemistry & cell biology*, **41**, 603-614.

65. Andrews, N.C. and Faller, D.V. (1991) A rapid micropreparation technique for extraction of DNA-binding proteins from limiting numbers of mammalian cells. *Nucleic acids research*, **19**, 2499.
66. Morelli, C., Garofalo, C., Sisci, D., del Rincon, S., Cascio, S., Tu, X., Vecchione, A., Sauter, E.R., Miller, W.H., Jr. and Surmacz, E. (2004) Nuclear insulin receptor substrate 1 interacts with estrogen receptor alpha at ERE promoters. *Oncogene*, **23**, 7517-7526.
67. Catalano, S., Giordano, C., Rizza, P., Gu, G., Barone, I., Bonofiglio, D., Giordano, F., Malivindi, R., Gaccione, D., Lanzino, M. *et al.* (2009) Evidence that leptin through STAT and CREB signaling enhances cyclin D1 expression and promotes human endometrial cancer proliferation. *J Cell Physiol*, **218**, 490-500.
68. Lanzino, M., Garofalo, C., Morelli, C., Le Pera, M., Casaburi, I., McPhaul, M.J., Surmacz, E., Ando, S. and Sisci, D. (2009) Insulin receptor substrate 1 modulates the transcriptional activity and the stability of androgen receptor in breast cancer cells. *Breast cancer research and treatment*, **115**, 297-306.
69. Ariazi, E.A., Clark, G.M. and Mertz, J.E. (2002) Estrogen-related receptor alpha and estrogen-related receptor gamma associate with unfavorable and favorable biomarkers, respectively, in human breast cancer. *Cancer research*, **62**, 6510-6518.
70. Park, Y.Y., Ahn, S.W., Kim, H.J., Kim, J.M., Lee, I.K., Kang, H. and Choi, H.S. (2005) An autoregulatory loop controlling orphan nuclear receptor DAX-1 gene expression by orphan nuclear receptor ERRgamma. *Nucleic acids research*, **33**, 6756-6768.
71. Verrijdt, G., Haelens, A. and Claessens, F. (2003) Selective DNA recognition by the androgen receptor as a mechanism for hormone-specific regulation of gene expression. *Molecular genetics and metabolism*, **78**, 175-185.
72. Crawford, P.A., Dorn, C., Sadovsky, Y. and Milbrandt, J. (1998) Nuclear receptor DAX-1 recruits nuclear receptor corepressor N-CoR to steroidogenic factor 1. *Mol Cell Biol*, **18**, 2949-2956.
73. Hanley, N.A., Rainey, W.E., Wilson, D.I., Ball, S.G. and Parker, K.L. (2001) Expression profiles of SF-1, DAX1, and CYP17 in the human fetal adrenal gland: potential interactions in gene regulation. *Mol Endocrinol*, **15**, 57-68.
74. Jo, Y. and Stocco, D.M. (2004) Regulation of steroidogenesis and steroidogenic acute regulatory protein in R2C cells by DAX-1 (dosage-sensitive sex reversal, adrenal hypoplasia congenita, critical region on the X chromosome, gene-1). *Endocrinology*, **145**, 5629-5637.
75. Young, M. and McPhaul, M.J. (1998) A steroidogenic factor-1-binding site and cyclic adenosine 3',5'-monophosphate response element-like elements are required for the activity of the rat aromatase promoter in rat Leydig tumor cell lines. *Endocrinology*, **139**, 5082-5093.
76. Sirianni, R., Chimento, A., Malivindi, R., Mazzitelli, I., Ando, S. and Pezzi, V. (2007) Insulin-like growth factor-I, regulating aromatase expression through steroidogenic factor 1, supports estrogen-dependent tumor Leydig cell proliferation. *Cancer research*, **67**, 8368-8377.

77. Sasano, H. and Harada, N. (1998) Intratumoral aromatase in human breast, endometrial, and ovarian malignancies. *Endocrine reviews*, **19**, 593-607.
78. Straume, A.H., Lovas, K., Miletic, H., Gravdal, K., Lonning, P.E. and Knappskog, S. (2012) Elevated levels of the steroidogenic factor 1 are associated with over-expression of CYP19 in an oestrogen-producing testicular Leydig cell tumour. *European journal of endocrinology / European Federation of Endocrine Societies*, **166**, 941-949.
79. Clipsham, R. and McCabe, E.R. (2003) DAX1 and its network partners: exploring complexity in development. *Molecular genetics and metabolism*, **80**, 81-120.
80. Niakan, K.K., Davis, E.C., Clipsham, R.C., Jiang, M., Dehart, D.B., Sulik, K.K. and McCabe, E.R. (2006) Novel role for the orphan nuclear receptor Dax1 in embryogenesis, different from steroidogenesis. *Molecular genetics and metabolism*, **88**, 261-271.
81. Ikeda, Y., Swain, A., Weber, T.J., Hentges, K.E., Zanaria, E., Lalli, E., Tamai, K.T., Sassone-Corsi, P., Lovell-Badge, R., Camerino, G. *et al.* (1996) Steroidogenic factor 1 and Dax-1 colocalize in multiple cell lineages: potential links in endocrine development. *Mol Endocrinol*, **10**, 1261-1272.
82. Lalli, E., Melner, M.H., Stocco, D.M. and Sassone-Corsi, P. (1998) DAX-1 blocks steroid production at multiple levels. *Endocrinology*, **139**, 4237-4243.
83. Dowsett, M. and Dunbier, A.K. (2008) Emerging biomarkers and new understanding of traditional markers in personalized therapy for breast cancer. *Clinical cancer research : an official journal of the American Association for Cancer Research*, **14**, 8019-8026.
84. Zhang, H., Slewa, A., Janssen, E., Skaland, I., Yu, Y., Gudlaugsson, E., Feng, W., Kjellevold, K., Soiland, H. and Baak, J.P. (2011) The prognostic value of the orphan nuclear receptor DAX-1 (NROB1) in node-negative breast cancer. *Anticancer research*, **31**, 443-449.
85. Tamai, K.T., Monaco, L., Alastalo, T.P., Lalli, E., Parvinen, M. and Sassone-Corsi, P. (1996) Hormonal and developmental regulation of DAX-1 expression in Sertoli cells. *Mol Endocrinol*, **10**, 1561-1569.
86. Shan, J.D., Porvari, K., Ruokonen, M., Karhu, A., Launonen, V., Hedberg, P., Oikarinen, J. and Vihko, P. (1997) Steroid-involved transcriptional regulation of human genes encoding prostatic acid phosphatase, prostate-specific antigen, and prostate-specific glandular kallikrein. *Endocrinology*, **138**, 3764-3770.
87. Lu, S., Liu, M., Epner, D.E., Tsai, S.Y. and Tsai, M.J. (1999) Androgen regulation of the cyclin-dependent kinase inhibitor p21 gene through an androgen response element in the proximal promoter. *Mol Endocrinol*, **13**, 376-384.
88. Adler, A.J., Scheller, A., Hoffman, Y. and Robins, D.M. (1991) Multiple components of a complex androgen-dependent enhancer. *Mol Endocrinol*, **5**, 1587-1596.
89. Suzuki, T., Miki, Y., Moriya, T., Akahira, J., Ishida, T., Hirakawa, H., Yamaguchi, Y., Hayashi, S. and Sasano, H. (2007) 5Alpha-reductase type 1 and aromatase in breast carcinoma as regulators of in situ androgen production. *International journal of cancer. Journal international du cancer*, **120**, 285-291.
90. Chanplakorn, N., Chanplakorn, P., Suzuki, T., Ono, K., Wang, L., Chan, M.S., Wing, L., Yiu, C.C., Chow, L.W. and Sasano, H. (2011) Increased 5alpha-reductase type 2 expression in human breast carcinoma following aromatase

inhibitor therapy: the correlation with decreased tumor cell proliferation. *Hormones & cancer*, **2**, 73-81.

91. Li, X., Strauss, L., Kaatrasalo, A., Mayerhofer, A., Huhtaniemi, I., Santti, R., Makela, S. and Poutanen, M. (2006) Transgenic mice expressing p450 aromatase as a model for male infertility associated with chronic inflammation in the testis. *Endocrinology*, **147**, 1271-1277.
92. Coleman, G.L., Barthold, W., Osbaldiston, G.W., Foster, S.J. and Jonas, A.M. (1977) Pathological changes during aging in barrier-reared Fischer 344 male rats. *Journal of gerontology*, **32**, 258-278.
93. Jacobs, B.B. and Huseby, R.A. (1967) Neoplasms occurring in aged Fischer rats, with special reference to testicular, uterine, and thyroid tumors. *Journal of the National Cancer Institute*, **39**, 303-309.

Cell Cycle 11:14, 2699-2710; July 15, 2012; © 2012 Landes Bioscience

Chenodeoxycholic acid through a TGR5-dependent CREB signaling activation enhances cyclin D1 expression and promotes human endometrial cancer cell proliferation

Ivan Casaburi,[1,†,*] Paola Avena,[1,†] Marilena Lanzino,[1] Diego Sisci,[1] Francesca Giordano,[2] Pamela Maris,[1] Stefania Catalano,[1] Catia Morelli[1] and Sebastiano Andò[2,*]

[1]Department of Pharmaco-Biology; University of Calabria; Cosenza, Italy; [2]Department of Cellular Biology; University of Calabria; Cosenza, Italy

[†]These authors contributed equally to this work.

Keywords: bile acid, TGR5, cyclin D1, endometrial cancer, obesity

Endometrial cancer exhibits a strong incidence in western developed countries mainly due to fat-rich diet and obesity. Processing of dietary lipids is triggered by bile acids, amphipathic detergents that are synthesized in the liver and stored in the gallbladder. In addition to their well-recognized role in dietary lipid absorption and cholesterol homeostasis, bile acids can also act as signaling molecules with systemic endocrine functions.

In the present study we investigated the biological effects of the primary bile chenodeoxycholic acid (CDCA) on a human endometrial cancer cell line, Ishikawa. Low concentrations of CDCA are able to stimulate Ishikawa cell growth by inducing a significant increase in cyclin D1 protein and mRNA expression through the activation of the membrane G protein-coupled receptor (TGR5)-dependent pathway. Dissecting the molecular mechanism underlying this effect by mutagenesis, EMSA and ChIP analysis revealed that CDCA-induced cyclin D1 expression requires the enhanced recruitment of the transcription factor CREB on the cyclic AMP-responsive element motif within the *cyclin D1* gene proximal promoter.

Our results suggest a novel molecular mechanism explaining the potential contribution of high-fat diet and obesity to endometrial cancer growth and progression opening the rationale for strategies to prevent the risk of this obesity-related cancer in women.

Introduction

Endometrial cancer incidence rate is higher in western industrialized than in developing countries.[1] The most relevant environmental risk factors include fat-rich diet, excess of body weight and physical inactivity.[2] Fat exerts its effect by stimulating the synthesis and secretion of bile acids (BAs), amphipathic detergents that are synthesized from cholesterol and actively secreted into bile by the liver and stored in the gallbladder.[3] Despite the efficient enterohepatic recirculation of bile acids, a small amount can spill over into the systemic circulation.[4-6] Bile acids' physiological and pathophysiological effects have been well established in liver and intestine, where they play an essential role in dietary lipid absorption and cholesterol homeostasis. Conversely, BAs effects on tissues outside of the enterohepatic circulation still need to be clarified. Recent studies indicate that bile acids are able to affect intracellular signaling and gene expression, which, in turn, may have an effect on cell growth and tumor development.[7]

Indeed, BAs can act as signaling molecules through the activation of specific receptors controlling different systemic endocrine functions. Specifically, BAs have been recognized as ligands for the nuclear farnesoid X receptor (FXR) and pregnane X receptor,[8-10] through which BAs regulate the transcription of many genes involved in the enterohepatic recycling and feedback regulation of bile acid biosynthesis as well as in the control of the lipid and carbohydrate metabolism. More recently, in addition to their genomic action, BAs have also been shown to be able to induce rapid non-genomic signaling pathways through the activation of a novel plasma membrane G protein-coupled receptor, TGR5, also known as M-BAR or BG37.[11,12] TGR5 is ubiquitously expressed in various human tissues, such as heart, spleen, skeletal muscle, kidney, liver, small intestine, placenta, lung, mammary gland, prostate, testis as well as uterus.[11] Bile acids, including taurine-conjugated lithocholic acid (TLCA), lithocholic acid (LCA), deoxycholic acid (DCA), chenodeoxycholic acid (CDCA) and cholic acid (CA), are natural endogenous ligands for this G-protein coupled receptor, able to activate

*Correspondence to: Ivan Casaburi and Sebastiano Andò; Email: icasaburi@yahoo.it and sebastiano.ando@unical.it
Submitted: 05/04/12; Revised: 06/05/12; Accepted: 06/06/12
http://dx.doi.org/10.4161/cc.21029

Table 1. Distribution of Ishikawa cells in the various phases of cell cycle

	G_0/G_1	G_2/M	S-Phase
untreated	52.0 ± 1.7	19.6 ± 1.2	27.6 ± 1.2
CDCA 5 μM	29.3 ± 2	20.6 ± 1.2	49.6 ± 2.1*
CDCA 100 μM	69.0 ± 2*	14.0 ± 1.1	17.0 ± 1*

*p ≤ 0.01 compared with untreated cells.

it with the following order of potency: TLCA (0.33 μM) > LCA (0.53 μM) > DCA (1.01 μM) > CDCA (4.43 μM) > CA (7.72 μM). TGR5 activation is followed by various cellular responses, including receptor internalization, extracellular signal-regulated kinase activation and intracellular cAMP production.[12]

To date, the role of bile acid on endometrial cancer growth has not been evaluated yet. The current study has been designed to investigate the biological effects of the primary bile acid chenodeoxycholic on the human endometrial cancer cell line, Ishikawa.

Here we demonstrate how low doses of CDCA, through the activation of the G-coupled membrane receptor, TGR5, promote Ishikawa cell proliferation through a complex molecular mechanism involving the activation of ERK signaling responsible for an enhanced recruitment of CREB onto the *cyclin D1* gene promoter. This cascade of events leads to an increased expression of cyclin D1, which is responsible for the induction of endometrial cancer cell growth. Our results reveal a new molecular mechanism explaining how obesity may contribute to the pathogenesis of endometrial cancer.

Indeed, our proposed model could represent at least one of the mechanisms through which bile acids in pathophysiological conditions, such as obesity, may exert positive effects on the growth of extrahepatic tissues and specifically on endometrial cells.

Results

Effects of CDCA on endometrial cancer cell growth. Opposite biological effects by bile acids, such as induction of proliferation or apoptosis, have been reported by several authors in different experimental conditions.[13,14]

To better understand this issue, we examined the effect of increasing doses of the primary bile acid chenodeoxicholyc (CDCA) on endometrial carcinoma cell growth by thymidine incorporation assay. As shown in **Figure 1A**, CDCA exerted divergent effects depending on its concentration. Indeed, low doses (2.5 and 5 μM) of CDCA strongly stimulated Ishikawa cell proliferation, while, by contrast, the higher CDCA dose (100 μM) markedly suppressed cell growth. These data correlated well with cell cycle analysis showing a decrease of the percentage of cells in the G_0/G_1-phase (**Table 1**) and a concurrent increase in the S-phase (**Fig. 1B**) following 72 h of 5 μM CDCA treatment. On the contrary, 100 μM CDCA treatment inhibited cell cycle progression as pointed out by the significant decrease of cell population in S-phase (**Table 1 and Fig. 1B**).

Since cyclin D1 is a critical modulator of the cell cycle G_1/S transition, and its overexpression is a hallmark of human endometrial cancers,[15-17] we aimed to evaluate the potential ability of CDCA to modulate cyclin D1 expression in Ishikawa human endometrial cancer cells. In the same vein, cellular levels of $p21^{WAF1/Cip1}$, the major cyclin-dependent-kinase inhibitor, were also analyzed. As shown in **Figure 1**, cyclin D1 mRNA (**Fig. 1C and D**) and protein content (**Fig. 1D and F**) were significantly increased by low doses (2.5 or 5 μM) of CDCA administration. In contrast, elevated concentrations of CDCA induced a dose-dependent downregulation of cyclin D1 expression concomitantly with an increase of $p21^{WAF1/Cip1}$ mRNA (**Fig. 1C and D**) and protein levels (**Fig. 1E and F**). The latter result appears to rely on a p53-independent pathway, since the expression of the tumor suppressor p53 was unaffected by CDCA exposure (**Fig. 1C–F**). These findings indicate that CDCA exerts a biphasic effect on Ishikawa cell proliferation as well as on cell cycle-regulating proteins, depending on its concentration.

CDCA effects are specifically mediated by TGR5 receptor. BAs are signaling molecules that can activate BA receptors to initiate signaling pathways and regulate gene expression. Two major receptors for BAs have been identified, namely the nuclear receptor FXR[10] and the G protein-coupled receptor TGR5.[11,12] To identify effects of the receptor involved in the above-described CDCA on endometrial cell proliferation, Thymidine incorporation assay was performed in Ishikawa cells, exposed to 5 or 100 μM CDCA, in which the expression of either TGR5 or FXR receptors was silenced by siRNA technology. As shown in **Figure 2A**, mRNA levels of both receptors were effectively knocked-down following 48 h of silencing. The effects of low doses of CDCA were specifically mediated by TGR5, since they were abrogated by silencing *TGR5* gene expression but not in the presence of siRNA for *FXR*. Notably, the effect of high doses of CDCA was unaffected by knocking-down both receptors accounting for a general cytotoxic and/or apoptotic effect (**Fig. 2B**).

CDCA modulates cyclin D1 expression through TGR5 receptor activation. Since GPCRs signal transduction involves the activation of extracellular signal-regulated kinase (ERK),[18] we examined whether CDCA might promote 42/44 ERK activation. To this aim, serum-starved Ishikawa cells were left untreated or treated with 5 μM CDCA. As shown in **Figure 3A**, CDCA significantly induced a rapid 42/44 ERK phosphorylation, while no changes were observed on the levels of total ERK.

To verify the involvement of TGR5 in CDCA-dependent activation of ERK signaling, we knocked down *TGR5* gene by siRNA technology in Ishikawa cells. *TGR5* gene silencing significantly affected CDCA-dependent 42/44 ERK activation/phosphorylation, since in this experimental condition, it was not any more detectable following treatment with 5 μM CDCA (**Fig. 3B**). Interestingly, the involvement of the TGR5/ERK pathway in CDCA-dependent effects is further evidenced by the disappearance of the positive modulation of cyclin D1 expression observed in TGR5 knocked-down Ishikawa cells following administration of 5 μM CDCA (**Fig. 3C**). The same inhibitory effect was reproduced upon treatment with PD 98059, a specific chemical inhibitor of ERK signaling (**Fig. 3D**), indicating that TGR5 may mediate CDCA-induced increase of cyclin D1 expression by rapid activation of ERK signaling.

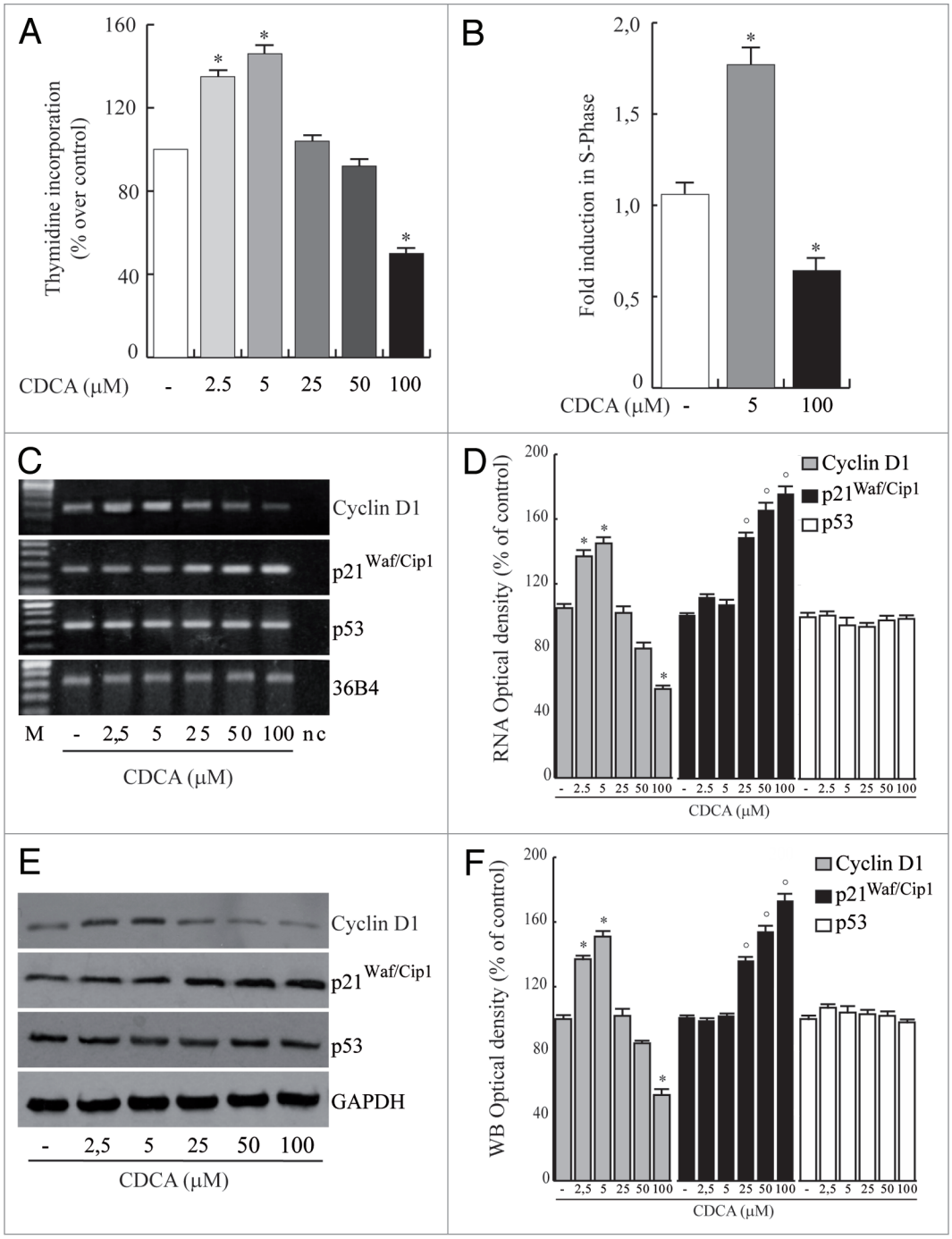

Figure 1. Divergent effects of CDCA treatment on Ishikawa cells. (A) Cell proliferation was determined by [^{3}H]thymidine incorporation assay after 72 h of treatment with different concentrations of CDCA as indicated in the figure. 5 x 10^4/well Ishikawa cells were seeded on 12-well plates, cultured as described in Materials and Methods and left untreated (-) or treated with CDCA as indicated. Results represent the mean ± SE of three independent experiments each performed in triplicate. *p ≤ 0.01 compared with untreated cells (-). (B) Synchronized Ishikawa cells were left untreated (-) or exposed to 5 μM or 100 μM CDCA for 72 h. Cell cycle distribution was determined as described in Materials and Methods. The results indicate the fold increase of Ishikawa cells in S-phase after CDCA treatments. (C and D) Total RNA from Ishikawa cells left untreated (-) or treated with CDCA as indicated for 24 h was reverse transcribed and subjected to PCR using specific primers for cyclin D1, $p21^{WAF1/Cip1}$, p53; 36B4 mRNA levels were determined as loading control; nc: negative control. (E and F) Protein extracts from Ishikawa cells left untreated (-) or treated with CDCA, as indicated, for 24 h were resolved by SDS-PAGE and subjected to immunoblot analysis using specific antibody against human cyclin D1, $p21^{WAF1/Cip1}$ and p53. GAPDH served as loading control. Histograms in (D and F) represent the mean ± SE of band intensities evaluated as optical density arbitrary units and expressed as the percentage of the control assumed as 100%, *.°p ≤ 0.01 compared with untreated cells.

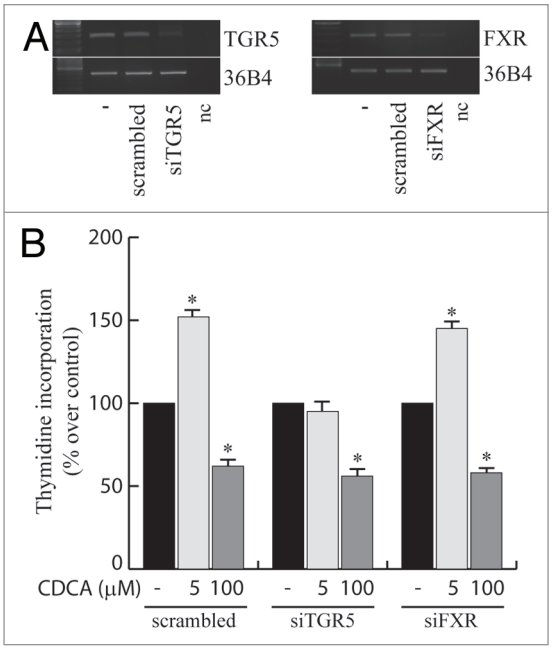

Figure 2. CDCA-effects on Ishikawa cell proliferation depend on TGR5 receptor. (A) RT-PCR analysis was performed in Ishikawa cells to evaluate the expression of TGR5 or FXR mRNA in the absence (-) or presence of control siRNA (scrambled) or siRNAs specific for TGR5 or FXR, respectively. nc, negative control. 36B4 mRNA was used as internal control. (B) [^{3}H]thymidine incorporation assay was performed on Ishikawa cells transfected with specific siRNA for TGR5, or FXR or control siRNA for 48 h, as indicated in Materials and Methods, and then left untreated (-) or treated with CDCA as indicated for 72 h. Data represent the mean ± SE of three separate experiments each in triplicate. *p ≤ 0.01 compared with untreated cells.

Characterization of functional CDCA responsive region(s) within the cyclin D1 gene promoter. The aforementioned observations prompted us to evaluate whether CDCA signaling could affect the transcriptional activity of the *cyclin D1* gene promoter. To this aim, Ishikawa cells were transiently transfected with a luciferase reporter construct containing the upstream region of the *cyclin D1* gene spanning from -2.966 to +142 bp. **Figure 4A** showed a significant increase of the *cyclin D1* gene promoter transcriptional activity following exposure to 5 μM CDCA for 24 h.

To delimit the cis element involved in cyclin D1 transcriptional activation by CDCA, a series of 5'-promoter-deleted mutants were used in transient transfection experiments. All the tested constructs, pCD1Δ-944, pCD1Δ-848, pCD1Δ-136 and pCD1Δ-96, which include, 0.944 kb, 0.848 kb, 0.136 kb and 0.096 kb of the cyclin D1 promoter fragments, respectively, showed an increased transcriptional activity upon CDCA administration with respect to untreated cells (**Fig. 4A**). These results suggest that CDCA-dependent transactivation of the *cyclin D1* promoter requires the region spanning from -96 to +142 bp that contains, at position -52 bp, a CRE binding motif, a well-known downstream target of ERK signaling. Indeed, mutation of CRE site (**Fig. 4B**, left panel) completely abolished the CDCA induced promoter (**Fig. 4B**, right panel) responsiveness, demonstrating its involvement in the modulation of cyclin D1 expression.

CDCA administration increases CREB-DNA binding activity to cyclin D1 promoter. To further investigate the specific role of CRE motif in the transcriptional activation of *cyclin D1* by CDCA, we performed EMSA experiments.

Using synthetic oligodeoxyribonucleotides corresponding to CRE motif, we observed the formation of a complex in nuclear extracts from Ishikawa cells (**Fig. 5A**, lane 1), which was abrogated by 100-fold molar excess of unlabeled probe (**Fig. 5A**, lane 2) as well as by the use of a mutated probe (**Fig. 5**, lane 3), demonstrating the specificity of the DNA-binding complex. CDCA administration induced an increase in the DNA binding activity compared with untreated sample (**Fig. 5A**, lane 4). Incubation of nuclear extracts with a specific anti-CREB antibody determined the appearance of a super-shifted band (**Fig. 5A,** lane 5). Finally, using transcribed and translated in vitro CREB protein, a complex migrating at the same level as that of Ishikawa nuclear extracts was obtained (**Fig. 5A**, lane 6).

To better determine the physiological relevance of the CRE site in the modulation of cyclin D1 promoter upon CDCA exposure, we investigated whether CREB interacts with *cyclin D1* gene promoter as it exists in native chromatin, performing chromatin immunoprecipitation (ChIP) assay. Using a specific anti-CREB antibody, CREB occupancy of the CRE containing region of *cyclin D1* promoter was induced in a CDCA-dependent manner (**Fig. 5B and C**). The enhanced recruitment of CREB was concomitant with an increased association of Polymerase II (Pol II) to the same cyclin D1 regulatory region, consistent with the previously demonstrated enhancement of cyclin D1 promoter activity (**Fig. 5B and C**). Our results suggest that the molecular mechanism leading to CDCA-mediated cyclin D1 upregulation in Ishikawa cells may involve the recruitment of CREB transcription factor on its responsive region within the cyclin D1 promoter.

CREB siRNA prevents CDCA-induced cyclin D1 expression and cell proliferation. In order to define more clearly the contribution of CREB in CDCA-induced cyclin D1 expression and cellular proliferation, we knocked-down CREB cellular levels by siRNA technology. CREB protein expression was effectively silenced as revealed by western blotting after 48 h of siRNA transfection (**Fig. 5D**). CREB gene silencing significantly abrogated the upregulation of cyclin D1 levels induced by CDCA administration, while no changes were observed after transfection of cells with scrambled siRNA upon identical experimental conditions (**Fig. 5D**). We, thus, determined the effect of CREB siRNA on growth stimulation induced by CDCA by measuring changes in the rate of DNA synthesis. The growth stimulatory effect of 5 μM CDCA was severely affected following CREB silencing (**Fig. 5E**). These results confirm the involvement of CREB in CDCA mediated upregulation of cyclin D1 and its biological significance for Ishikawa cell proliferation.

CDCA effects on Ishikawa anchorage-independent cell growth. Since the described CDCA effects are mediated by the activation of ERK, a downstream effector mostly involved in

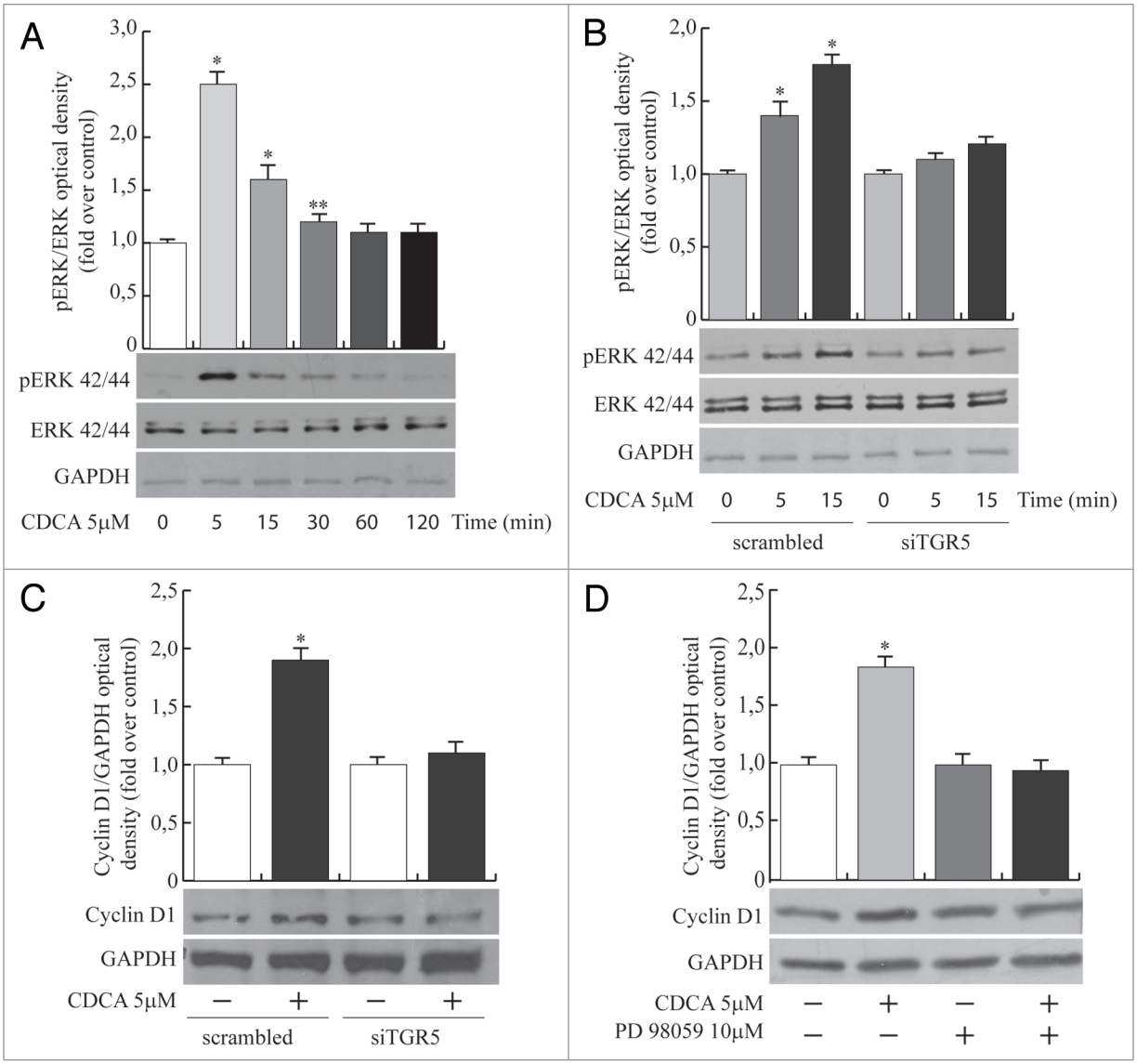

Figure 3. TGR5/ERK signaling is required for CDCA-dependent modulation of cyclin D1 expression. (A) Serum-starved Ishikawa cells were treated with 5 μM CDCA for various time intervals as indicated. Protein extracts were resolved by SDS-PAGE and subjected to immunoblot analysis with specific antibodies against phosphorylated (p), and total 42/44 ERK. GAPDH was used as a protein loading control. Upper histograms summarize densitometric analyses of results from three separate experiments, expressed as fold change (means ± SE) of phosphorylated ERK/total ERK ratio respect to untreated cells (time 0). Data were normalized to GAPDH content. *p ≤ 0.01, **p ≤ 0.05 compared with untreated cells. (B) Ishikawa cells were transfected with control siRNA (scrambled), or TGR-5 siRNA and treated with 5 μM CDCA for various time intervals as indicated. Total proteins were extracted and imunoblotting analysis was performed to evaluate the expression of phosphorylated, total 42/44 ERK and GAPDH as a protein loading control. Upper histograms represent the mean ± SE as described in (A). *p ≤ 0.01, compared with scrambled untreated cells. (C) Ishikawa cells were transfected with control siRNA (scrambled), or TGR-5 siRNA and then left untreated (-) or treated with 5 μM CDCA for 24 h. Total proteins were extracted and immunoblotting analysis was performed to evaluate the expression of cyclin D1. Filters were stripped and reprobed with antibody against GAPDH as loading control. Upper histograms represent the mean ± SE of band intensities from three separate experiments, evaluated as optical density arbitrary units and expressed as fold induction over control (-). *p ≤ 0.01 compared with untreated cells.

growth factors signaling, we investigated whether this primary bile acid could cooperate in promoting Ishikawa cell growth in the presence of EGF, the main growth factor sustaining endometrial cancer growth,[19] and IGF-1, whose levels are positively correlated with obesity.[20] As shown in **Figure 6**, anchorage-independent growth assays demonstrated that low doses of CDCA as well as administration of EGF or IGF induced a significant increase in the number of colonies formation in soft agar. Interestingly, combined treatment of low doses of CDCA (5 μM) with EGF (20 ng/ml) or IGF-1 (50 ng/ml) elicited an additive effect with respect to that observed in the presence of the two mitogens alone. These data reasonably address how, in pathophysiologic circumstances in which growth factor signaling systems are dysregulated, as in obese women, a small amount of bile acid may contribute to potentiate growth factor stimulatory effects on endometrial tumor growth.

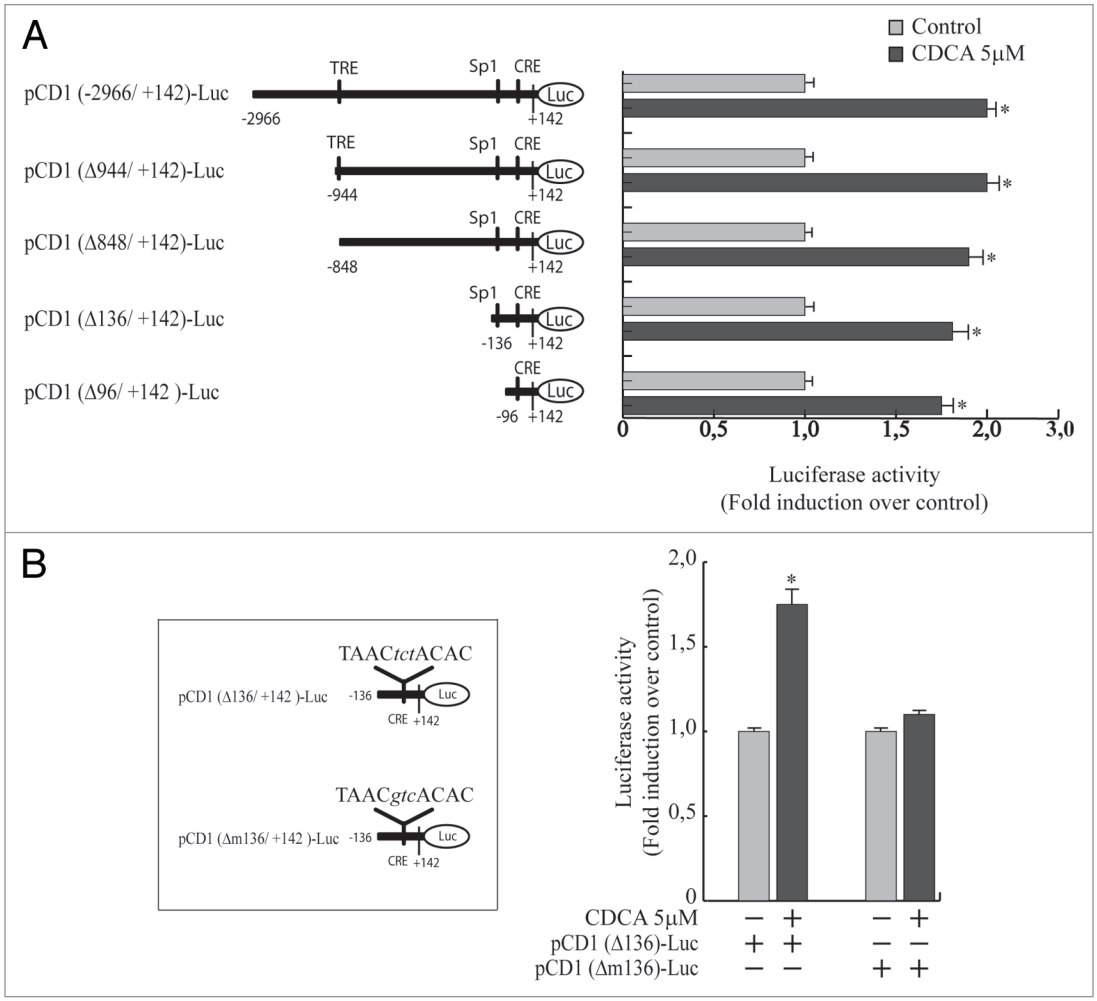

Figure 4. CDCA-dependent cyclin D1 gene promoter transactivation involves a CRE motif. (A, left panel) Schematic representation of human cyclin D1 promoter fragments used in this study: all the promoter constructs contain the same 3′ boundary (+142); the 5′ boundaries of the promoter fragments varied from -2,966 to -96. (A, right panel) Ishikawa cells were transfected, as described in Materials and Methods, with a cyclin D1 full-length promoter plasmid or with different deleted constructs as indicated. Cells were then left untreated (Control) or treated with 5 μM CDCA for 24 h. (B, left panel) Schematic representation of the mutated pCD1Δ136 construct obtained by site directed mutagenesis as described in Materials and Methods. (C, right panel) Ishikawa cells were transfected, as described in Materials and Methods, with pCD1Δ136 plasmid or the corresponding mutated construct and left untreated (-) or treated with 5 μM CDCA for 24 h. Values represent the mean ± SE of three separate experiments each performed in triplicate. *p ≤ 0.01 compared with untreated cells.

Discussion

Endometrial cancer is the most common gynecological malignant disorder in more developed countries. Its incidence is ten times higher in North America and Europe than in less developed countries, where risk factors are less common and endometrial cancer is rare.[1,2] The most significant risk factors for endometrial cancer include "unopposed estrogen," a sedentary lifestyle and obesity.[21] Specifically, increasing epidemiologic data indicate being overweight and obesity as important risk factors for type-I endometrial cancer, which is the most common malignancy in women and accounts for 80% of all endometrial tumors.[21,22]

Many causative and correlative links between obesity and cancer have been proposed.[23] At present, the strongest support for mechanisms linking obesity and cancer risk involves the metabolic and endocrine effects of obesity, which lead to an altered production of peptide and steroid hormones.[21] Fat may exert its effects by stimulation of bile acids synthesis and secretion. In addition to their classic function facilitating hepatobiliary secretion of endogenous metabolites and xenobiotics and intestine absorption of lipophilic nutrients, bile acids also have been recognized as signaling molecules with diverse endocrine and paracrine functions, including regulation of their own synthesis and lipids biogenesis in the enterohepatic system as well as glucose metabolism and energy expenditure in peripheral tissues.[24,25]

Our results show that CDCA exerts opposite proliferative effects depending on its own concentration. Specifically, high doses of the primary bile acid CDCA, up to 100 μM, induce cell death, whereas low doses of CDCA stimulate cell proliferation in Ishikawa endometrial tumor cells that represent an experimental model for type-I endometrial cancer.[26]

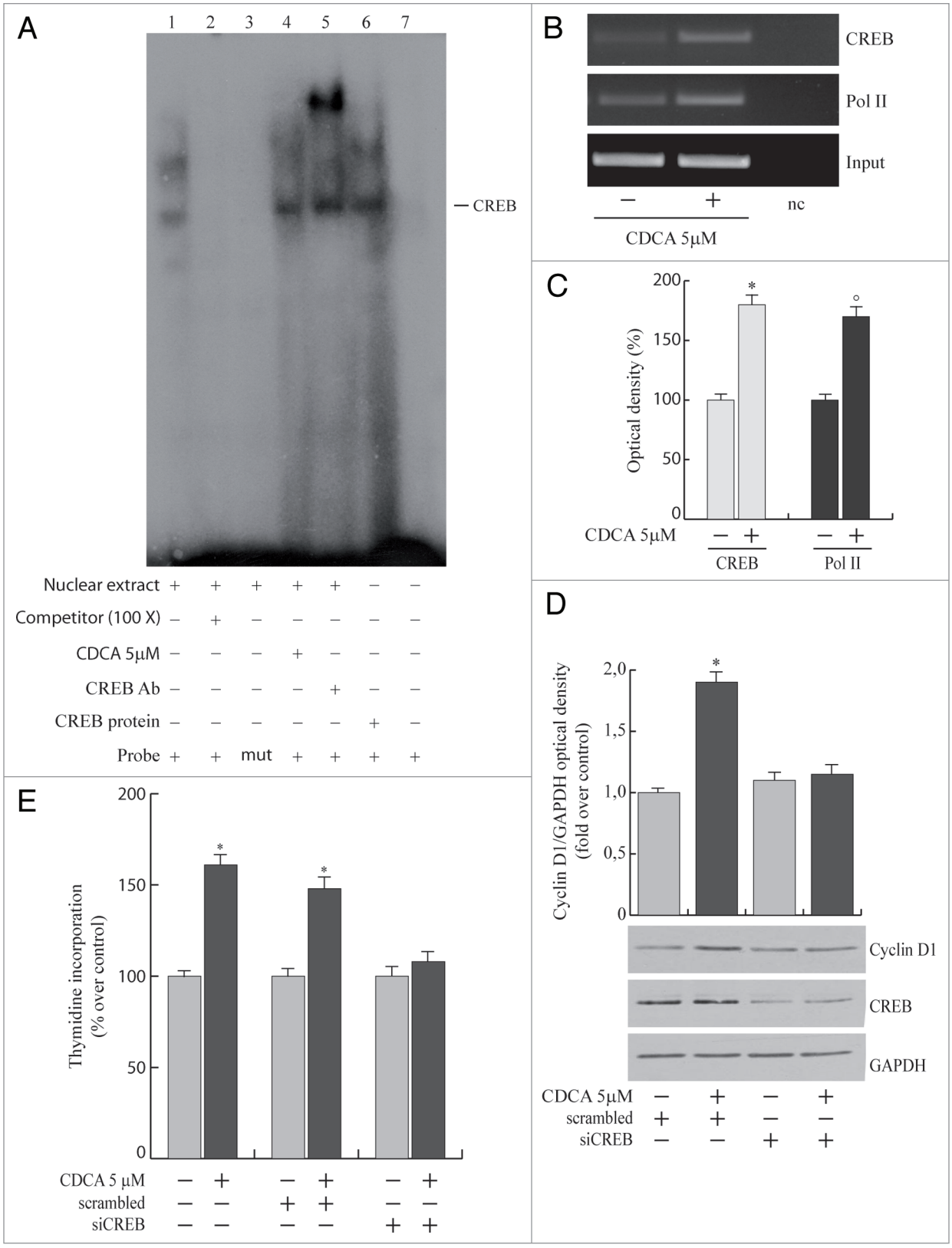

Figure 5. For figure legend, see page 2706.

Figure 5 (See previous page). CDCA-dependent effects in Ishikawa cells require the involvement of the transcription factor CREB. (A) Nuclear extracts from Ishikawa cells were incubated with a CREB-specific consensus sequence probe labeled with [λ^{32}P] ATP and subjected to electrophoresis in a 6% polyacrylamide gel (lane 1); competition experiments were done by adding as competitor a 100-fold molar excess of unlabeled probe (lane 2) or with a 100-fold molar excess of labeled mutated (mut) CRE oligonucleotide (lane 3); Ishikawa nuclear extracts treated with 5 μM CDCA for 2 h and incubated with probe (lane 4); the specificity of the binding was tested by adding to the reaction mixture a CREB antibody (lane 5). We used as positive control a transcribed and translated in vitro CREB protein (lane 6). Probe alone (lane 7). (B) Serum-starved Ishikawa cells were left untreated (-) or treated with 5 μM CDCA for 2 h. The preacleared chromatin was immunoprecipitated with specific antibody anti-CREB, anti-polymerase II (Pol II) antibody and with a normal mouse serum IgG as negative control (nc). Cyclin D1 promoter sequence containing CRE site was detected by PCR using specific primers. DNA inputs were obtained by amplifying 30 μl of purified soluble chromatin prior immunoprecipitation. (C) Histograms represent the mean ± SE of band intensities from three separate ChIP experiments, evaluated as optical density arbitrary unit and expressed as percentages of the control assumed as 100%. *,°p ≤ 0.01 compared with untreated cells (-). (D) Ishikawa cells were transfected with control siRNA (scrambled) or siRNA for CREB, and left untreated (-) or treated with 5 μM CDCA for 24 h. Total proteins were extracted and immunoblotting analysis was performed to evaluate the expression of cyclin D1 and CREB proteins. GAPDH was used as a loading control on the same stripped blot. The upper histograms represent the mean ± SE of band intensities from three separate experiments, evaluated as optical density arbitrary unit and expressed as fold induction over control (-). *p ≤ 0.01 compared with untreated cells. (E) Ishikawa cells were transfected with control siRNA (scrambled) or siRNA for CREB, and left untreated (-) or treated with 5 μM CDCA for 72 h. Thymidine incorporation assay was performed as described in Materials and Methods. Data represent the mean ± SE of three separate experiments each in triplicate. *p ≤ 0.01 compared with untreated cells.

The proliferative effect operated by low doses of CDCA in our experimental cell system is biologically relevant on the basis of the observations that the same order of serum bile acids concentration has been found in either overweight or obese subjects with respect to normal weight subjects. For instance, in obesity, an increased production of precursors of cholesterol and bile acids synthesis could reflect an abnormal liver function[27] sustaining bile acids spillover into the systemic circulation.

It is now clear that, in addition to their important roles in nutritional absorption, bile acids are signaling molecules that can activate BA receptors to initiate signaling pathways and regulate gene expression. Two major receptors for BAs have been identified, the nuclear receptor FXR[10] and the G protein-coupled receptor TGR5.[11,12] Our results indicate that the stimulatory effect of low doses of CDCA on Ishikawa cell proliferation is specifically mediated by TGR5, since it is abrogated by silencing TGR5 gene expression but not influenced by FXR knockout. Instead, the effect on Ishikawa cell proliferation of high doses of CDCA is unaffected by silencing both receptors accounting for a general cytotoxic and/or apoptotic effect.

CDCA effects on Ishikawa cell proliferation are consistent with cell cycle analysis showing a decrease of the percentage of cells in the G_0/G_1-phase and a concurrent increase in the S-phase, following low doses of CDCA long-term exposure.

The cell cycle is strictly regulated by the coordinate action of cyclin-dependent kinases (cdk), specific cyclin proteins and cdk inhibitors. Alterations of the mechanisms controlling cell cycle progression play a relevant role in the pathogenesis of different human neoplasia. Among the molecules involved in cell cycle regulation, cyclin D1 abnormalities may contribute to such malignant transformation.[17,28-30] Altered expression of cyclin D1 may result from rearrangement,[31] translocation,[32] amplification and/or overexpression in different types of cancer.[33,34] In endometrial glands, cyclin D1 overexpression has been reported to be progressively increased in intensity and extent from normal endometrium to complex hyperplasia and carcinoma.[35]

Of interest, we found that exposure to low doses of CDCA upregulates cyclin D1 mRNA and protein levels. By contrast, elevated concentrations of CDCA induced a downregulation of cyclin D1 expression in a dose dependent-manner concomitantly with an increase of $p21^{WAF1/Cip1}$ expression without affecting the tumor suppressor p53 expression levels. Moreover, CDCA upregulation of cyclin D1 expression requires the activation of the ERK signaling through the involvement of the G-protein-coupled receptor TGR5 as it emerges by the observation that silencing of *TGR5* gene abrogated both CDCA-induced ERK phosphorylation and cyclin D1 expression.

The observed effect of CDCA on Ishikawa cell proliferation and cyclin D1 expression rely on a membrane TGR5-mediated signaling cascade eliciting genomic effects. Indeed, CDCA administration induces the transcriptional activity of the full-length *cyclin D1* gene promoter. We documented that the region spanning from -96 to +142, fwhich contains a CRE site, is required for the responsiveness to CDCA, as demonstrated by site-directed mutagenesis analysis of the CRE site showing that this motif is a crucial mediator of *cyclin D1* regulation by CDCA. Our observation leads us to previous findings evidencing how *cyclin D1* is transcriptionally regulated by CRE in endometrial cancer cells.[36]

The specific role of CREB is revealed by EMSA and ChIP experiments showing the ability of CDCA to enhance the recruitment of CREB to the CRE-containing region within the *cyclin D1* promoter. The relative contribution of this transcription factor also emerges from our data showing that silencing of *CREB* gene expression is able to reverse the upregulatory effect of CDCA on cyclin D1 expression and growth in Ishikawa cells.

Finally, the biological significance of CDCA effect on Ishikawa cell growth rises from its ability to potentiate the anchorage-independent cell growth sustained by growth factors, which represent a hallmark of cell transformation and closely resembles the cancer cell phenotypic behavior in vivo. For instance, this assumes a particular relevance in the circumstance, wherein growth factor signaling systems are deregulated and bile acid synthesis and secretion are enhanced as it occurs in obese women.[3,27]

In conclusion, our results, as schematically illustrated in **Figure 7**, evidence for the first time how low doses of CDCA are able to induce a rapid non-genomic signaling through the activation of the G-protein-coupled receptor, TGR5, that in turn activates ERK signaling allowing the transcription factor CREB

to upregulate *cyclin D1* gene expression and endometrial cancer cell growth.

These results indicate a new mechanism by which high-fat diet and obesity could potentially contribute to endometrial cancer risk and clarify the molecular basis underlying the role of bile acid-dependent signaling in tumor growth and progression. Our observation may open new avenues for a number of rational strategies to prevent the hormonal and metabolic imbalances associated with obesity-related cancer.

Materials and Methods

Materials. Modified Eagle's medium (MEM), L-glutamine, Eagle's non-essential amino acids, penicillin, streptomycin, fetal bovine serum (FBS), bovine serum albumin (BSA), phosphate-buffered saline, RNase A were purchased by Sigma. TRIzol and Lipofectamine 2000 reagent by Invitrogen, FuGENE 6 by Roche Applied Science. TaqDNA polymerase, RETROscript kit, 100-bp DNA ladder, Dual Luciferase kit and TK Renilla luciferase plasmid were provided by Promega. Aprotinin, leupeptin, phenylmethylsulfonyl fluoride (PMSF), sodium orthovanadate and CDCA were purchased by Sigma. Antibodies against phosphor-p44/42 MAPK (Thr202/Tyr204) (9101S), 44/42 MAPKinase (9102S) and CREB (48H2), were provided by Cell Signaling. Antibodies against cyclin D1 (M-20), GAPDH (FL-335), $p21^{WAF1/Cip1}$ (H164), p53 (DO-1) and polymerase II (N20) by Santa Cruz Biotechnology. ECL system and Sephadex G-50 spin columns were purchased from Amersham Biosciences. [^{32}P] ATP and [^{3}H]thymidine from PerkinElmer Life Sciences PD 98,059.

Cell culture. Ishikawa human endometrial cancer cells were obtained from D. Picard (University of Geneva). Ishikawa cells were maintained in MEM without phenol red supplemented with 10% fetal bovine serum, 1% L-glutamine, 1% penicillin/streptomycin and 1% non-essential amino acids. Before each experiment cells were switched to serum free medium or medium additioned with 5% charcoal-stripped FBS for 24 h.

Plasmids. Plasmids containing the human cyclin D1 promoter or its deletions (p -2966/þ142, p -944/þ142, p -848/þ142, p -136/þ142, p -096/þ142) were kindly provided by Prof A. Weisz (University of Naples). These fragments were inserted into the luciferase vector pXP2.

Site-directed mutagenesis. The cyclin D1 promoter plasmids bearing cyclic AMP-responsive element (CRE) mutated site (pCRE mut) were created by site-directed mutagenesis using QuickChange kit (Stratagene). Briefly, this was based on a PCR reaction with two complementary oligonucleotide primers containing the mutation. The PCR was performed with the Pfu DNA polymerase during 16 cycles (30 sec at 95°C, 30 sec at 55°C and 8 min at 68°C), using as template the human cyclin D1 promoter pCD1Δ136/þ142, and the following mutagenic primer mutations are shown as lowercase letters:

5'-GAT CTT TGC TTA ACA ACA GTA ACc tcA CAC GGA CTA CAG GGG AG-3' and

5'-CTC CCC TGT AGT CCG TGT aga GTT ACT GTT GTT AAG CAA AGA TC-3' (pCD1Δm136/þ142).

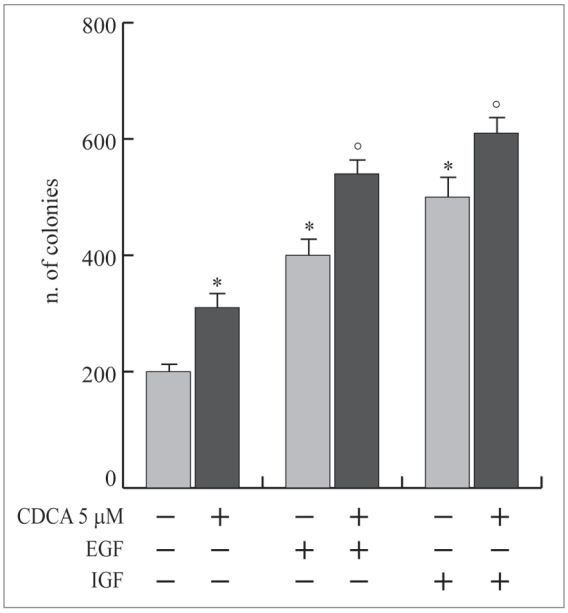

Figure 6. Additive effects of CDCA on anchorage-independent Ishikawa cell growth sustained by growth factors. Anchorage-independent growth was performed as described in Materials and Methods. Ishikawa cells were seeded (5,000 cells/well) in six-well plates in 0.5% agarose and left untreated (-) or treated with CDCA (5 μM), EGF (20 ng/ml) and IGF-1 (50 ng/ml) or with combined treatments, as indicated. Cells were allowed to grow for 14 d, and then the number of colonies > 50 μm were quantified and the results graphed. Results represent the mean ± SE of three different experiments each in triplicate. *p ≤ 0.01 CDCA (or EGF, or IGF-1) treated compared with untreated cells. °p ≤ 0.01 CDCA + EGF (or IGF-1) treated vs. EGF (or IGF-1) alone.

The PCR products were then incubated with DpnI, which only digests the parental methylated cDNA and the constructed mutated expression vectors were confirmed by DNA sequencing.

DNA flow cytometry. Ishikawa cells were harvested, fixed and stained with Propidium iodide (100 μg/ml) after treatment with RNase A (20 μg/ml). Stained cells were analyzed for DNA content by Flow Cytometry using FAC-Scan (Becton Dickingson and Co.).

Total RNA extraction and reverse transcription-PCR assay. Total cellular RNA was extracted from Ishikawa cells using Triazol reagent as suggested by the manufacturer. Evaluation of genes expression was performed by the reverse transcription-PCR method using a RETROscript kit as suggested by the manufacturer.

The cDNAs obtained were amplified by PCR using the following primers: cyclin D1 forward 5'-TCT AAG ATG AAG GAG ACC ATC-3' and reverse 5'-GCG GTA GTA GGA CAG GAA GTT GTT-3'; $p21^{WAF1/Cip1}$ forward 5'-GCT TCA TGC CAG CTA CTT CC-3' and reverse 5'-CTG TGC TCA CTT CAG GGT CA-3'; p53 forward 5'-GTG GAA GGA AAT TTG CGT GT-3' and reverse 5'-CCA GTG TGA TGA TGG TGA GG-3'; 36B4 forward 5'-CTC AAC ATC TCC CCC TTC TC-3' and reverse 5'-CAA ATC CCA TAT CCT CGT CC-3'; human TGR5 forward 5'-TCG TCT ACT TGG CTC CCA ACT TCT-3' and reverse 5'-AGC CCA TAG ACT TCG AGG

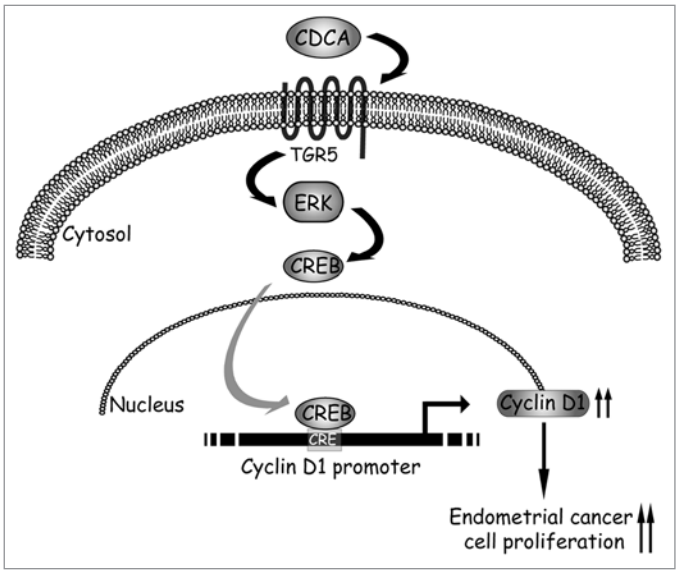

Figure 7. Proposed model for CDCA-mediated upregulation of *cyclin D1* gene in endometrial cancer cells. Low doses of CDCA activates TGR5 receptor inducing rapid non-genomic effects through the stimulation of ERK pathway. The latter, in turn, enables CREB transcription factor to be recruited to the CRE site within the proximal *cyclin D1* promoter, increasing its transcription.

TAC AGG T-3'; human FXR forward 5'-GCA GCC TGA AGA GTG GTA CTC TC-3' and reverse 5'-CAT TCA GCC AAC ATT CCC ATC TC-3' The PCR was performed for 30 cycles for cyclin D1 (94°C for 1 min, 60°C for 1 min and 72°C for 2 min), 30 cycles for p21 (94°C for 1 min, 58°C for 1 min and 72°C for 2 min), 28 cycles for p53 (95°C for 1 min, 56°C for 1 min and 72°C for 2 min), 32 cycles for TGR-5 (95°C for 1 min, 68°C for 1 min and 72°C for 2 min), 35 cycles for FXR (94°C for 30 s, 57°C for 30s, 72°C for 30 s) and 15 cycles (94°C for 1 min, 58°C for 1 min and 72°C for 2 min) to amplify 36B4 in the presence of 1 μl of first strand cDNA, 1 μM each of the primers mentioned above, 0.5 mM dNTP, Taq DNA polymerase (2 units/tube) and 2.2 mM magnesium chloride in a final volume of 25 μl. To check for the presence of DNA contamination, a reverse transcription-PCR was performed on 1 μg of total RNA without Moloney murineleukemia virus reverse transcriptase (the negative control). DNA quantity in each lane was analyzed by scanning densitometry.

Immunoblotting analysis. Ishikawa cells were grown in 10 cm dishes to 50–60% confluence and lysed in 500 μl of 50 mM Tris-HCl, 150 mM NaCl, 1% NP-40, 0.5% sodium deoxycholate, 2 mM sodium fluoride, 2 mM EdTA, 0.1% SDS and a mixture of protease inhibitors (aprotinin, PMSF and sodium ortho-vanadate). Equal amounts of total proteins were resolved on an 11% SDS-polyacrylamide gel, transferred to a nitrocellulose membrane and probed with the appropriated antibody. As internal control, all membranes were subsequently stripped (glycine 0.2 M, pH 2.6 for 30 min at room temperature) of the first antibody and reprobed with anti GADPH antibody. The antigen-antibody complex was detected by incubation of the membranes for 1 h at room temperature with peroxidase-coupled goat anti-mouse or anti-rabbit IgG and revealed using the ECL System.

The blots were then exposed to film and the bands of interest were quantified by Scion Image laser densitometry scanning program. The results obtained as optical density arbitrary values were transformed to percentages of the control (percent control) taking the samples from cells not treated as 100%.

Transient transfection assay. Ishikawa cells were starved with serum free medium for 24 h and then transfected using the FuGENE 6 reagent with the mixture containing 0.25 μg of human cyclin D1 promoter constructs.

Twenty-four hours after transfection, the cells were untreated or treated with CDCA for 24 h. Empty vectors were used to ensure that DNA concentrations were constant in each transfection. Thymidine kinase Renilla luciferase plasmid was used to normalize the efficiency of the transfection. Firefly and Renilla luciferase activities were measured by the Dual Luciferase kit. The firefly luciferase data for each sample were normalized based on transfection efficiency measured by Renilla luciferase activity.

Electrophoretic mobility shift assay (EMSA). Nuclear extracts from Ishikawa cells were prepared as previously described.[36] The probe was generated by annealing single-stranded oligonucleotides, labeled with [λ^{32}P] ATP and T4 polynucleotide kinase, and purified using Sephadex G50 spin columns.

The DNA sequences used as probe or as cold competitors are the following (the nucleotide motifs of interest are underlined and mutations are shown as lowercase letters): 5'-TTA ACA ACA GTA ACG TCA CAC GGA CTA-3' and 5'-TAG TCC GTG TGA CGT TAC TGT TGT TAA-3' (CRE); 5'-CTT AAC AAC AGT AAt tgC ACA CGG ACT A-3' and 5'-TAG TCC GTG TGc aaT TAC TGT TGT TAA G-3' (CRE MUT); in vitro transcribed and translated CREB protein was synthesized using the T7 polymerase in the rabbit reticulocyte lysate system. The protein-binding reactions were performed in 20 μl of buffer [20 mmol/L HEPES (pH 8), 1 mmol/L EDTA, 50 mmol/L KCl, 10 mmol/L DTT, 10% glycerol, 1 mg/ml BSA, 50 μg/ml poly(dI/dC)] with 50,000 cpm of labeled probe, 20 μg of Ishikawa nuclear protein or an appropriate amount of CREB protein and 5 μg of poly (dI-dC). The mixtures were incubated at room temperature for 20 min in the presence or absence of unlabeled competitor oligonucleotides. For experiments involving CREB antibody, the reaction mixture was incubated with these antibody at 4°C for 12 h before addition of labeled probe. The entire reaction mixture was electrophoresed through a 6% polyacrylamide gel in 0.25x Tris borate-EDTA for 3 h at 150 V.

Chromatin immunoprecipitation assay (ChIP). Serum-starved Ishikawa cells were untreated or treated with 5 μM CDCA for 2 h. The cells were then cross-linked with 1% formaldehyde and sonicated. Supernatants were immunocleared with salmon sperm DNA/protein A and immunoprecipitated with specific anti-CREB and anti-polymerase II antibodies or a normal mouse serum IgG as negative control. Pellets were washed as reported, eluted with elution buffer (1% SDS, 0.1 M $NaHCO_3$) and digested with proteinase K. DNA was obtained by phenol/chloroform/isoamyl alcohol extractions and precipitated with

ethanol; 3 ml of each sample were used for PCR amplification with the following primers flanking CRE sequence present in the cyclin D1 promoter region: 5'-TGC GCC CGC CCC CGC CCC CCT C-3' and 5'-TGT TCC ATG GCT GGG GCT CTT-3'.

The PCR conditions were 1 min at 94°C, 1 min at 65°C and 2 min at 72°C. The amplification products obtained in 35 cycles were analyzed in a 2% agarose gel and visualized by Ethidium bromide staining.

RNA silencing (siRNA). Cells were plated in 6-well dishes with regular growth medium the day before transfection to 50–60% confluence. On the second day the medium was changed with SFM without P/S, and cells were transfected with validated ON-TARGET plus SMART pool of siRNA targeted human TGR-5 or FXR[37] or control siRNA, purchased from Thermo Scientific Dharmacon (sequence information is patented and protected by Dharmacon), or with RNA duplex of validate RNAi targeted human CREB mRNA sequence 5'- GGC UAA CAA UGG UAC CGA Utt-3', or with a stealth RNAi control (Ambion) to a final concentration of 50 nM using Lipofectamine 2000 as recommended by the manufacturer. After 5 h, the transfection medium was changed with SFM (MAPK and cyclin D1 analysis by immunoblotting) or 5% charcoal-treated FBS (cell proliferation by [^{3}H]thymidine incorporation) in order to avoid Lipofectamine 2000 toxicity and cells were exposed to CDCA as indicated in figures.

[^{3}H]thymidine incorporation. Ishikawa cells were starved for 24 h and then were untreated or treated with different doses of CDCA for 72 h in MEM supplemented with 5% charcoal-stripped FBS. For the last 6 h, [^{3}H]thymidine (1 μCi/ml) was added to the culture medium. After rinsing with phosphate-buffered saline, cells were washed once with 10% and three times with 5% trichloroacetic acid. The cells were lysed by adding 0.1 N NaOH and then incubated for 30 min at 37°C. Thymidine incorporation was determined by scintillation counting.

Anchorage-independent soft agar growth assays. Ishikawa cells were plated in 4 ml of MEM with 0.5% agarose and 5% charcoal-stripped FBS, in 0.7% agarose base in 6-well plates. Two days after plating, medium containing hormonal treatments (CDCA, EGF and IGF) was added to the top layer, and the appropriate medium was replaced every 2 d. After 14 d, 150 μl of 3-(4,5-dimethylthiazol-2-yl)-2,5-diphenyltetrazolium bromide was added to each well and allowed to incubate at 37°C for 4 h. Plates were then placed at 4°C overnight, and colonies > 50 μm diameter from triplicate assays were counted. Data are the mean colony number of three plates and representative of two independent experiments.

Statistical analysis. Each datum point represents the mean ± SE of three different experiments. Statistical analysis was performed using ANOVA followed by Newman-Keuls testing to determine differences in means. $p < 0.05$ was considered as statistically significant.

Disclosure of Potential Conflict of Interest

No potential conflicts of interest were disclosed.

Acknowledgments

Special thanks to Società Italiana di Patologia (SIP) for the Young Life Scientist Awards to P. Avena and D. Sturino (Faculty of Pharmacy, University of Calabria) for the English review of the manuscript. This work was supported by Associazione Italiana Ricerca sul Cancro (AIRC) grant 2011–2014; Ministero Istruzione Università Ricerca (MIUR)-Ex 60%-2011.

References

1. Cancer Research UK. CancerStats: corpus uteri cancer. http://info.cancerresearchuk.or/cancerstats/(9 March 2012, date last accessed).
2. Madison T, Schottenfeld D, James SA, Schwartz AG, Gruber SB. Endometrial cancer: socioeconomic status and racial/ethnic differences in stage at diagnosis, treatment and survival. Am J Public Health 2004; 94:2104-11; PMID:15569961; http://dx.doi.org/10.2105/AJPH.94.12.2104.
3. Key TJ, Allen NE, Spencer EA, Travis RC. The effect of diet on risk of cancer. Lancet 2002; 360:861-8; PMID:12243933; http://dx.doi.org/10.1016/S0140-6736(02)09958-0.
4. Monte MJ, Marin JJ, Antelo A, Vazquez-Tato J. Bile acids: chemistry, physiology and pathophysiology. World J Gastroenterol 2009; 15:804-16; PMID:19230041; http://dx.doi.org/10.3748/wjg.15.804.
5. Engelking LR, Dasher CA, Hirschowitz BI. Within-day fluctuations in serum bile-acid concentrations among normal control subjects and patients with hepatic disease. Am J Clin Pathol 1980; 73:196-201; PMID:7188830.
6. Everson GT. Steady-state kinetics of serum bile acids in healthy human subjects: single and dual isotope techniques using stable isotopes and mass spectrometry. J Lipid Res 1987; 28:238-52; PMID:3553403.
7. Debruyne PR, Bruyneel EA, Li X, Zimber A, Gespach C, Mareel MM. The role of bile acids in carcinogenesis. Mutat Res 2001; 480-481:359-69; PMID:11506828; http://dx.doi.org/10.1016/S0027-5107(01)00195-6.
8. Makishima M, Okamoto AY, Repa JJ, Tu H, Learned RM, Luk A, et al. Identification of a nuclear receptor for bile acids. Science 1999; 284:1362-5; PMID:10334992; http://dx.doi.org/10.1126/science.284.5418.1362.
9. Parks DJ, Blanchard SG, Bledsoe RK, Chandra G, Consler TG, Kliewer SA, et al. Bile acids: natural ligands for an orphan nuclear receptor. Science 1999; 284:1365-8; PMID:10334993; http://dx.doi.org/10.1126/science.284.5418.1365.
10. Wang H, Chen J, Hollister K, Sowers LC, Forman BM. Endogenous bile acids are ligands for the nuclear receptor FXR/BAR. Mol Cell 1999; 3:543-53; PMID:10360171; http://dx.doi.org/10.1016/S1097-2765(00)80348-2.
11. Maruyama T, Miyamoto Y, Nakamura T, Tamai Y, Okada H, Sugiyama E, et al. Identification of membrane-type receptor for bile acids (M-BAR). Biochem Biophys Res Commun 2002; 298:714-9; PMID:12419312; http://dx.doi.org/10.1016/S0006-291X(02)02550-0.
12. Kawamata Y, Fujii R, Hosoya M, Harada M, Yoshida H, Miwa M, et al. A G protein-coupled receptor responsive to bile acids. J Biol Chem 2003; 278:9435-40; PMID:12524422; http://dx.doi.org/10.1074/jbc.M209706200.
13. Martinez JD, Stratagoules ED, LaRue JM, Powell AA, Gause PR, Craven MT, et al. Different bile acids exhibit distinct biological effects: the tumor promoter deoxycholic acid induces apoptosis and the chemopreventive agent ursodeoxycholic acid inhibits cell proliferation. Nutr Cancer 1998; 31:111-8; PMID:9770722; http://dx.doi.org/10.1080/01635589809514689.
14. Goldberg AA, Beach A, Davies GF, Harkness TA, Leblanc A, Titorenko VI. Lithocholic bile acid selectively kills neuroblastoma cells, while sparing normal neuronal cells. Oncotarget 2011; 2:761-82; PMID:21992775.
15. Lukas J, Pagano M, Staskova Z, Draetta G, Bartek J. Cyclin D1 protein oscillates and is essential for cell cycle progression in human tumour cell lines. Oncogene 1994; 9:707-18; PMID:8108113.
16. Nikaido T, Li SF, Shiozawa T, Fujii S. Coabnormal expression of cyclin D1 and p53 protein in human uterine endometrial carcinomas. Cancer 1996; 78:1248-53; PMID:8826947; http://dx.doi.org/10.1002/(SICI)1097-0142(19960915)78:6<1248::AID-CNCR12>3.0.CO;2-0.
17. Fu M, Wang C, Li Z, Sakamaki T, Pestell RG. Minireview: cyclin D1: normal and abnormal functions. Endocrinology 2004; 145:5439-47; PMID:15331580; http://dx.doi.org/10.1210/en.2004-0959.
18. Rozengurt E. Mitogenic signaling pathways induced by G protein-coupled receptors. J Cell Physiol 2007; 213:589-602; PMID:17786953; http://dx.doi.org/10.1002/jcp.21246.
19. Albitar L, Pickett G, Morgan M, Wilken JA, Maihle NJ, Leslie KK. EGFR isoforms and gene regulation in human endometrial cancer cells. Mol Cancer 2010; 9:166; PMID:20579378; http://dx.doi.org/10.1186/1476-4598-9-166.
20. Renehan AG, Frystyk J, Flyvbjerg A. Obesity and cancer risk: the role of the insulin-IGF axis. Trends Endocrinol Metab 2006; 17:328-36; PMID:16956771; http://dx.doi.org/10.1016/j.tem.2006.08.006.

21. Calle EE, Kaaks R. Overweight, obesity and cancer: epidemiological evidence and proposed mechanisms. Nat Rev Cancer 2004; 4:579-91; PMID:15286738; http://dx.doi.org/10.1038/nrc1408.
22. Amant F, Moerman P, Neven P, Timmerman D, Van Limbergen E, Vergote I. Endometrial cancer. Lancet 2005; 366:491-505; PMID:16084259; http://dx.doi.org/10.1016/S0140-6736(05)67063-8.
23. Blagosklonny MV. NCI's provocative questions on cancer: some answers to ignite discussion. Oncotarget 2011; 2:1352-67; PMID:22267462.
24. Russell DW. Fifty years of advances in bile acid synthesis and metabolism. J Lipid Res 2009; 50:120-5; PMID:18815433; http://dx.doi.org/10.1194/jlr.R800026-JLR200.
25. Houten SM, Watanabe M, Auwerx J. Endocrine functions of bile acids. EMBO J 2006; 25:1419-25; PMID:16541101; http://dx.doi.org/10.1038/sj.emboj.7601049.
26. Albitar L, Pickett G, Morgan M, Davies S, Leslie KK. Models representing type I and type II human endometrial cancers: Ishikawa H and Hec50co cells. Gynecol Oncol 2007; 106:52-64; PMID:17490735; http://dx.doi.org/10.1016/j.ygyno.2007.02.033.
27. Halmy L, Fehér T, Steczek K, Farkas A. High serum bile acid level in obesity: its decrease during and after total fasting. Acta Med Hung 1986; 43:55-8; PMID:3774418.
28. Cordon-Cardo C. Mutations of cell cycle regulators. Biological and clinical implications for human neoplasia. Am J Pathol 1995; 147:545-60; PMID:7677168.
29. Knudsen KE, Diehl JA, Haiman CA, Knudsen ES. Cyclin D1: polymorphism, aberrant splicing and cancer risk. Oncogene 2006; 25:1620-8; PMID:16550162; http://dx.doi.org/10.1038/sj.onc.1209371.
30. Wang C, Lisanti MP, Liao DJ. Reviewing once more the c-myc and Ras collaboration: converging at the cyclin D1-CDK4 complex and challenging basic concepts of cancer biology. Cell Cycle 2011; 10:57-67; PMID:21200143; http://dx.doi.org/10.4161/cc.10.1.14449.
31. Arnold A, Kim HG, Gaz RD, Eddy RL, Fukushima Y, Byers MG, et al. Molecular cloning and chromosomal mapping of DNA rearranged with the parathyroid hormone gene in a parathyroid adenoma. J Clin Invest 1989; 83:2034-40; PMID:2723071; http://dx.doi.org/10.1172/JCI114114.
32. Withers DA, Harvey RC, Faust JB, Melnyk O, Carey K, Meeker TC. Characterization of a candidate bcl-1 gene. Mol Cell Biol 1991; 11:4846-53; PMID:1833629.
33. Hall M, Peters G. Genetic alterations of cyclins, cyclin-dependent kinases and Cdk inhibitors in human cancer. Adv Cancer Res 1996; 68:67-108; PMID:8712071; http://dx.doi.org/10.1016/S0065-230X(08)60352-8.
34. Caldon CE, Sutherland RL, Musgrove E. Cell cycle proteins in epithelial cell differentiation: implications for breast cancer. Cell Cycle 2010; 9:1918-28; PMID:20473028; http://dx.doi.org/10.4161/cc.9.10.11474.
35. Ruhul Quddus M, Latkovich P, Castellani WJ, James Sung C, Steinhoff MM, Briggs RC, et al. Expression of cyclin D1 in normal, metaplastic, hyperplastic endometrium and endometrioid carcinoma suggests a role in endometrial carcinogenesis. Arch Pathol Lab Med 2002; 126:459-63; PMID:11900573.
36. Catalano S, Giordano C, Rizza P, Gu G, Barone I, Bonofiglio D, et al. Evidence that leptin through STAT and CREB signaling enhances cyclin D1 expression and promotes human endometrial cancer proliferation. J Cell Physiol 2009; 218:490-500; PMID:18988190; http://dx.doi.org/10.1002/jcp.21622.
37. Rizzo G, Passeri D, De Franco F, Ciaccioli G, Donadio L, Rizzo G, et al. Functional characterization of the semisynthetic bile acid derivative INT-767, a dual farnesoid X receptor and TGR5 agonist. Mol Pharmacol 2010; 78:617-30; PMID:20631053; http://dx.doi.org/10.1124/mol.110.064501.

Anticancer Activity of a Quercetin-based Polymer Towards HeLa Cancer Cells

FRANCESCO PUOCI[1,2], CATIA MORELLI[3], GIUSEPPE CIRILLO[1,2], MANUELA CURCIO[1,2], ORTENSIA ILARIA PARISI[1,2], PAMELA MARIS[3], DIEGO SISCI[3] and NEVIO PICCI[1,2]

[1]*Department of Pharmaceutical Sciences, University of Calabria, Arcavacata di Rende (CS), Italy;*
[2]*Macrofarm Srl, University of Calabria, Edificio Polifunzionale, Arcavacata di Rende (CS), Italy;*
[3]*Departimento Pharmaco-Biology, University of Calabria, Arcavacata di Rende (CS), Italy*

Abstract. *Background: Quercetin is one of the most potent antioxidants showing anti-inflammatory, antiproliferative and antitumoral effects; however its short half-life in buffered solution (e.g. body fluids) has so far hampered its introduction into clinical practice. Aim: To overcome this inconvenience, quercetin was covalently conjugated into a polymethacrylic acid backbone and the conjugate was tested on HeLa cancer cells. Materials and Methods: FT-IR, UV-Vis, Gel Permeation Chromatography analyses and the Folin-Ciocalteu test were performed to characterize the conjugate. Antioxidant properties were assessed by the DPPH test and the viability experiments by trypan blue exclusion assay. Results: The conjugate showed a functionalization degree of 2.01 mg of Q per g, an IC_{50} of 2.62 mg ml^{-1} in the DPPH assay and was able to induce a 90% cell death after one day treatment, while the value for free Quercetin was 40% after three days. Conclusion: Polymer conjugation significantly increases quercetin stability, leading to a sustained activity of the flavonoid.*

In recent years, an emerging research field aimed to improve the performance of natural and synthetic polymers concerning the synthesis of antioxidant polymers by covalent insertion of antioxidant molecules into polymeric chains (1, 2). The resulting functional materials show innovative application in biomedical and pharmaceutical fields; they could be applied in pharmaceutical and cosmetic formulations in order to avoid the oxidation of their components, as preservative agents in food packaging and in biomedicine as innovative materials (*e.g.* haemodialysis membranes, contact lenses, *etc.*) (3, 4). The advantage in the use of these bioconjugates is related to the possibility of combining the advantages of both the components: the unique properties of antioxidant molecules and the high stability and slow degradation rate of macromolecular systems (5).

In the realm of biomedicine, a recent therapeutic approach is related to the discovery of the role of free radicals in cardiovascular diseases, cancer, diabetes, neurodegenerative disorders, autoimmune diseases, aging and other diseases, opening a new application field for antioxidant materials (6, 7). In particular, the first therapeutic strategies related to the use of polymer therapeutics were to improve the performance of poorly water-soluble anticancer drugs. The conjugation of such molecules with water-soluble polymers, indeed, results in enhancing the pharmacokinetics of the therapeutics by mean of increased water solubility, reduced side-effects and easier administration (8, 9).

Several different approaches have been proposed to synthesize biopolymers coupled with antioxidant compounds, indicating the need for synthetic procedures to generate multifunctional polymeric systems *via* straightforward and efficient chemistries. In this work, the adopted synthetic strategy is the coupling reaction between the antioxidant molecule and a growing polymeric chain in a single-step reaction. With this approach, it is possible to synthesize polymer antioxidant conjugates without the generation of toxic reaction by-products, while also preserving the antioxidant from the degradation processes (10). The selected antioxidant molecule was quercetin, while methacrylic acid (MAA) was the chosen co-monomer for the synthesis of a polymer-quercetin conjugate (Pol-Q). The choice of MAA is dictated by the wide use of methacrylate polymers in biomedicine and biotechnology as base materials for drug delivery systems, contact lenses, food technology, quality control systems and biosensors (11).

Quercetin (3,3',4',5,7-pentahydroxylflavone), a flavonoid ubiquitously present in fruits and vegetables, such as tea,

Correspondence to: Francesco Puoci, Department of Pharmaceutical Sciences, University of Calabria, Arcavacata di Rende (CS), 87036, Italy. Tel: +39 0984493151, Fax: +39 0984493298, e-mail: francesco.puoci@unical.it

Key Words: Anticancer activity, antioxidants, polymeric drugs, radical grafting, quercetin, HeLa cells.

apples, onion and berries, was selected due to its high biological benefits, including antioxidative, anti-genotoxic, anti-inflammatory, vasodilating effects, and because it has been recently proposed as a chemopreventive and anticancer agent (12). Its antitumoral effects have been attributed to various mechanisms, including the inhibition of enzymes that activate carcinogens, the modification of signal transduction pathways, and the interactions with receptors and other proteins (13). Various cellular receptors have indeed been reported to be involved in the anticancer activities of quercetin, including the androgen receptor (14), the epidermal growth factor receptor (EGFR) family (15) and the death receptor (DR) (16). In particular, quercetin has also been reported to suppress viability of HeLa cells *via* AMP-activated protein kinase (AMPK)-induced heat shock protein (HSP)70 and EGFR down-regulation (17). However, the sensitivity of quercetin to fast auto-oxidation results in its poor stability in aqueous aerobic environments (18), thus its half-life, generally ranges between 2 h (*e.g.* in McCoy's 5A cell culture medium) to 10 h [in (PBS) pH 7.2] (19), due to chemical decomposition in biologically active products, such as protocatechuic acid and phloroglucinol carboxylic acid (20).

Our hypothesis is that polymer conjugation significantly increases quercetin stability, leading to a sustained activity of the flavonoid.

Materials and Methods

Materials, cell line and culture conditions. MAA, 2,2'-azoisobutyronitrile (AIBN), quercetin, 2,2'-diphenyl-1-picrylhydrazyl radical (DPPH), Folin-Ciocalteu reagent (FCR), disodium hydrogen phosphate, sodium dihydrogen phosphate, and polymethacrylic acid (pMAA) standard samples for size-exclusion chromatography (M_n=600-500000; M_w/M_n=1.06-1.10) were obtained from Sigma-Aldrich (Sigma Chemical Co., St Louis, MO, USA). *N,N*-Dimethylformamide (DMF), water and ethanol were HPLC-grade and provided by Carlo Erba reagents (Milan, Italy). Human HeLa cervical adenocarcinoma cells (Interlab Cell Line Collection, ICLC, Genoa, Italy) were maintained in a humified tissue culture incubator at 5% CO_2 and 37°C and cultured in modified Eagle's medium (MEM, Sigma-Aldrich, Gillingham, Dorset, UK) supplemented with 10% fetal bovine serum (FBS), 100 IU ml^{-1} penicillin, 100 mg ml^{-1} streptomycin, and 0.2 mM L-glutamine. HeLa cells were maintained in a humidified tissue culture incubator at 5% CO_2 and 37°C and cultured in Modified Eagle's Medium, supplemented with 10% fetal bovine serum (FBS), 100 IU ml^{-1} penicillin, 100 mg ml^{-1} streptomycin, and 0.2 mM L-glutamine.

Synthesis of Pol-Q conjugate. The polymerization of MAA with quercetin was carried out as follows: in a 10 ml glass tube, 0.1, 0.25, and 0.5 g of quercetin were dissolved in 8.0 ml of DMF and then 5.0 g of MAA and 100 mg of AIBN were added and the solution was magnetically stirred at 60°C. After 24 h, the mixture was poured into acetone, and then the precipitated polymer was filtered by sintered glass filter funnel (Pyrex, Ø30 mm; porosity 3), submitted to three dissolution/precipitation cycles (methanol/acetone), and vacuum dried at room temperature.

The polymer was checked to be free of unreacted quercetin and any other compounds by HPLC analysis after each purification step.

Blank polymer (pMAA) was prepared under the same conditions without using quercetin.

Pol-Q analysis. The liquid chromatography consisted of a Jasco PU-2089 Plus liquid chromatography apparatus equipped with a Rheodyne 7725i injector (fitted with a 20 µl loop), a Jasco UV-2075 HPLC detector and Jasco-Borwin integrator (Jasco Europe s.r.l., Milan, Italy). A reverse-phase C18 Hibar column, 250 mm × 4 µm, particle size=5 µm, pore size=120Å (Merck, Darmstadt, Germany), was employed. In accordance with literature data (21), the mobile phase adopted for the detection of quercetin was a 1% (v/v) aqueous solution of formic acid-acetonitrile-2-propanol (70:22:8) at a flow rate of 0.2 ml min^{-1}. Chromatograms were recorded at 370 nm. For pMAA and Pol-Q, Mn and Mw/Mn were measured by Gel permeation chromatography (GPC) using water as eluent at 45°C and at flow rate, 1.0 ml min-1on Waters Ultrahydrogel-1000 column connected to a Jasco PU-2089 pump and a Jasco 930-RI refractive-index detector. The columns were calibrated with standard pMAA samples (22). (FT-IR) spectra were recorded as KBr pellets on a Jasco FT-IR 4200. (UV-Vis) absorption spectra were obtained with a Jasco V-530 UV/Vis spectrometer (Jasco Europe s.r.l., Milan, Italy).

Evaluation of disposable phenolic groups by Folin-Ciocalteu procedure. The amount of total phenolic equivalents was determined using the Folin-Ciocalteu reagent procedure, according to the literature, with some modifications (23). Briefly, 20 mg of Pol-Q conjugate were dispersed in distilled water (6.0 ml) in a volumetric flask. Folin-Ciocalteu reagent (1.0 ml) was added and the contents of the flask were mixed thoroughly. After 3 min, 3 ml of Na_2CO_3 (2%, w/w) were added, and then the mixture was allowed to stand for 2 h with intermittent shaking. The absorbance was measured at 760 nm against a control prepared using the blank polymer under the same reaction conditions. The amount of total phenolic groups in the polymeric material was expressed as quercetin equivalents (mg) by using the equation obtained from the calibration curve of the free antioxidant, recorded by employing five different standard solutions of quercetin; 0.5 ml of each solution were added to the Folin-Ciocalteu system to raise the final concentration to 8.0, 16.0, 24.0, 32.0, and 40.0 µM, respectively. After 2 h, the absorbance of the solutions was measured to record the calibration curve and the correlation coefficient (R^2), slope and intercept of the regression equation obtained were calculated by the method of least squares.

Determination of scavenging effect of Pol-Q on the DPPH radical. In order to evaluate the free radical scavenging properties of Pol-Q, its reactivity towards a stable free radical DPPH, was evaluated (24). For this purpose, in each of seven test tubes, 5.0, 10.0, 15.0, 20.0 mg of Pol-Q were dissolved in 6 ml of ethanol and then 4 ml of ethanol solution of the DPPH (250 µM) were added, obtaining a solution of the DPPH with a final concentration of 100 µM. The sample was incubated in a water bath at 25°C and after 30 min, the absorbance of the remaining DPPH was determined colorimetrically at 517 nm. The same reaction conditions were applied for the blank pMAA and standard quercetin solutions (positive control). The scavenging activity of the tested polymeric materials was measured as the decrease in the absorbance of DPPH and was expressed as percentage inhibition of the DPPH radical calculated according to the following equation (1):

$$\text{Inhibition (\%)} = \frac{A_0 - A_1}{A_0} \times 100 \qquad \text{(Eqtn 1)}$$

where A_0 is the absorbance of a standard prepared under the same conditions, but without any polymer, and A_1 is the absorbance of polymeric samples.

Cell viability on treatment with quercetin and Pol-Q. The effect of Q and Pol-Q on cell proliferation was assessed by the trypan blue exclusion assay. HeLa cells in the exponential growth phase were plated in triplicates in 12-well plates at a density of 10^5 cells/well and grown overnight. The following day, cells were synchronized in phenol red-free serum-free media (PRF-SFM) for 24 h to avoid growth differences among cells. Following starvation, free quercetin (100 μM) or Pol-Q (corresponding to ~100 μM quercetin) were added to the cells in PRF-MEM plus 0.5% FBS. Comparable amounts of (DMSO) and polymer alone were also tested. Untreated cells were used as control. After 1, 2 or 3 days, cells were harvested by trypsinization and incubated in a 0.5% trypan blue solution for 10 min at room temperature. Cell viability was determined microscopically by counting trypan blue-negative cells in a hemacytometer (Burker, Brand, Germany).

Statistical analyses. Each measurement was carried out in five independent experiments, data are expressed as means (±SD), and analysed using one-way analysis of variance (ANOVA). For the inhibitory experiment, the IC_{50} value was determined as the concentration of antioxidant that provides 50% inhibition of DPPH.

Results and Discussion

Synthesis and Characterization of Pol-Q conjugate. The Pol-Q conjugate was synthesized by free radical coupling reaction between MAA and quercetin based on literature data which suggest that quercetin can be incorporated in a growing polymeric chain by the reaction between the radical formed in the *ortho-* and *para-* positions relative to the hydroxyl group of the flavonoid and the MAA monomer (25).

Optimization of the reaction conditions was performed in order to maximize the incorporation of quercetin in the growing polymeric chain, and thus the selected amount of quercetin in the polymerization feed represents the highest amount of quercetin which can be dissolved in the reaction medium. Pol-Q conjugates synthesized using a lower amount of quercetin, indeed, were found to be less effective antioxidants.

The synthesized polymer was then conformed to be free of un-reacted quercetin by HPLC analyses of acetone used in the precipitation-dissolution cycles which Pol-Q conjugate underwent in the purification process.

After the synthesis and purification steps, chemical characterization of Pol-Q was carried out by determination of the molecular weight distributions, FT-IR and UV-Vis analyses and the determination of the amount of quercetin incorporated into the polymeric backbone. By specific (SEC) analyses, the molecular weight distribution of Pol-Q and blank polymers were determined and corresponded to average values of 71 000 Da and 77 000 Da for Pol-Q and pMAA, respectively, with M_w/M_n <1.7.

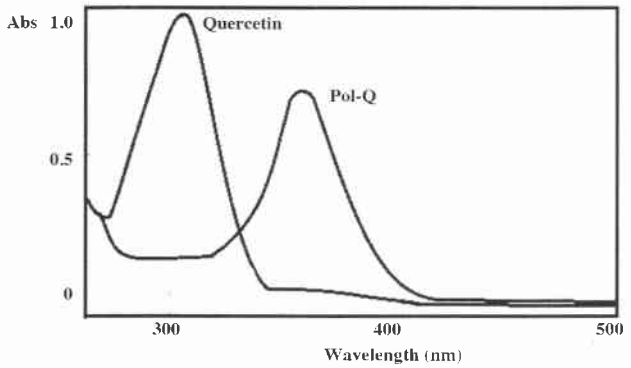

Figure 1. *UV-Vis absorption spectra of free and conjugated (Pol-Q) quercetin.*

FT-IR and UV-Vis analyses were performed to demonstrate the formation of covalent bond between quercetin and the polymeric backbone. In particular, FT-IR analysis of Pol-Q shows the presence of the carbon-to-carbon stretching band (1523 cm^{-1}) within the aromatic ring of the antioxidant which is absent from the pMAA, while the presence of a bathochromic shift of the absorption peaks of the aromatic region of quercetin from 310 nm to 367 nm after incorporation into the polymeric chain suggest the formation of a covalent linkage between Q and MAA residues (Figure 1).

A key characterization of the synthesized Pol-Q is the determination of the amount of quercetin bound into the polymeric backbone. This characterization was performed by using the Folin-Ciocalteu assay, by which it is possible to determine the efficiency of the antioxidant residues in reducing the molybdenum complex within the Folin-Ciocalteu reagent (23). Thus, a comparison between the reducing power of quercetin and Pol-Q to form the spectrophotometrically detectable blue species $(PMoW_{11}O_{40})^{4-}$ is a direct indication of the amount of quercetin incorporated into the conjugate. The assay was performed according to the literature and, as a result, it was determined that 1.0 g of Pol-Q contained 2.01±0.3 mg of quercetin.

A first functional characterization of the conjugate efficiency was performed in terms of antioxidant properties and scavenging activity in particular. In recent years, the DPPH assay has become quite popular in antioxidant studies because it is a simple and highly sensitive method to evaluate the free radical scavenging properties of a selected antioxidant (24). The antioxidant effect is proportional to the disappearance of DPPH in test samples due to the fact that DPPH accepts hydrogen from an antioxidant. Under our conditions, Pol-Q was found to be a powerful radical

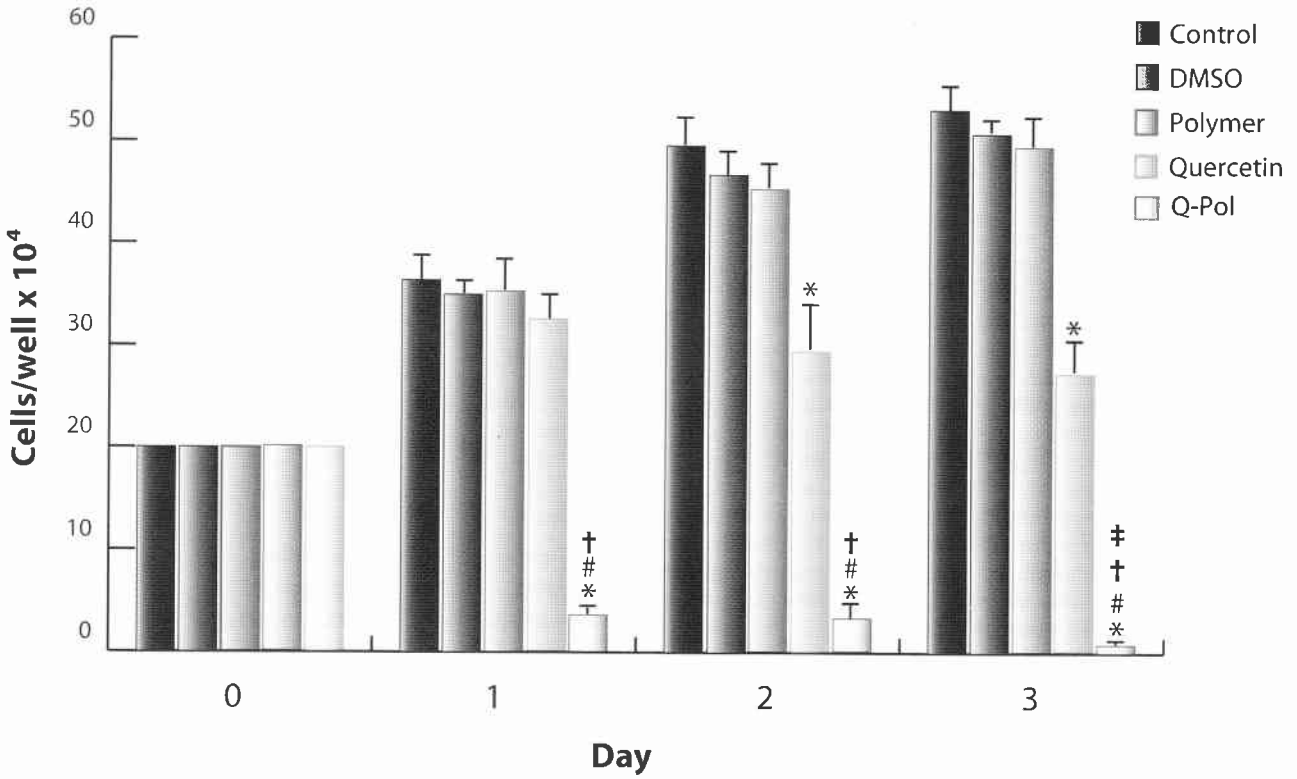

Figure 2. *Polymer conjugation accelerates and increases the efficacy of quercetin in inducing cancer cell death. Cancerous HeLa cells were treated with (DMSO), polymer alone, quercetin, polymer-conjugated quercetin (Pol-Q) or left untreated (control). Viability was determined after 1, 2 and 3 days. Values represent the mean of four triplicate independent experiments. Significance values were as follows: *p<0.01 vs. the respective control; #p<0.01 vs. the corresponding free quercetin treated samples; †p< 0.01 vs. the control at day 0; ‡p<0.01 vs. Pol-Q treated samples at day 1 and day 2. The error bars indicate SD.*

scavenger, with an IC_{50} value of 2.62 mg ml^{-1}, with pMAA exhibiting a low degree of interference with the assay. By considering the amount of quercetin per g of Pol-Q obtained by the Folin-Ciocalteu assay, this IC_{50} value corresponds to 17.7 μM of quercetin. The IC_{50} value of free quercetin (positive control) is 16.1±0.7 μM, confirming that the conjugation process did not interfere with the antioxidant properties of quercetin which are retained in the final polymer.

Anticancer activity of Pol-Q. To assess the effect of polymer conjugation on quercetin-induced tumour cell death, viability experiments were conducted on HeLa cells (Figure 2). After only two days of treatment, quercetin alone started to show a cytostatic effect (*vs.* day 0), which persisted at day 3, and caused a 40-50% growth retardation compared to the relative control at both time points. Notably, polymer conjugation dramatically increased toxicity of quercetin, inducing ~90% cell death vs control (~80% *vs.* control at day 0), as early as one day of treatment, and actually reaching 95% suppression of viability after three days. As expected, the vejicle used for free quercetin, DMSO, and polymer alone did not show any significant effect at any time point considered when compared to control samples (Figure 2).

It is worth mentioning that quercetin has recently been reported to induce a dose-dependent suppression of viability of HeLa cells (17). In agreement with our observations, the authors found a ~40% reduction of viability *vs.* the relative control after three days of quercetin treatment, but our data show that this effect is rather cytostatic, if compared to the starting cell number (day 0). On the contrary, Pol-Q is able to induce a prompt and almost complete cell kill, as early as after one day of treatment, and the cytotoxic activity persists and even increases with time. This effect cannot be ascribed to use of polymer alone, since no significant difference in HeLa cell viability was observed in polymer treated-cells, compared to controls (Figure 2).

Conclusion

A new antioxidant-polymer conjugate was synthesized and characterized in terms of anticancer activity. The quercetin flavonoid was incorporated into a methacrylate polymer by

free radical reaction and, after chemical characterization of the polymeric material, the so formed polymeric antioxidant was tested as anti-cancer agent towards HeLa cells. Our results show how polymer-bound quercetin exerts a rapid (as soon as after one day of treatment) and sustained cytotoxic effect, reaching almost 100% of cell kill within three days of exposure, if compared to free quercetin, which was only able to exert a cytostatic effect. This dramatic increase of toxicity on tumour cells observed in Pol-Q treated samples, could be most likely ascribed to a prolonged stability of the quercetin molecule following polymer conjugation. Our data support the idea that antioxidant conjugates represent a reliable and effective vehicle for anti-tumor agents, suggesting their possible implementation as co-adjuvant in the treatment of cancer disease.

Acknowledgements

This work was financially supported by MIUR (Programma di ricerca di rilevante interesse nazionale 2008) and University of Calabria funds. Financial support of Regional Operative Program (ROP) Calabria ESF 2007/2013 – IV Axis Human Capital – Operative Objective M2 - Action D.5 is gratefully acknowledged. Authors are solely responsible for the work.

References

1 Cirillo G, Kraemer K, Fuessel S, Puoci F, Curcio M, Spizzirri UG, Altimari I and Iemma F: Biological activity of a gallic acid – gelatin conjugate. Biomacromolecules *11*: 3309-3315, 2010.
2 Pasanphan W, Buettner GR and Chirachanchai S: Chitosan conjugated with deoxycholic acid and gallic acid: a novel biopolymer-based additive antioxidant for polyethylene. J Appl Polym Sci *109*: 38-46, 2008.
3 Menichetti S, Viglianisi C, Liguori F, Cogliati C, Boragno L, Stagnaro P, Losio S and Sacchi MC: Ethylene-based co-polymers with tunable content of polymerizable hindered phenols as non-releasing macromolecular additives. J Polym Sci Polym Chem *46*: 6393-6406, 2008.
4 Singh A and Kaplan DL: *In vitro* enzyme-induced vinyl polymerization. Adv Polym Sci 194: 211-222, 2006.
5 Dahe GJ, Teotia RS, Kadam SS and Bellare JR: The biocompatibility and separation performance of antioxidative polysulfone/vitamin E TPGS composite hollow fiber membranes. Biomaterials *32*: 352-365, 2011.
6 Halliwell B: Free radicals and antioxidants – Quo vadis? Trends Pharmacol Sci *32*: 125-130, 2011.
7 Nenkat Ratnam D, Ankola DD, Bhardwaj V, Sahana DK and Ravi Kumar MNV: Role of antioxidants in prophylaxis and therapy: a pharmaceutical perspective. J Control Rel *113*: 189-207, 2006.
8 Chen X, McRae S, Parelkar S and Emrick T: Polymeric phosphorylcholine-camptothecin conjugates prepared by controlled free radical polymerization and click chemistry. Bioconjugate Chem *20*: 2331-2341, 2009.
9 Ferguson EL and Duncan R: Dextrin-phospholipase A2: synthesis and evaluation as a bioresponsive anticancer conjugate. Biomacromolecules *10*: 1358-1364, 2009.
10 Puoci F, Iemma F, Curcio M, Parisi OI, Cirillo G, Spizzirri UG and Picci N: Synthesis of methacrylic – ferulic acid co-polymer with antioxidant properties by single-step free radical polymerization. J Agric Food Chem *56*: 10646-10650, 2008.
11 Herveas Perez JP, Lopez-Cabarcos E and Lopez-Ruiz B: The application of methacrylate-based polymers to enzyme biosensors. Biomol Eng *23*: 233-245, 2006.
12 Kook D, Wolf AH, Yu AL, Neubauer AS, Priglinger SG, Kampik A and Welge-Lussen UC: The protective effect of quercetin against oxidative stress in the human RPE. Invest Ophthalmol Vis Sci *49*: 1712-1720, 2008.
13 Moon YJ, Wang X and Morris ME: Dietary flavonoids: effects on xenobiotic and carcinogen metabolism. Toxicol In Vitro *20*: 187-210, 2006.
14 Xing N, Chen Y, Mitchell SH and Young CY: Quercetin inhibits expression and function of the androgen receptor in LNCaP prostate cancer cells. Carcinogenesis *22*: 409-414, 2001.
15 Kim WK, Bang MH, Kim ES, Kang NE, Jung KC, Cho HJ and Park JHY: Quercetin decreases the expression of ERBB2 and ERBB3 proteins in HT-29 human colon cancer cells. J Nutr Biochem *16*: 155-162, 2005.
16 Chen W, Wang X, Zhuang J, Zhang L and Lin Y: Induction of death receptor 5 and suppression of survivin contribute to sensitization of TRAIL-induced cytotoxicity by quercetin in non-small cell lung cancer cells. Carcinogenesis *28*: 2114-2121, 2007.
17 Jung JH, Lee JO, Kim JH, Lee SK, You GY, Park SH, Park JM, Kim EK, Suh PG, An JK and Kim HS: Quercetin suppresses HeLa cell viability *via* AMPK-induced HSP70 and EGFR down-regulation. J Cell Physiol *223*: 408-414, 2010.
18 Makris DP and Rossiter JT: Heat-induced, metal-catalyzed oxidative degradation of quercetin and rutin (quercetin-3-O-rhamnosylglucoside) in aqueous model systems. J Agric Food Chem *48*: 3830-3838, 2000.
19 Van der Woude H, Gliszczyńska-Swigło A, Struijs K, Smeets A, Alink GM and Rietjens IM: Biphasic modulation of cell proliferation by quercetin at concentrations physiologically relevant in humans. Cancer Lett *200*: 41-47, 2003.
20 Boulton DW, Walle KU and Walle T: Fate of the flavonoid quercetin in human cell lines: chemical instability and metabolism. J Pharm Pharmacol *51*: 353-359, 1999.
21 Careri M, Corradini C, Elviri L, Nicoletti I and Zagnoni I: Direct HPLC analysis of quercetin and trans-resveratrol in red wine, grape, and winemaking byproducts. J Agric Food Chem *51*: 5226-5231, 2003.
22 Bai F, Huang B, Yang X and Huang W: Synthesis of monodisperse poly(methacrylic acid) microspheres by distillation–precipitation polymerization. Eur Polym J *43*: 3923-3932, 2007.
23 Pan Y, Zhu J, Wang H, Zhang X, Zhang Y, He C, Ji X and Li H: Antioxidant activity of ethanolic extract of Cortex fraxini and use in peanut oil. Food Chem *103*: 913-918, 2007.
24 Magalhaes ML, Segundo MA, Reis S and Lima JLFC: Methodological aspects about *in vitro* evaluation of antioxidant properties. Anal Chim Acta *613*: 1-19, 2009.
25 Kobayashi S and Higashimura H: Oxidative polymerization of phenols revisited. Prog Polym Sci *28*: 1015-1048, 2003.

Received January 18, 2012
Revised February 17, 2012
Accepted February 20, 2012

Nanoscale

Dynamic Article Links

Cite this: *Nanoscale*, 2011, **3**, 3198

www.rsc.org/nanoscale

PAPER

PEG-templated mesoporous silica nanoparticles exclusively target cancer cells†

Catia Morelli,[b] Pamela Maris,[b] Diego Sisci,[b] Enrico Perrotta,[d] Elvira Brunelli,[d] Ida Perrotta,[d] Maria Luisa Panno,[c] Antonio Tagarelli,[e] Carlo Versace,[f] Maria Francesca Casula,[g] Flaviano Testa,[a] Sebastiano Andò,[c] Janos B. Nagy[a] and Luigi Pasqua*[a]

Received 9th March 2011, Accepted 11th May 2011
DOI: 10.1039/c1nr10253b

Mesoporous silica nanoparticles (MSNs) have been proposed as DNA and drug delivery carriers, as well as efficient tools for fluorescent cell tracking. The major limitation is that MSNs enter cells regardless of a target-specific functionalization. Here we show that non functionalized MSNs, synthesized using a PEG surfactant-based interfacial synthesis procedure, do not enter cells, while a highly specific, receptor mediated, cellular internalization of folic acid (FOL) grafted MSNs (MSN-FOL), occurs exclusively in folate receptor (FR) expressing cells. Neither the classical clathrin pathway nor macropinocytosis is involved in the MSN endocytic process, while fluorescent MSNs (MSN-FITC) enter cells through aspecific, caveolae-mediated, endocytosis. Moreover, internalized particles seem to be mostly exocytosed from cells within 96 h. Finally, cisplatin (Cp) loaded MSN-FOL were tested on cancerous FR-positive (HeLa) or normal FR-negative (HEK293) cells. A strong growth arrest was observed only in HeLa cells treated with MSN-FOL-Cp. The results presented here show that our mesoporous nanoparticles do not enter cells unless opportunely functionalized, suggesting that they could represent a promising vehicle for drug targeting applications.

Introduction

The major limitation of current chemotherapy is the dose-responsive effect, so that cell kill is proportional to drug exposure.[1] A highly aggressive style of dosing is thus necessary to eradicate tumours, although it is hindered by poor selectivity for cancer cells and severe toxicity to normal cells.[2] Therefore, localized drug delivery would, ideally, improve the therapeutic efficacy, minimizing side effects. In recent years a great effort has been made to develop tumour-selective devices by conjugating anti-cancer drugs to hormones, antibodies and vitamin derivatives. Among them, a low molecular weight vitamin compound, folic acid, shows great promise as a tumour-homing agent.[3] This essential vitamin has a high affinity for FR, a tumour associated glycosylphosphatidylinositol anchored protein, which can actively internalize bound folates and folate conjugated compounds *via* receptor-mediated endocytosis.[4] FR is up-regulated in more than 90% of ovarian carcinomas, and it is expressed at high to moderate levels in kidney, brain, lung, and breast carcinomas while it occurs at very low levels in most normal tissues.[5] Based on these observations, it has been hypothesized that folate conjugation to anti-cancer drugs will improve drug selectivity and decrease negative side effects.[6] We and other groups proposed mesoporous silica nanoparticles as the starting architecture for the development of such a conceived device.[7] Mesoporous silica nanoparticle biocompatibility has been demonstrated by several reports[8] and folic acid functionalization seemed to further reduce the already low toxic effect on cells, as recently described by Dubernet's group in their two-photon dye-doped mesoporous silica-based systems.[9] Slowing *et al.* demonstrated that the uptake of differently surface functionalized fluorescent MCM-41-Type MSNs by HeLa cells is dependent on the nature of the grafted groups.[10] Next, Liong *et al.* reported the uptake of MSNs synthesized employing a ionic surfactant with a magnetic core by pancreatic cancer cells. The internalization of the nanoparticles, loaded with hydrophobic anticancer drugs, caused *per se* an evident cellular toxicity, which increased when the folic acid function was added to the system only in FR overexpressing cell lines.[11] Recently, rattle-type magnetic

[a]*Department of Chemical Engineering and Material, University of Calabria, Via P. Bucci 87036, Rende, CS, Italy. E-mail: l.pasqua@unical.it; Fax: +39 0984 496655; Tel: +39 0984 496677*
[b]*Pharmaco- Biology Department, University of Calabria, Via P. Bucci 87036, Rende, CS, Italy*
[c]*Cellular Biology Department, University of Calabria, Via P. Bucci 87036, Rende, CS, Italy*
[d]*Ecology Department, University of Calabria, Via P. Bucci, 87036 Rende, CS, Italy*
[e]*Chemistry Department, University of Calabria, Via P. Bucci 87036, Rende, CS, Italy*
[f]*Physics Department, University of Calabria, Via P. Bucci 87036, Rende, CS, Italy*
[g]*Chemical Sciences Department and INSTM, University of Cagliari, Monserrato, Italy*
† Electronic supplementary information (ESI) available. See DOI: 10.1039/c1nr10253b

mesoporous silica nanospheres, functionalized with PEG and folic acid and loaded with the anticancer agent docetaxel, determined an increased cell death in FR+ HeLa cells, compared to FR− MCF-7 cancer cells. In addition, after intravenous injection, the nanospheres have been shown to be delivered to designated organs when an external magnetic field is applied.[12] Moreover, Rosenholm *et al.*[13] evaluated the targeting potential of hyperbranched polyethyleneimine MSNs functionalized with fluorescein and folic acid. The authors observed that particles were internalized five times more by FR expressing cancer cells as compared to normal cells bearing only low levels of the receptor. Finally, a very recent *in vivo* study showed that MCM-41 type MSNs preferentially accumulate in tumors and that drug-delivery capability of camptothecin-loaded MSNs increases when folic acid function is added to the system.[14] Even though, in all the above mentioned reports, the targeting function has always improved MSN internalization by FR expressing cells, it is worth noting that particles are able to enter cells regardless of the presence of the targeting function folic acid.[15] Interestingly, the mesoporous silica nanoparticles used in this study seem to behave differently, since cellular uptake does not occur unless opportunely functionalized. Once inside, particles localize in endosomal cavities, and seem to be mostly expelled from the cells in a 96 h time period.

Results and discussion

Mesoporous silica nanoparticles used in this study were synthesized by modifying an interfacial synthesis procedure carried out at room temperature (RT),[7] introducing decane as the organic phase.[16] The aim was to limit mesoporous silica particle size, an essential parameter in drug targeting applications. To prevent a dramatic pore volume reduction in the final systems, the as-synthesized materials were functionalized before surfactant extraction to preferentially address the siloxane modifying agent on the external surface of the mesoporous particles. In this way, as previously reported,[16] a considerable pore volume is recovered after surfactant extraction of a PEG-templated folic acid-functionalized hybrid mesoporous silica, thus folic acid modification takes place preferentially on the external surface since it does not block the pore mouths nor does it substantially fill the pores, allowing a consistent drug loading. Non functionalized, as-synthesized, particles (MSN_{surf}) were either calcined (MSN) and used as blank in all *in vitro* experiments, or else extracted (MSN-E) for pore structure characterization. Aminopropyl-functionalized particles (MSN-AP) were prepared by covalent grafting of aminopropyltriethoxysilane (APTES) on MSN_{surf}. Folic acid-functionalized particles (MSN-FOL) were synthesized by amide bond formation between the amino group of MSN-AP and folic acid. To track the particles route within the cells, a fluorescent tracer (fluorescein isothiocyanate, FITC) was employed to obtain MSN-FITC and MSN-FITC-FOL materials (see Electronic Supplementary Information, ESI, Methods, Discussion and Fig. S-1 to Fig. S-4 for chemico-physical characterization). Fig. 1 shows a schematic representation of the MSN-FOL tested in our experiments (panel a); panels b and c show the Transmission Electron Microscopy (TEM) micrographs of MSN-FOL material that exhibits a porous texture in adherence with materials of the MSU family (see ESI, Discussion),[17] while Scanning Electron Microscopy (SEM) images (panels d and e) show that this synthesis procedure yields nanoscaled particles without a regular morphology appearing as aggregates of up to 500 nm. Indeed, Dynamic Light Scattering (DLS) measurements of all functionalized particles showed that, when suspended in water, their average size distribution ranges between 100 to 300 nm (Fig. 1 f and data not shown), presumably for aggregates disassembly deriving from repulsive hydration forces occurring between silanol groups and hydrogen bonded water molecules.[18]

All synthesized MSNs have been preliminarily tested for toxicity in our cellular models. As similarly reported by other authors,[10,13,14] MSNs were clearly non-toxic up to 30 μg/10^6 cells (see ESI Fig.S-6 and data not shown), while higher amounts showed cytostatic effects at later time points (data not shown). Thus, the choice of an adequate range of concentrations is an essential requirement for a proper use of the material. For this reason, in all the experimental procedures we used the maximum non-toxic amount of particles (30 μg/10^6 cells).

To investigate if our MSNs could be internalized by cells, flow cytometry analysis was conducted on MSN-FITC-FOL treated HeLa cells, which express very high levels of FR (Fig. 2a). The degree of endocytosis was determined by quantifying living cells that exhibited green fluorescence due to the FITC dye: only the fluorescence deriving from inside the cells was revealed, since that coming from the outer surface was quenched by trypan blue treatment (see *Experimental*). Our results showed a consistent positive distribution of particles into the cells already after 1 h of incubation, which persisted up to 24 h, while a prolonged exposure (96 h) led to a complete loss of fluorescence, probably due to MSN-FITC-FOL expulsion into the medium, as discussed later (Fig. 2b). Interestingly, in accordance with other authors' observations,[8,10] MSN-FITC were also internalized by cells, with a trend comparable to MSN-FITC-FOL, although to a lesser extent, as emerges from the shift to the left (*i.e.* lower intensity of the fluorescent signal) of the distribution curves at each time point considered (Fig. 2b and c). It can be excluded that the difference in fluorescence intensity could be due to uneven amounts of FITC on the MSN-FITC and MSN-FITC-FOL particles, since the latter derives from the former after an additional step during preparation, thus with comparable saturation of reactive sites (AP sites) by FITC molecules (see ESI, Methods). We postulated that the higher degree of endocytosis of MSN-FITC-FOL, with respect to MSN-FITC, could rather be ascribed to the recognition of the targeting function folic acid on MSN-FITC-FOL by FR and the subsequent internalization of the particles into the cells.

In agreement with these results, our previous confocal microscopy observations showed that both MSN-FITC and MSN-FITC-FOL enter HeLa and MCF-7 cancer cells,[16] regardless of FR cellular content; in fact MCF-7 cells do not express FR, while HeLa cells express very high levels of the receptor (Fig. 2a). Whilst MSN-FITC-FOL were expected to be internalized by HeLa, probably through FR, the presence of MSN-FITC inside both cell lines, led us to hypothesize the existence of a non specific mechanism for MSNs bearing the fluorescent dye, despite the presence of the folic acid function.

To investigate if specific endocytic pathways are activated depending on MSN surface functionalization, we conducted TEM observations on differently functionalized nanoparticles at

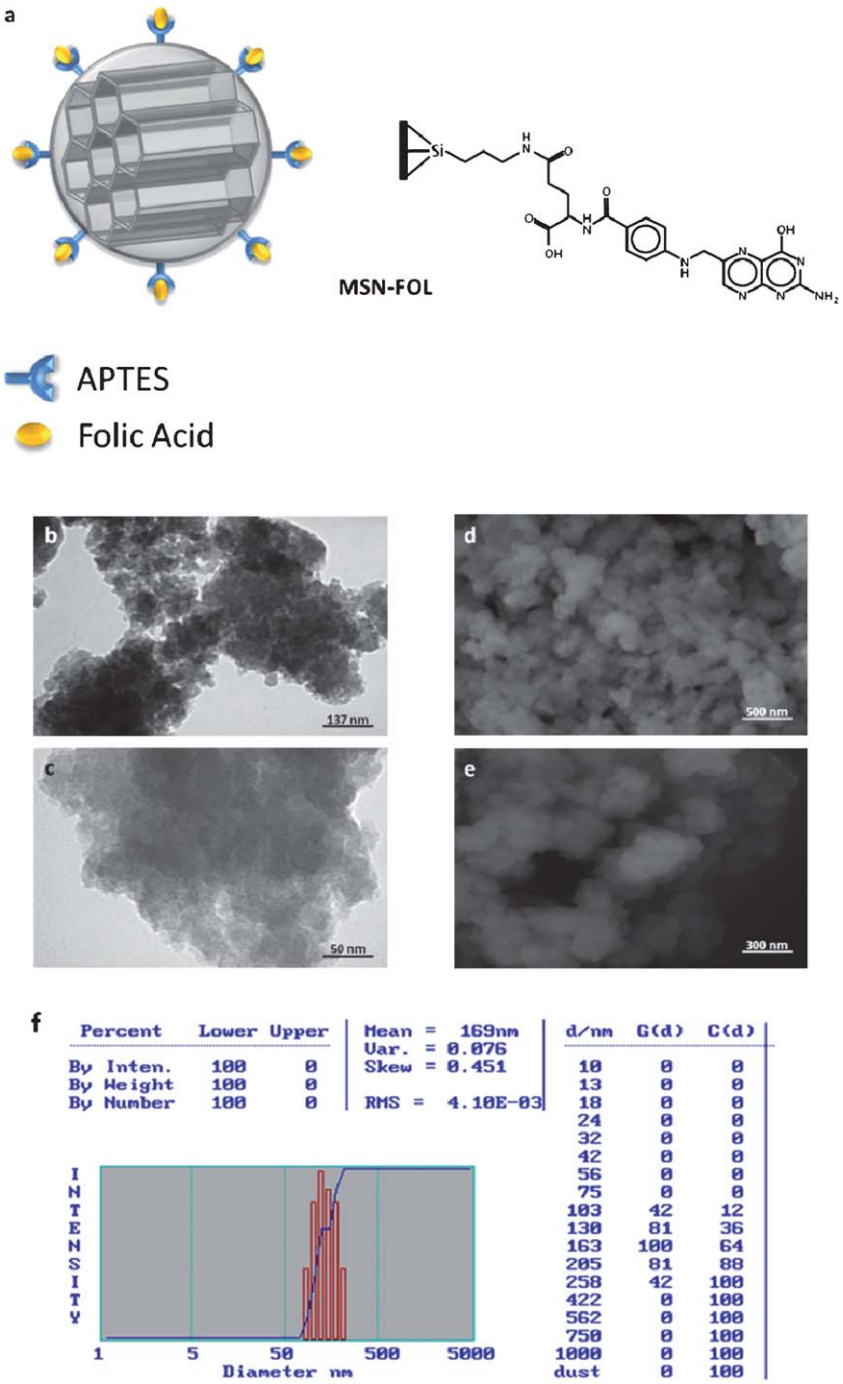

Fig. 1 Folate conjugated mesoporous silica nanoparticles for drug targeting applications. **a**, Schematic representation, **b–c**, TEM and **d–e**, SEM micrographs of MSN-FOL. **f**, 120μg of MSN-FOL were added to 4ml of pure water (30μg ml^{-1} final concentration) and resuspended by gentle stirring; then particle size distribution was determined through DLS.

various time points. Interestingly, MSN never entered HeLa (Fig. 3a), nor other cancerous (T47D, MCF-7 and SKBR3) and normal (HEK293) cell lines (Fig. 3b), indicating that calcined, non functionalized, particles are inert and do not interact with the biological systems. This result corroborates several recent reports, indicating that silanol groups on mesoporous silica nanoparticles tend to establish electrostatic interactions with the lipid head groups of the biological membranes,[19] and such interaction has been proposed to be accountable for particles cellular internalization. We suppose that our MSN do not enter cells most likely because silanol groups condensed upon calcination, thus preventing any possible interaction with membrane surface constituents. On the contrary, extracted particles (MSN-E) were able to enter cells in great amount, confirming that silanol groups are responsible for cellular uptake. However, it is worth mentioning that water suspensions of calcined, non

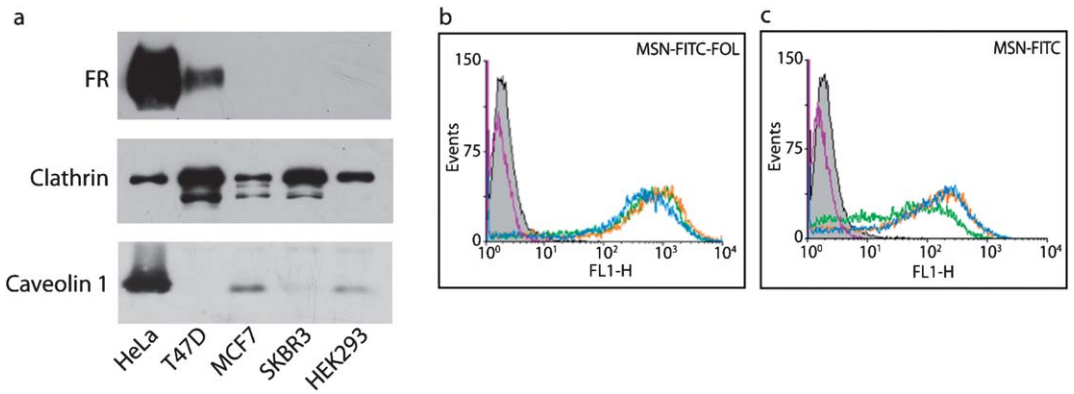

Fig. 2 **a**, Protein expression of FR, clathrin and caveolin-1 in different cell lines. 50 μg of non-denatured proteins from total lysates were loaded and subjected to WB analysis. **b** and **c**, MSN-FITC-FOL and MSN-FITC are internalized by HeLa cancer cells with different dynamics. Flow cytometry assay of HeLa cells incubated with MSN-FITC-FOL (**b**) and MSN-FITC (**c**) for 1 h (green), 6 h (orange), 24 h (blue) and 96 h (violet). Samples were analyzed by measuring the relative fluorescence intensity of FITC per cell at the FL-1H channel. Data were normalized *versus* an untreated control. The results are representative of three independent experiments.

functionalized MSN, did show a particle size distribution similar to MSN-E and to all the other functionalized materials (exemplified by MSN-FOL in Fig. 1f), evidencing the absence of water-induced hydrophobic interactions among calcined particles, which could potentially lead to their assembly into bigger aggregates (DLS data not shown). This means that differences in behaviour of calcined MSN compared to extracted/functionalized MSNs in biological contexts, cannot be ascribed to larger aggregate formation in aqueous suspensions, but only to the differences in their surface functionalization.

Successively, we questioned whether the cellular uptake could be ascribed to electrostatic interactions between the protonated aminopropyl (AP) groups bound to the particles surface and the negatively charged cell membranes. Our results showed that AP groups do not significantly affect the endocytotic process, since only a negligible amount of particles was internalized by the different cell lines (Fig. 3c and Fig. 4).

However, the saturation of AP sites by the folic acid function is sufficient to completely abrogate the already low reactivity of the AP groups. In fact MSN-FOL, where AP sites are mostly bound to folate function, enter only FR expressing HeLa and T47D cells, but cannot enter FR-negative cells (Fig. 2a, 3a–c and Fig. 4b). On the other hand, FITC binding to AP sites allows particles to penetrate only into caveolin-1 (the major constituent of caveolae[20]) expressing cells (Fig. 2a) and in a greater extent, if compared to MSN-AP (Fig. 3c and Fig. 4). Finally, the addition of the folic acid function to MSN-FITC (MSN-FITC-FOL) increases their uptake only in FR expressing HeLa cells (Fig. 3c and Fig. 4).

Moreover, in all cell lines, particle uptake occurs as soon as after 1 h of incubation and the majority of cells appear free of particles within 96 h, clearly underlining MSNs biocompatibility (Fig. 3a, c and data not shown).

As expected, colloidal-gold labelling for FR unambiguously demonstrated that MSN-FOL enter HeLa cells through FR mediated endocytosis. Fig. 3e shows how MSN-FOL A) approach the cell membrane within a region enriched in FR clusters, B) are engulfed through folic acid recognition by FR, C) are internalized by the cell and D) co-localize with FR, most likely in glycosylphosphatidylinositol (GPI) enriched early endosomal compartments, GEECs, as recently proposed.[21] Indeed, a strong FR immunopositive reaction was always evident on the edges of the membranes involved in the overall MSN-FOL endocytic process.

This result was corroborated by the observation that a folic acid excess was able to completely inhibit only MSN-FOL and reduce MSN-FITC-FOL uptake, antagonizing their binding to FR, without influencing the cellular uptake of all the other functionalized MSNs. On the other hand, hyperosmolar sucrose treatment, known to inhibit the clathrin endocytic machinery, did not significantly reduce the internalization of any of the functionalized MSNs, leading to the assumption that clathrin coated pits, though expressed in all cell lines tested (Fig. 2a), are not the preferential route for MSN entry into the cell. Furthermore genistein, an inhibitor of caveolae, selectively reduced MSN-FITC and MSN-FITC-FOL uptake (though the latter could still occur through FR), with no effect on MSN-FOL internalization (Fig. 3d).

These observations where further emphasized by the fact that MSN-FITC, as aforementioned, could not enter caveolin-1 negative cells, such as T47D and SKBR3, while MSN-FITC-FOL only did not enter SKBR3, which lacks both FR and caveolin-1 (Fig. 2a and Fig.4). It is worth underlining that MSN-FOL can enter FR positive, but caveolin-1 negative, T47D cells (Fig. 2a, 3b and Fig. 4b), indicating, as recently suggested,[21] a caveolae independent mechanism for the internalization of GPI-anchored proteins, such as FR. Moreover, confocal microscopy observations confirmed that MSNs neither enter cells through clathrin coated pits, since no merge was found with any of the well characterized markers of this classical endocytic pathway (Rab5, for the early endosomes, Rab7, for late endosomes, and Lamp1, for lysosomes), nor through the Golgi network, which did not seem to be involved in the overall process at all time points tested (see Fig. S-7 in the ESI). These results are in agreement with other author's observations, showing that FITC labelled mesoporous silica nanoparticles can escape from endo-lysosomal vesicles, albeit they report a clathrin-mediated endocytosis for their particles.[22,23] On the other hand recent

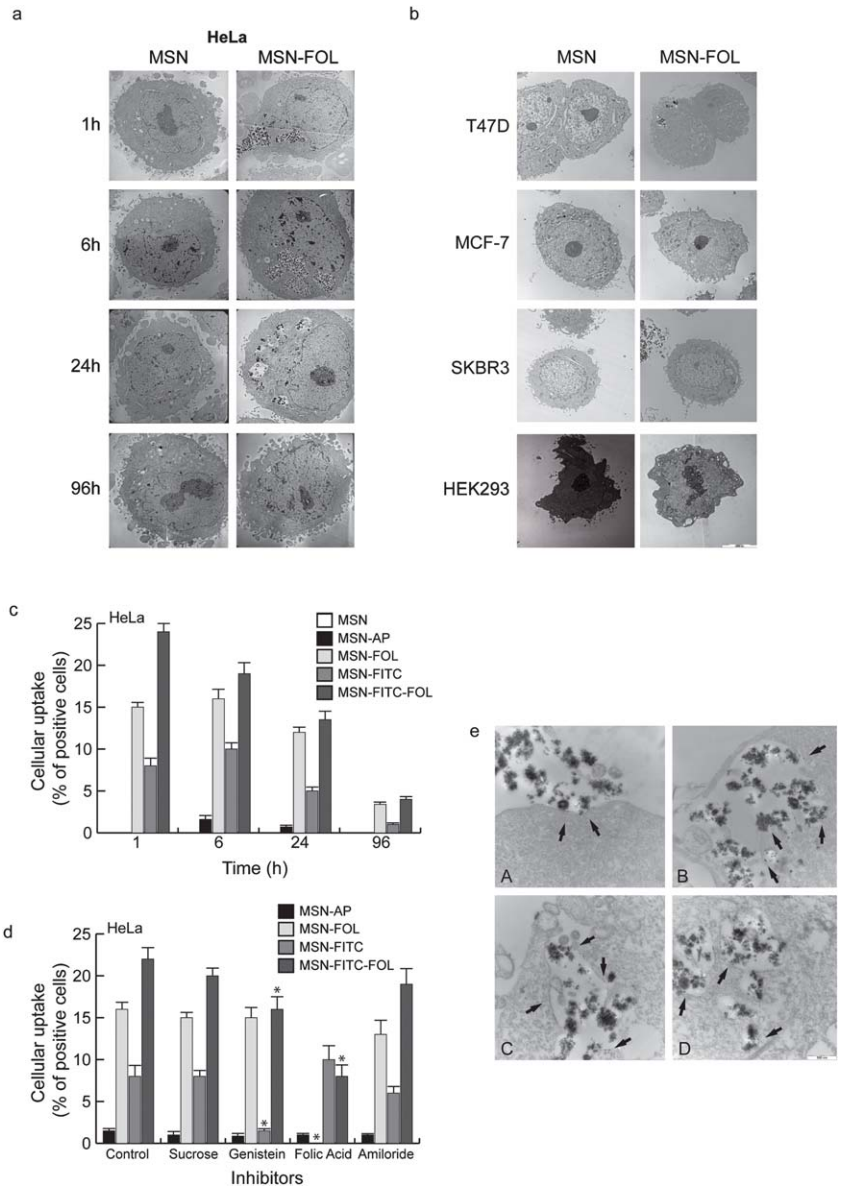

Fig. 3 Effect of functionalization on MSN uptake. TEM investigation of MSN and MSN-FOL uptake in **a**, FR expressing HeLa cells at indicated time points, and **b**, other cells lines at 6 h. Images were taken at 5000× magnification. **c**, time dependent endocytosis of differently functionalized MSNs by HeLa cells (expressed as % of positive cells) and **d**, effect of uptake inhibitors after 6 h of exposure to MSNs (*$p < 0.01$ *vs.* the respective untreated control). See *Experimental* for details on quantitative determination of particle uptake. Values represent the mean ± s.d. of two independent experiments. **e**, Colloidal-gold immunocytochemistry for FR (black dots indicated by arrows) in MSN-FOL treated HeLa cells. Images were taken at 40 000× magnification.

reports from Rosenholm *et al.* showed that their particles remain compartmentalized in endo-lysosomes up to 72 h in HeLa cells.[24] The inconsistency of the data available could reasonably rely on the different nature (*e.g.* size and morphology) of the particles tested in this and the other studies.

Interestingly, although TEM images (Fig. 3e, panel B) suggest that macropinocytosis could represent an additional endocytotic route (other than the FR mediated uptake) used by MSN-FOL to enter cells, inhibition of membrane ruffling (which is an essential feature for macropinosome formation) by the ion exchange inhibitor amiloride, did not lead to any significant decrease in MSN-FOL, nor in MSN-FITC and MSN-FITC-FOL internalization (Fig. 3d).

Once clarified that MSN uptake occurs through specific endocytotic mechanisms, depending on the nature of their functionalization, we questioned whether, once inside, the particles are retained in the cells or rather expelled outside with the elapsing of time. To this aim, we determined the size distribution of particles dispersed in culture medium collected up to 96 h following 1 h treatment of HeLa cells with MSN-FOL. DLS measurements for treated samples after 6 and 24 h did not show any substantial difference from those of control samples (data

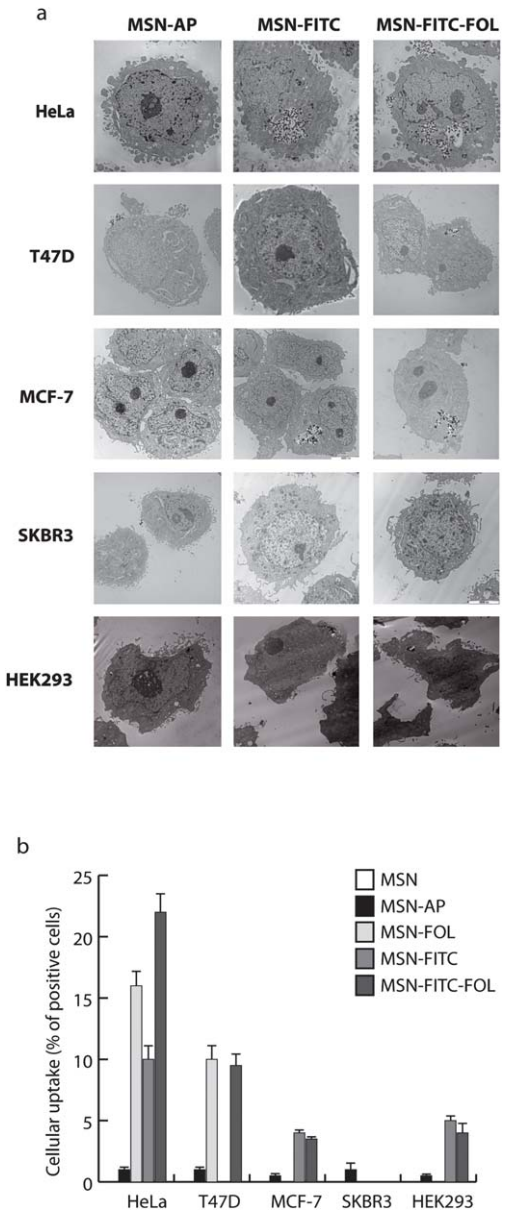

Fig. 4 Effect of functionalization on MSN uptake. **a**, TEM investigation and **b**, quantitative analysis (see *Experimental*) of functionalized MSN uptake in different cells lines after 6 h of incubation. Images were taken at 5000× magnification.

not shown), while sample collected at 48, 72 and 96 h showed comparable particle distributions, ranging around two main peaks at 25 nm and ~250 nm, which were very different respect to non treated control samples (see Fig. S-8 in the ESI and data not shown). These data indicate that most of the particles could be exocytosed from the cells starting from 48 h either as unmodified units (as suggested from the peak around 250 nm, corresponding to the average size of particle aggregates as they are added to the cultures: see Fig. 1f), or as smaller units, probably due to aggregate disassembly (peak around 25nm). On the other hand, we could speculate that the presence of a tail exceeding 250 nm in the particle size distribution could be attributed to aggregate formation in the culture medium,[25] since they do not appear either in control samples or in water suspensions (see Fig. S-8 in the ESI and Fig. 1f). Particle expulsion from the cell is in line with the dramatic drop of MSN positive cells observed at 96 h (Fig. 2b and c and Fig.3a and c).

Finally, to assess if MSN-FOL could represent a reliable tool for drug targeting purposes, we loaded the particles with the chemotherapeutic drug cisplatin (see ESI, Methods), and tested the obtained MSN-FOL-Cp on FR over-expressing HeLa cells and on normal FR negative HEK293 cells. As expected, a strong growth arrest was observed as soon as after one day in MSN-FOL-Cp treated HeLa cells, if compared to the less dramatic growth retardation caused by comparable amounts of free Cp, while, as already shown in Fig. S-6 in the ESI, MSN-FOL did not affect cell proliferation (Fig. 5a). On the contrary, FR-negative HEK293 cells, showed no difference between the growth inhibition observed in MSN-FOL-Cp and free Cp treated samples, with respect to control and MSN-FOL samples (Fig. 5b). Similar results were obtained in other FR negative cells, SKBR3 breast cancer cells and mouse embryonic fibroblast, 3T3L1 (data not shown). These data confirmed our TEM observations, evidencing that folate receptor on HeLa cells mediates the recognition of MSN-FOL and the subsequent endocytosis. Thus, folic acid grafting on the Cp-loaded MSN selectively increases the delivery of the drug to cells that over-express FR, but not to FR-negative cells. Moreover, it is worth underlining that, on the basis of our previous observations,[7] toxicity of MSN-FOL-Cp

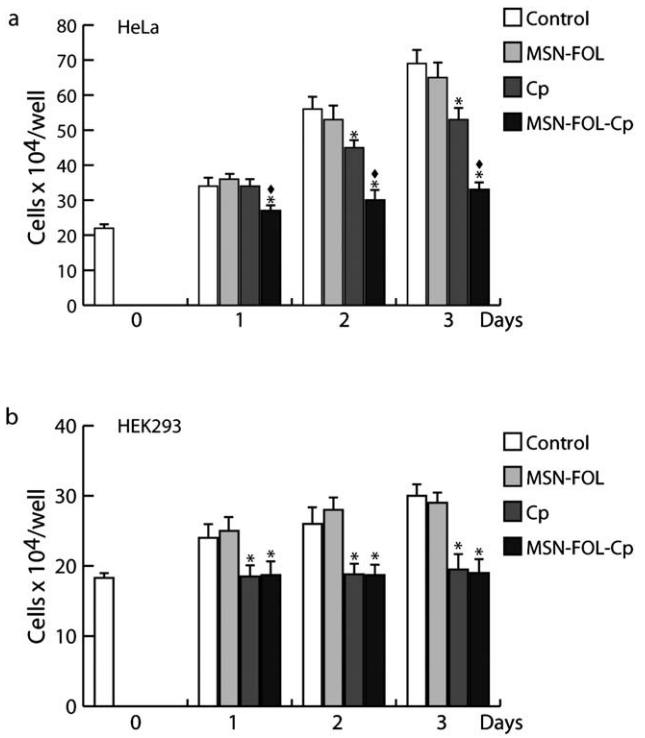

Fig. 5 Cp loaded MSN-FOL inhibit growth in FR-expressing HeLa cancer cells. **a**, cancerous FR+ HeLa and **b**, normal FR- HEK293 cells were separately treated for 1 h with MSN-FOL, Cp alone, MSN-FOL-Cp or left untreated. Viability was determined after 1, 2 or 3 days. Values represent the mean ± s.d. of four triplicate independent experiments. *$p <$ 0.01 *vs.* the respective control; ◆ $p < 0.01$ *vs.* the corresponding free Cp treated samples.

can only in part be ascribed to the release of small amounts of drug in the medium occurring during the 1 h exposure of the cells to the particles. To overcome this inconvenience, as recently reported by Chen *et al.* for doxorubicin,[26] an intracellular pH-sensitive drug delivery device, able to release the drug (covalently bound to the vehicle) once reached the more acidic environment of the endosomal cavities,[27] is currently under development in our laboratories.

Conclusion

All together, our results clearly demonstrate a highly specific, FR mediated, endocytosis for MSNs bearing the folic acid function, and a non specific, caveolae dependent, mechanism for FITC bearing MSNs. As aforementioned, other authors reported that mesoporous silica nanoparticles were found within the cytoplasm of different cell lines,[10,13,22,28] independent of their surface functionalization, thus hampering their potential implementation as a targeting device. Here we propose a system in which the vehicle alone (MSN) is not able to enter cells (or enter in negligible amounts, as for MSN-AP), unless opportunely functionalized. However, since MSN-FITC uptake is not specific, we wouldn't relay on their diagnostic use, *e.g.* in cancer imaging, although they, at least in principle, could passively accumulate at the tumour site on account of the enhanced permeability and retention (EPR) effect.[29]

In conclusion, as schematically illustrated in Fig. 6, our mesoporous silica nanoparticles with controlled size, ranging around 200 nm (Fig. 1f), as required for drug targeting purposes,[30] represent a great potential for localized drug release since they are able to be internalized, in a highly specific way, exclusively by FR over-expressing tumour cells, from where they appear to be mostly exocytosed as soon as after 48 h following particles uptake. The results obtained with drug loaded MSN-FOL encourage us to pursue this aim. In fact the toxic effect of MSN-FOL-Cp is much stronger than free Cp exclusively in FR-expressing cells, while it is comparable in FR negative cells, confirming that the folic acid function is the activator in the cellular uptake process. Ongoing studies in our laboratories are considering other tumour markers for the development of new MSNs based devices against a broader range of tumours.

Experimental

Mesoporous silica nanoparticles

A detailed description of the synthesis and the characterization, as well as the drug loading procedure of MSN is reported in the ESI†.

Materials, cell lines and culture conditions

Human HeLa cervix adenocarcinoma cells and HEK293 embryonic kidney cells (American Type Culture Collection, ATCC) were cultured in Dulbecco's Modified Eagle's Medium (DMEM) supplemented with 10% fetal bovine serum (FBS); human breast cancer cells MCF-7, SKBR3 and T47D (Interlab Cell Line Collection, ICLC, Genova, Italy) were maintained in DMEM:F12 containing 5% FBS (MCF-7) and RPMI medium plus 10% FBS (SKBR3 and T47D). Culture media were supplemented with 100 IU ml^{-1} penicillin, 100 μg ml^{-1} streptomycin, and 0.2 mM L-glutamine. All media and reagents were purchased from Sigma-Aldrich, United Kingdom.

Western blotting

Protein expression of FR, clathrin and caveolin-1 was assessed by Western blotting (WB) using total protein lysates from different cell lines. Cells were plated in growing medium and lysed with RIPA buffer (50 mM Tris-HCl, pH 7.4, 150 mM NaCl, 1% NP-40, 0.25% Na deoxycholate, plus inhibitors). The protein content was determined using Bradford dye reagent (Bio-Rad). 50 μg of non-denatured proteins were run on an 11% polyacrylamide gel and transferred to nitrocellulose membranes. Proteins of interest were detected with specific antibodies (Abs), recognized by peroxidase-coupled secondary Abs, and developed using the ECL Plus Western Blotting detection system (Amersham Pharmacia Biotech, United Kingdom). The primary Ab used for FR detection was anti-human FOLR1 (R&D Systems Inc., USA); for clathrin and caveolin-1 were anti-Clathrin Heavy Chain and anti-Caveolin-1 Abs (Cell Signalling Technology Inc., USA), respectively.

Fluorescence assisted cell sorting (FACS) analysis

To investigate if MSN undergo endocytosis, HeLa cells were seeded on 60 mm tissue culture-treated Petri dishes and incubated at 37 °C in growing medium for 1 h, 6 h, 24 h and 96 h with 30 μg of MSN-FITC or MSN-FITC-FOL/10^6 cells. Cells were then harvested using trypsin, washed three times with phosphate-buffered saline (PBS) and resuspended in cold PBS. Cell fluorescence was measured using a FACS Calibur flow cytometer (Cell Feet software, Becton Dickinson, NJ). A fluorescence quencher, Trypan Blue, was included in the cell suspension, so that only the intracellular fluorescence could be detected, since the dye cannot penetrate the membranes of living cells. At least 1×10^4 cells/sample were measured. Data were normalized *versus* an untreated control.

Transmission electron microscopy (TEM)

Cells were seeded on 60 mm tissue culture-treated Petri dishes and incubated at 37 °C for opportune time points, with MSN-E, MSN-AP, MSN-FOL, MSN-FITC and MSN-FITC-FOL. Endocytic mechanisms were examined by pre-treating cells for 30 min, before adding the particles, either with folic acid (FA) 5 mM (Sigma Aldrich, UK), or each of the following inhibitors: sucrose 100 mM, Genistein 100 μg ml^{-1} or Amiloride 500 μM, all purchased from Sigma Aldrich, UK (inhibitor concentrations were chosen by titration, and the highest non toxic to cells were used). After 6 h of incubation, cells were centrifuged to form a pellet and immediately fixed in 3% glutaraldehyde solution in 0.1 M phosphate buffer (pH. 7.4) for 2 h, postfixed in osmium tetroxide (3%) for 2 h, dehydrated in graded acetone and embedded in Araldite (Fluka, Buchs, Switzerland). Ultrathin sections were collected on 300 mesh copper grids and contrasted using both lead citrate and uranyl acetate and then examined with a "Zeiss EM 900" electron microscope.

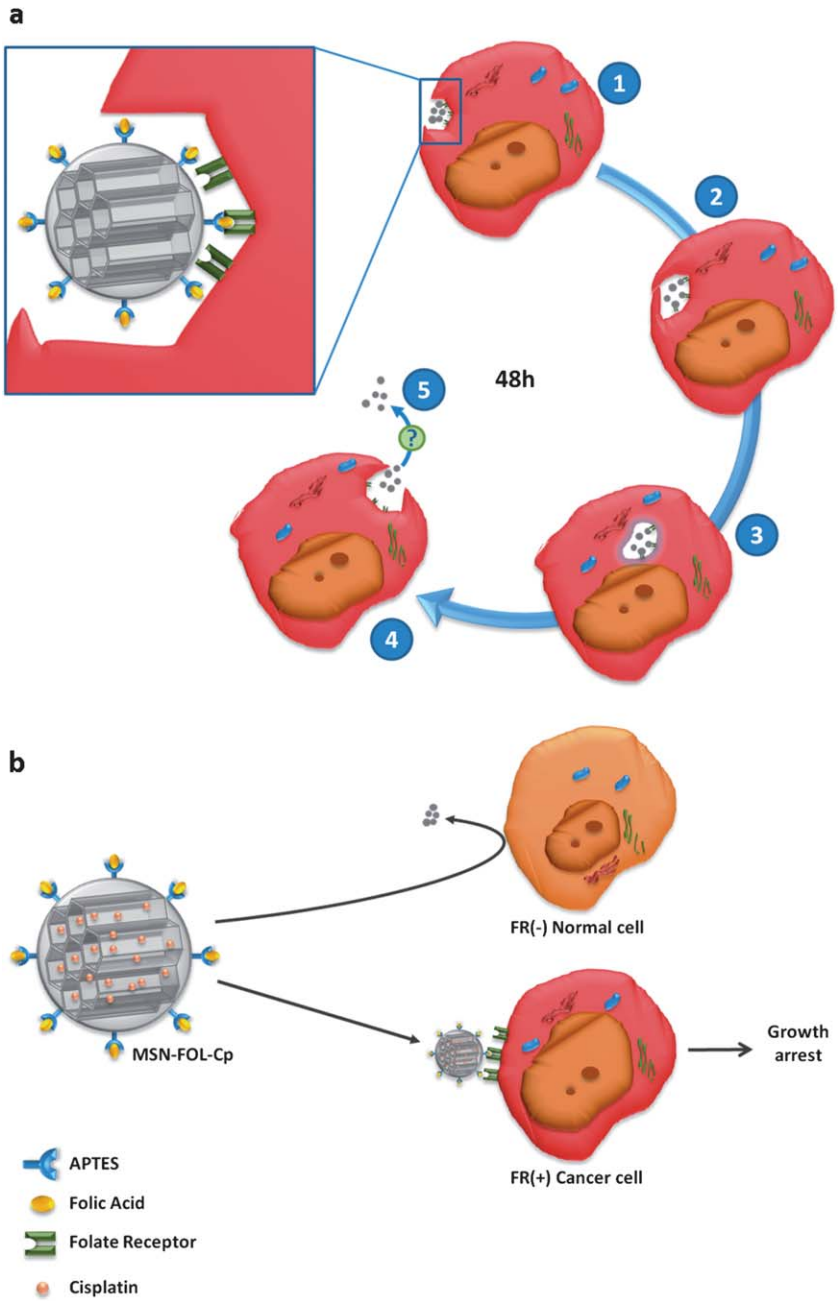

Fig. 6 Schematic representation of MSN-FOL intracellular fate and mechanism of action. **a**, MSN-FOL enter the cell *via* FR mediated endocytosis (1), are sequestered together with FR in endosomal structures (2–3), are probably exocytosed outside the cell starting from 48 h (4–5). **b**, MSN-FOL-Cp do not enter FR-negative cells, and only induce growth arrest in FR-positive cells.

For quantitative determination of particle uptake, positive and negative cells were counted in 150 out of 300 fields for each sample.

Colloidal-gold immunocytochemistry

HeLa cells, seeded on 60 mm tissue culture dishes, were incubated at 37 °C for 30 min with MSN-FOL, and then harvested by trypsin, centrifuged and immediately fixed overnight at 4 °C in 4% paraformaldehyde + 1% glutaraldehyde solution in 0.1 M phosphate buffer (pH. 7.4) and then dehydrated in 30% ethanol (4 °C, 30 min), 50% ethanol (RT, 30 min), 70% ethanol (RT, 1 h), 90% ethanol and absolute ethanol at RT 3 times for each step. Infiltration with LR white acrylic resin (London Resin Company; Berkshire, UK) was carried out using 1 : 1 and then 2 : 1 LR white: ethanol mixtures, followed by pure LR white overnight. The samples were embedded in fresh LR white in gelatine capsules and polymerized for 24 h at 50 °C. Ultrathin sections of the LR-embedded specimens were prepared using a diamond knife and were collected up on formvar-carbon coated nickel grids.

For indirect immunolabelling, the grids with sections were first floated for 15 min on 1% bovine serum albumin (BSA) in PBS, to reduce non-specific binding. Sections were successively incubated

at 4 °C overnight with a mouse monoclonal antibody to FR (R&D Systems), then rinsed with PBS to remove unbound antibody molecules and incubated with 10 nm anti-mouse goat γ-globulin-gold particle complex at a dilution of 1 : 10 for 1 h at room temperature. A non-immune goat serum was used in place of the primary antibody as negative control. After immunolabelling, the sections were washed with PBS, rinsed with distilled water, incubated in 1.25% glutaraldehyde for 3 min, further washed with distilled water, dried, and then stained with uranyl acetate and lead citrate. All sections were examined with a "Zeiss EM 900" electron microscope.

Confocal laser scanning microscopy (CLSM)

For MSN-FITC-FOL tracking through the clathrin endocytic pathway, HeLa cells were transfected in suspension using Lipofectamine 2000 (Invitrogen, Italy) with one the following plasmids, bearing a red-fluorescent tag: mRFP-Rab5, DsRed-rab7 WT and Lamp1-RFP (Addgene, USA), markers for early endosomes, late endosomes and lysosomes, respectively. Cells were then seeded on cover slips in 35 mm Petri dishes, and after 6 h the medium was replaced with fresh growing medium. After additional 48 h, cells were treated for opportune time points with 30 μg/10^6 cells of MSN-FITC-FOL.

For particle tracking through the Golgi network, Organelle Lights, targeting the human Golgi-resident enzyme *N*-acetylgalactosaminyl-transferase 2, was used, following the manufacturer's instructions (Molecular Probes, Invitrogen, Italy). MSN-FITC-FOL were then added for different time points. Following treatment, cells were fixed in 4% paraformaldehyde, washed 3 times with PBS, and mounted with Fluoromount aqueous mounting medium (Sigma, Italy). The cellular localization of MSM-FITC-FOL, was examined under a Leica TCS SP2 Confocal Laser Scanning Microscope at 6000× magnification. The fluorophores were imaged separately to ensure no excitation/emission wavelength overlap.

Dynamic light scattering (DLS)

Changes in size distribution of the nanoparticles have been determined by means of dynamic light scattering experiments. In short, the linearly polarized light beam of a 35 mW HeNe laser (Spectra Physics mod. 127) has been focused by a 300 mm focal length lens on the sample cell, which consists of a quartz cylindrical cuvette (2 cm inner diameter). The autocorrelation functions of the scattered light have been constructed by a Brookhaven Instruments 2030AT digital correlator processing the photocurrent pulse produced by a 9863A Thorn-EMI photomultiplier with built-in amplifier-discriminator. Light was collected at a fixed scattering angle of 90°, a light collimator with a 50 μm pin-hole allowed us to operate always with at least one coherence in the regime of pure homodyne detection. The autocorrelation function has been Laplace inverted by the CONTIN routine.

Cell viability

The effect of cisplatin (Cp) loaded MSN on cell proliferation was assessed by trypan blue exclusion assay. HeLa cells in the exponential growth phase were plated in growing medium in 12-well plates at a concentration of 10^5 cells/well and grown overnight. The following day, cells were synchronized in serum free media (SFM) for 24 h, so that most of the cells belonged to a population in the same cell cycle phase, to avoid growth differences among cells. Following starvation, MSN-FOL, free Cp (0,5 μg/10^5 cells) or MSN-FOL-Cp (1 μg/10^5 cells, bearing ~0.5 μg of Cp, since the amount of Cp detected in MSN-Fol-Cp material resulted to be 48.8% in weight) were added to the cells for 1 h; the medium was then replaced with fresh medium plus 1% FBS and after 1, 2 or 3 days, cells were harvested by trypsinization and incubated in a 0.5% trypan blue solution for 10 min at room temperature. Cell viability was determined microscopically by counting trypan blue negative cells in a hemacytometer (Burker, Brand, Germany).

Acknowledgements

Financial support has been provided by: PRIN (Progetti di Ricerca di Interesse Nazionale) 2007- Prot. 2007N9A3A4_002), AIRC (Associazione Italiana Ricerca Cancro) grants, MIUR Ex 60% - 2009. We thank Desiderio Giovanni (LICRYL – Liquid Crystal Laboratory CNR-IPCF) for precious help during ESEM measurements.

References

1 L. H. Reddy, Drug delivery to tumours: recent strategies, *J. Pharm. Pharmacol.*, 2005, **57**, 1231–42.
2 S. Jaracz, J. Chen, L. V. Kuznetsova and I. Ojima, Recent advances in tumor-targeting anticancer drug conjugates, *Bioorg. Med. Chem.*, 2005, **13**, 5043–54.
3 A. R. Hilgenbrink and P. S. Low, Folate receptor-mediated drug targeting: from therapeutics to diagnostics, *J. Pharm. Sci.*, 2005, **94**, 2135–46.
4 B. A. Kamen and A. Capdevila, Receptor-mediated folate accumulation is regulated by the cellular folate content, *Proc. Natl. Acad. Sci. U. S. A.*, 1986, **83**, 5983–7; C. P. Leamon and P. S. Low, Delivery of macromolecules into living cells: a method that exploits folate receptor endocytosis, *Proc. Natl. Acad. Sci. U. S. A.*, 1991, **88**, 5572–6.
5 B. A. Kamen and A. K. Smith, A review of folate receptor alpha cycling and 5-methyltetrahydrofolate accumulation with an emphasis on cell models *in vitro*, *Adv. Drug Delivery Rev.*, 2004, **56**, 1085–97.
6 P. S. Low and A. C. Antony, Folate receptor-targeted drugs for cancer and inflammatory diseases, *Adv. Drug Delivery Rev.*, 2004, **56**, 1057–1238.
7 L. Pasqua, F. Testa, R. Aiello, S. Cundari and J. B. Nagy, Preparation of bifunctional hybrid mesoporous silica potentially useful for drug targeting, *Microporous Mesoporous Mater.*, 2007, **103**, 166–173.
8 Y. S. Lin, C. P. Tsai, H. Y. Huang, C. T. Kuo, Y. Hung, D. M. Huang, Y. C. Chen and C. Y. Mou, Well-ordered mesoporous silica nanoparticles as cell markers, *Chem. Mater.*, 2005, **17**, 4570–4573.
9 V. Lebret, L. Raehm, J. O. Durand, M. Smaihi, M. H. V. Werts, M. Blanchard-Desce, D. Methy-Gonnod and C. Dubernet, Surface functionalization of two-photon dye-doped mesoporous silica nanoparticles with folic acid: cytotoxicity studies with HeLa and MCF-7 cancer cells, *J. Sol-Gel Sci. Technol.*, 2008, **48**, 32–39; V. Lebret, L. Raehm, J. O. Durand, M. Smaihi, M. H. V. Werts, M. Blanchard-Desce, D. Methy-Gonnod and C. Dubernet, Folic Acid-Targeted Mesoporous Silica Nanoparticles for Two-Photon Fluorescence, *J. Biomed. Nanotechnol.*, 2010, **6**, 176–180.
10 I. Slowing, B. G. Trewyn and V. S. Lin, Effect of surface functionalization of MCM-41-type mesoporous silica nanoparticles on the endocytosis by human cancer cells, *J. Am. Chem. Soc.*, 2006, **128**, 14792–3.

11 M. Liong, J. Lu, M. Kovochich, T. Xia, S. G. Ruehm, A. E. Nel, F. Tamanoi and J. I. Zink, Multifunctional inorganic nanoparticles for imaging, targeting, and drug delivery, *ACS Nano*, 2008, **2**, 889–96.
12 H. X. Wu, G. Liu, S. J. Zhang, J. L. Shi, L. X. Zhang, Y. Chen, F. Chen and H. R. Chen, Biocompatibility, MR imaging and targeted drug delivery of a rattle-type magnetic mesoporous silica nanosphere system conjugated with PEG and cancer-cell-specific ligands, *J. Mater. Chem.*, 2011, **21**, 3037–3045.
13 J. M. Rosenholm, A. Meinander, E. Peuhu, R. Niemi, J. E. Eriksson, C. Sahlgren and M. Linden, Targeting of porous hybrid silica nanoparticles to cancer cells, *ACS Nano*, 2009, **3**, 197–206.
14 J. Lu, M. Liong, Z. Li, J. I. Zink and F. Tamanoi, Biocompatibility, biodistribution, and drug-delivery efficiency of mesoporous silica nanoparticles for cancer therapy in animals, *Small*, 2010, **6**, 1794–805.
15 Z. Tao, B. Toms, J. Goodisman and T. Asefa, Mesoporous silica microparticles enhance the cytotoxicity of anticancer platinum drugs, *ACS Nano*, 2010, **4**, 789–94.
16 L. Pasqua, C. Morelli, F. Testa, D. Sisci, E. Brunelli, R. Aiello, S. Andò and J. B. Nagy, Preparation and cell inclusion of fluorescent folic acid functionalized mesoporous silica microspheres potentially useful for drug targeting, *Stud. Surf. Sci. Catal.*, 2007, **170**, 1956–1962.
17 S. A. Bagshaw, E. Prouzet and T. J. Pinnavaia, Templating of mesoporous molecular sieves by nonionic polyethylene oxide surfactants, *Science*, 1995, **269**, 1242–4.
18 L. Gunther and W. Peukert, The relevance of interactions in nanoparticle systems - Application to particulate thin films, *Part. Part. Syst. Charact.*, 2002, **19**, 312–320.
19 Y. Roiter, M. Ornatska, A. R. Rammohan, J. Balakrishnan, D. R. Heine and S. Minko, Interaction of nanoparticles with lipid membrane, *Nano Lett.*, 2008, **8**, 941–4; I. I. Slowing, C. W. Wu, J. L. Vivero-Escoto and V. S. Lin, Mesoporous silica nanoparticles for reducing hemolytic activity towards mammalian red blood cells, *Small*, 2009, **5**, 57–62.
20 B. Nichols, Caveosomes and endocytosis of lipid rafts, *J. Cell Sci.*, 2003, **116**, 4707–14.
21 P. Bhagatji, R. Leventis, J. Comeau, M. Refaei and J. R. Silvius, Steric and not structure-specific factors dictate the endocytic mechanism of glycosylphosphatidylinositol-anchored proteins, *J Cell Biol*, 2009, **186**, 615–28.
22 D. M. Huang, Y. Hung, B. S. Ko, S. C. Hsu, W. H. Chen, C. L. Chien, C. P. Tsai, C. T. Kuo, J. C. Kang, C. S. Yang, C. Y. Mou and Y. C. Chen, Highly efficient cellular labeling of mesoporous nanoparticles in human mesenchymal stem cells: implication for stem cell tracking, *FASEB J.*, 2005, **19**, 2014.
23 M. Fisichella, H. Dabboue, S. Bhattacharyya, G. Lelong, M. L. Saboungi, F. Warmont, P. Midoux, C. Pichon, M. Guerin, T. Hevor and J. P. Salvetat, Uptake of Functionalized Mesoporous Silica Nanoparticles by Human Cancer Cells, *J. Nanosci. Nanotechnol.*, 2010, **10**, 2314–2324.
24 J. M. Rosenholm, E. Peuhu, L. T. Bate-Eya, J. E. Eriksson, C. Sahlgren and M. Linden, Cancer-cell-specific induction of apoptosis using mesoporous silica nanoparticles as drug-delivery vectors, *Small*, 2010, **6**, 1234–41.
25 Q. He, J. Zhang, J. Shi, Z. Zhu, L. Zhang, W. Bu, L. Guo and Y. Chen, The effect of PEGylation of mesoporous silica nanoparticles on nonspecific binding of serum proteins and cellular responses, *Biomaterials*, 2010, **31**, 1085–92.
26 F. H. Chen, L. M. Zhang, Q. T. Chen, Y. Zhang and Z. J. Zhang, Synthesis of a novel magnetic drug delivery system composed of doxorubicin-conjugated Fe3O4 nanoparticle cores and a PEG-functionalized porous silica shell, *Chem. Commun.*, 2010, **46**, 8633–8635.
27 S. Mukherjee, R. N. Ghosh and F. R. Maxfield, *Endocytosis. Physiol Rev*, 1997, **77**, 759–803.
28 I. I. Slowing, B. G. Trewyn and V. S. Lin, Mesoporous silica nanoparticles for intracellular delivery of membrane-impermeable proteins, *J. Am. Chem. Soc.*, 2007, **129**, 8845–9.
29 H. Maeda, J. Wu, T. Sawa, Y. Matsumura and K. Hori, Tumor vascular permeability and the EPR effect in macromolecular therapeutics: a review, *J. Controlled Release*, 2000, **65**, 271–84.
30 B. Borak, J. Arkowski, M. Skrzypiec, P. Ziolkowski, B. Krajewska, M. Wawrzynska, B. Grotthus, H. Gliniak, A. Szelag, W. Mazurek, D. Bialy and K. Maruszewski, Behavior of silica particles introduced into an isolated rat heart as potential drug carriers, *Biomed. Mater.*, 2007, **2**, 220–3.

MOLECULAR AND CELLULAR BIOLOGY, Feb. 2010, p. 857–870 Vol. 30, No. 3
0270-7306/10/$12.00 doi:10.1128/MCB.00824-09

Akt2 Inhibition Enables the Forkhead Transcription Factor FoxO3a To Have a Repressive Role in Estrogen Receptor α Transcriptional Activity in Breast Cancer Cells▽

Catia Morelli,[1] Marilena Lanzino,[1] Cecilia Garofalo,[1] Pamela Maris,[1] Elvira Brunelli,[3] Ivan Casaburi,[1] Stefania Catalano,[1] Rosalinda Bruno,[1] Diego Sisci,[1]*† and Sebastiano Andò[2]*†

Department of Pharmaco-Biology,[1] Department of Ecology,[3] and Department of Cell Biology,[2] University of Calabria, 87036 Arcavacata di Rende (CS), Italy

Received 24 June 2009/Returned for modification 23 July 2009/Accepted 16 November 2009

Estrogen receptor alpha (ER) and the insulin-like growth factor I receptor (IGF-IR) pathways are engaged in a functional cross talk in breast cancer, promoting tumor progression and increased resistance to anticancer treatments and radiotherapy. Here, we introduce new mechanisms through which proteins of the IGF-I/IGF-IR signaling pathway may regulate ER function in the absence of ligand. Our results indicate that in ER-positive breast cancer cells, Akt2 modulates ER transcriptional activity at multiple levels, including (i) the regulation of ER expression and its nuclear retention and (ii) the activation of one of its downstream targets, the Forkhead transcription factor FoxO3a. FoxO3a colocalizes and coprecipitates with ER in the nucleus, where it binds to Forkhead-responsive sequences on the ER target pS2/*TFF-1* promoter; in addition, FoxO3a silencing leads to an increase of ER transcriptional activity, suggesting a repressive role of the Forkhead transcription factor in ER function. Moreover, 17β-estradiol upregulates FoxO3a levels, which could represent the basis for an ER-mediated homeostatic mechanism. These findings provide further evidence of the importance of mediators of the growth factor signaling in ER regulation, introducing the Akt2/FoxO3a axis as a pursuable target in therapy for ER-positive breast cancer.

Ovarian steroids are essential for the development, proliferation, and differentiation of normal human breast tissue (2). Cell response to 17β-estradiol (E2) is mostly mediated through estrogen receptor alpha (ER) (14), although E2 can elicit physiological events that are independent of ER (57, 60). ER is expressed at low levels in normal human mammary epithelial cells and is absent in stromal cells. However, during breast cancer development, the number of cells expressing ER and the abundance of this receptor tend to increase (48). The causative role of ER in the development of breast cancer has been substantiated by numerous *in vivo* and *in vitro* studies that documented the ability of estrogens to stimulate proliferation and differentiation in normal and cancerous mammary epithelium (24, 42). The analysis of clinical samples indicated that more than 60% of breast tumors express ER (13, 25). ER expression (i) has been defined as a marker for breast cancer diagnosis and prognosis (50), (ii) is correlated with a higher degree of tumor differentiation (35, 38), (iii) increases disease-free survival (41), and (iv) is a target for antiestrogen therapy and prevention.

In breast cancer, the expression and/or activity of specific growth factor receptors, such as the insulin-like growth factor receptor or epidermal growth factor receptor family members, including EGFR and Her-2/neu (6, 29, 44), is inversely related to ER expression and activity (16, 27, 59) and confers E2-independent growth properties (23) and antiestrogen resistance (21, 26).

Growth factors have been shown to enhance the transcriptional activity of ER in a ligand-independent manner through activation of mitogen-activated protein kinase (MAPK) or the phosphatidylinositol 3-kinase (PI3-K)/Akt pathway (23, 53, 55). In human breast cancers, PI3-K/Akt signaling is frequently deregulated either by loss of the suppressor protein PTEN or by the expression of active isoforms of PI3-K or downstream elements, such as Akt and mTOR (7).

Akt is known to play an important role in controlling cell proliferation, survival, and inhibition of apoptosis (22). Akt is a serine/threonine kinase belonging to the AGC superfamily. The Akt family is composed of three closely related isoforms, Akt1, Akt2 and Akt3, which are expressed at the mRNA level by virtually all normal human tissues (21, 64).

Since tumorigenesis has been reported not to involve a dramatic change in the RNA expression patterns of the three AKT isoforms, it has been proposed that differences in the Akt1, -2, and-3 kinase activities may be more important in clinical disease (64). For instance, elevated Akt1 kinase activity has been detected in primary tumors of the breast, prostate, and ovary (52, 56); sustained Akt2 kinase activity has been reported in breast and ovarian carcinomas (52, 55, 61); while the expression levels of Akt3 have been shown to be upregulated in ER-negative breast cancer tumors (40).

Recently, the Forkhead box class O (FoxO) family members transcription factors FoxO1a, FoxO3a, FoxO4 (formerly FKHR, FKHRL1, and AFX, respectively), and the more recent FoxO6 (20) have been identified as targets of the PI-3K/

* Corresponding author. Mailing address for Sebastiano Andò: Dipartimento di Biologia Cellulare, Università della Calabria, 87036 Arcavacata di Rende (CS), Italy. Phone: 39 0984 493110. Fax: 39 0984 492911. E-mail: sebastiano.ando@unical.it. Mailing address for Diego Sisci: Dipartimento Farmaco-Biologico, Università della Calabria, 87036 Arcavacata di Rende (CS), Italy. Phone: 39 0984 496211. Fax: 39 0984 496203. E-mail: dsisci@unical.it.

† D.S. and S.A. contributed equally to this study.

▽ Published ahead of print on 23 November 2009.

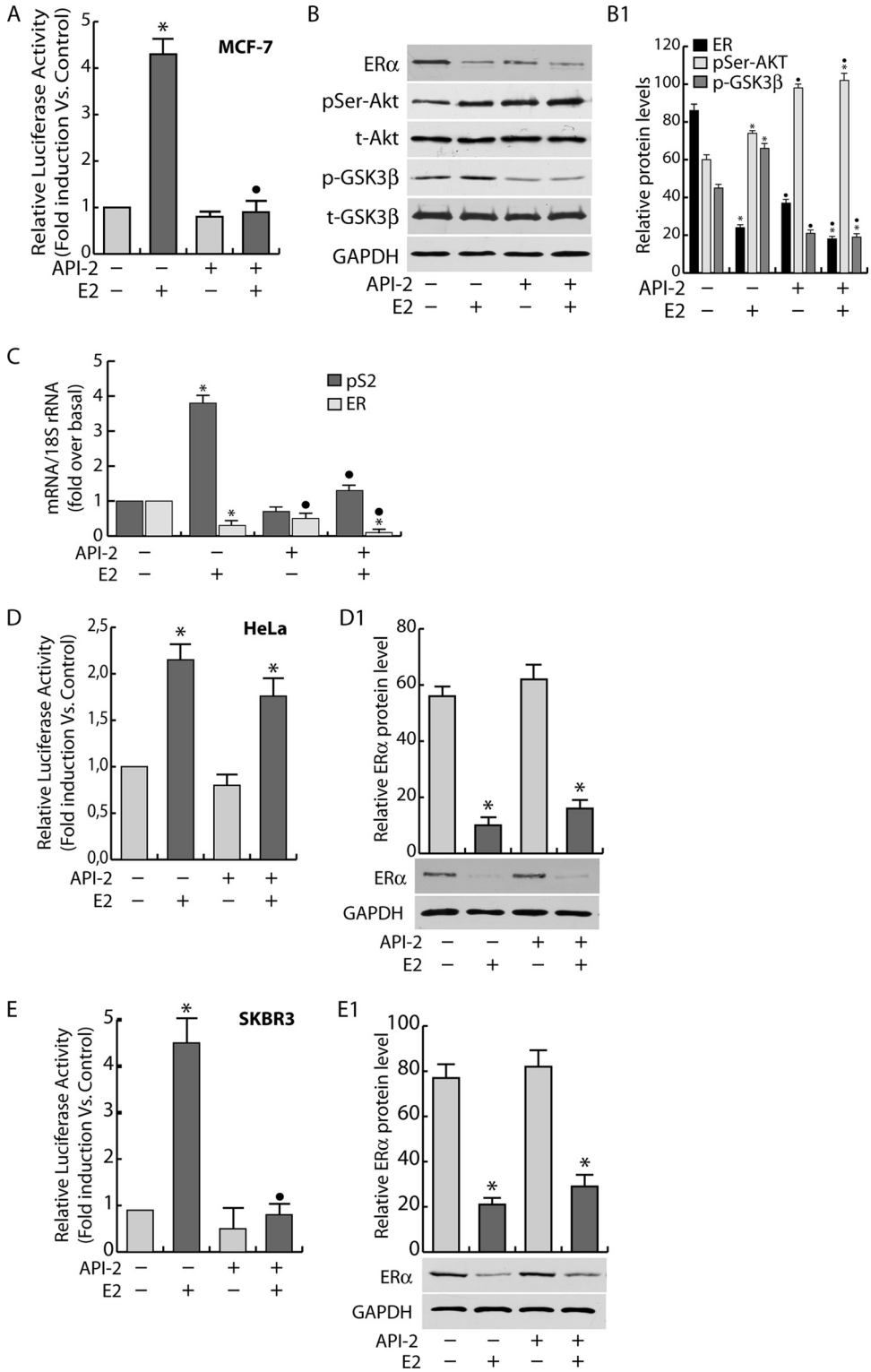

FIG. 1. Akt inhibition decreases ER transcriptional activity. (A) MCF-7 cells were transfected with a mixture of XETL (1 μg/well) and pRL-Tk (50 ng/well) plasmids for 6 h. The medium was then replaced with fresh PRF-SFM, and the cells were pretreated with 1 μM API-2 for 1 h or left untreated and then stimulated with 100 nM E2 for an additional 16 h. Firefly luciferase was detected and expressed as relative luciferase activity with respect to the untreated samples (fold induction versus the control). (B) The whole-cell lysates obtained were then collected and analyzed by WB using specific Abs. (C) MCF-7 cells were treated as in panel A; total RNA was extracted, and the abundance of pS2 and ER mRNAs was detected in real time, as described in Materials and Methods. Each sample was normalized to its 18S rRNA content. (D and E) HeLa and SKBR3 cells were transfected with a mixture of XETL (0.5 μg/well), HeG0 (0.5 μg/well), and pRL-Tk (50 ng/well) plasmids for 6 h and then treated as in panel A. (D1 and E1) The ER content in total lysates. (B1, D1, and E1) Densitometric analysis of protein levels reported as means ± SD of samples normalized over GAPDH. In all experiments, significance values were as follows: *, $P < 0.05$ versus non-E2-treated samples; ●, $P < 0.05$ versus the corresponding non-API-2-treated samples.

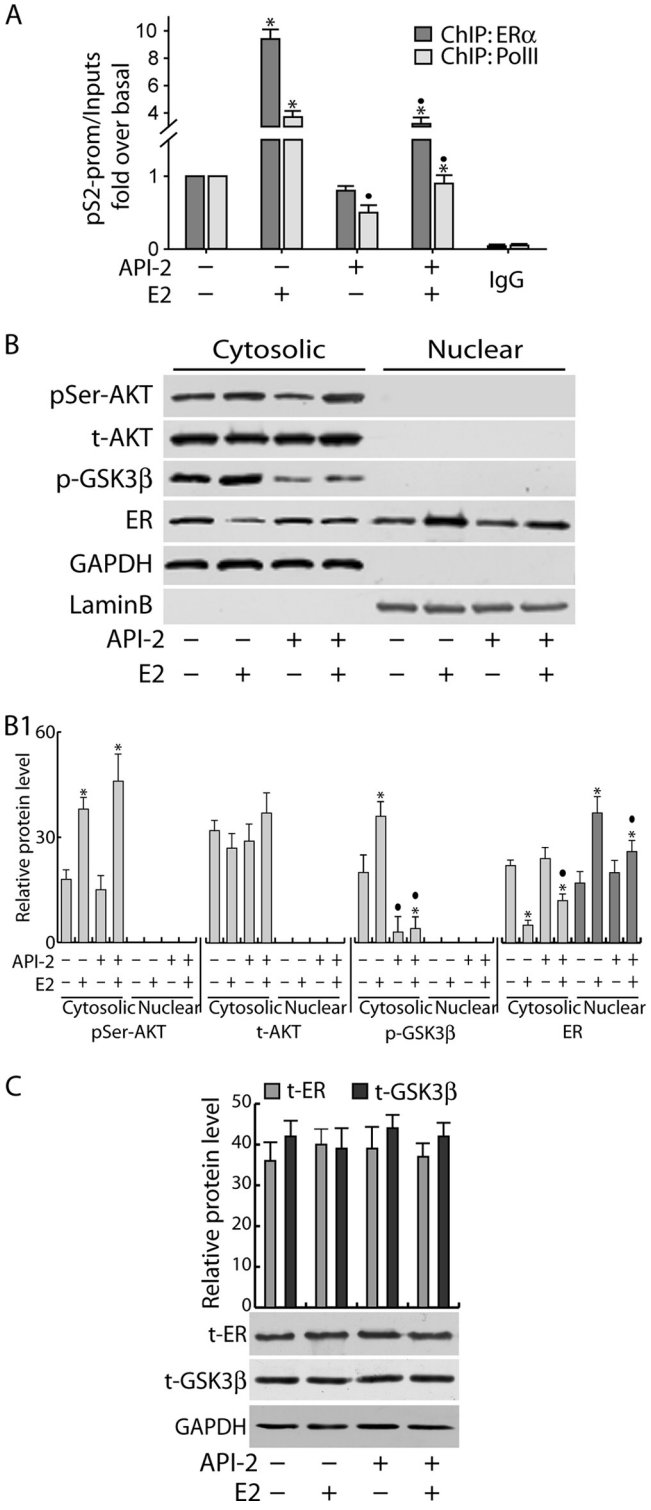

FIG. 2. Short-term Akt inhibition affects ER retention in the nucleus. (A) MCF-7 cells synchronized in PRF-SFM for 24 h were pretreated with API-2 for 1 h and then treated with 100 nM E2 or left untreated for 45 min. Then, samples were processed for ChIP analysis as described in Materials and Methods. The ERE-containing pS2 promoter region was amplified using a specific pair of primers (data available on request). A mixture of normal rabbit IgG and normal mouse IgG was used as a negative control for both primary Abs to precipitate the E2-treated samples. (B) MCF-7 cells were serum starved for 24 h, pretreated for 1 h with API-2, and then treated with 100 nM E2 for 5 min or left untreated. Cytoplasmic and nuclear protein extracts were collected as described in Materials and Methods and subjected to WB (50 μg/lane) using different Abs. (B1) The relative protein levels were analyzed, and the optical density is reported. (C) MCF-7 cells were treated as in panel B, and total protein extracts were collected with RIPA buffer (see Materials and Methods) and processed by WB. Samples were normalized over input (A), GAPDH (for cytosolic proteins [B] and total proteins [C]), and lamin B (for nuclear proteins [B]). In all experiments, significance values were as follows: ∗, $P < 0.05$ versus non-E2-treated samples; ●, $P < 0.05$ versus the corresponding non-API-2-treated samples. The error bars indicate SD.

Akt pathway (8). Some reports showed evidence that the overexpression of any of these Forkhead transcription factors induced either cell cycle arrest or apoptosis (1, 8, 39, 45). Activation of PI-3K controls cell cycle entry by inactivating FoxO factors, which have been shown to regulate expression of p27/Kip1 (36), cyclin D1, and cyclin E (46). FoxO transcription factors have been shown to be functional in mammary cells and to be regulated by Akt (19); in fact, Akt-phosphorylated FoxO binds to 14-3-3 proteins, and the complex is translocated from the nucleus to the cytoplasm (8). When hypophosphorylated, Forkhead proteins are released from 14-3-3 and translocate into the nucleus, where they transactivate specific proapoptotic target genes (36, 47, 54). Recently, several reports have suggested a functional interaction between ER and FoxO members. E2 has been noted to determine ER binding to FKHR, FKHRL1, and AFX (49, 62, 65) and to induce FKHR phosphorylation in breast cancer cells (34). Particularly, E2-dependent ER binding to FKHR seems to be involved in ER nucleocytoplasmic shuttling, since site-directed mutagenesis of the ER nuclear export sequence inhibits FKHR nuclear export, the estradiol-induced cytoplasmic relocalization of receptor, and DNA synthesis (33). In transient-transfection experiments, FoxO members seemed also to regulate ER-mediated transcription, showing either coactivator or corepressor functions on estrogen-responsive element (ERE) sites, depending on the cellular model (49, 62, 65). Additionally, FoxO3a has recently been reported to suppress cell growth and tumorigenesis in breast cancer cells and in an orthotopic mouse model of breast cancer (65).

The aim of this study was to better elucidate the molecular mechanisms underlying the regulation exerted by the Akt/FoxO axis on ER in human breast cancer cells.

MATERIALS AND METHODS

Cell culture, conditions, and treatments. The ER-positive human breast cancer epithelial cell line MCF-7 was maintained in monolayer culture in Dulbecco's modified Eagle's/Ham's F-12 medium (1:1) (DMEM/F-12), supplemented with 5% fetal bovine serum (FBS) and 1% Eagle's nonessential amino acids. Human cervical cancer (HeLa) cells (ATCC, United Kingdom) were grown in modified Eagle's medium (MEM) containing 10% calf serum, and human breast cancer (SKBR3) cells (ATCC, United Kingdom) were cultured in RPMI medium plus 10% FBS. Additionally, culture media were supplemented with 100 IU/ml penicillin, 100 μg/ml streptomycin, and 0.2 mM L-glutamine (all media and reagents were purchased from Sigma-Aldrich, United Kingdom).

For experimental purposes, cells were synchronized in phenol red-free and serum-free DMEM/F-12 (PRF-SFM) (Sigma-Aldrich, United Kingdom) for 24 h in the absence of steroids and growth factors. Following starvation, the cells were pretreated or not with 1 μM API-2 (triciribine; Calbiochem), an inhibitor of Akt activity, for 1 h and then treated with 100 nM E2 (Sigma) for 5 min (for Western

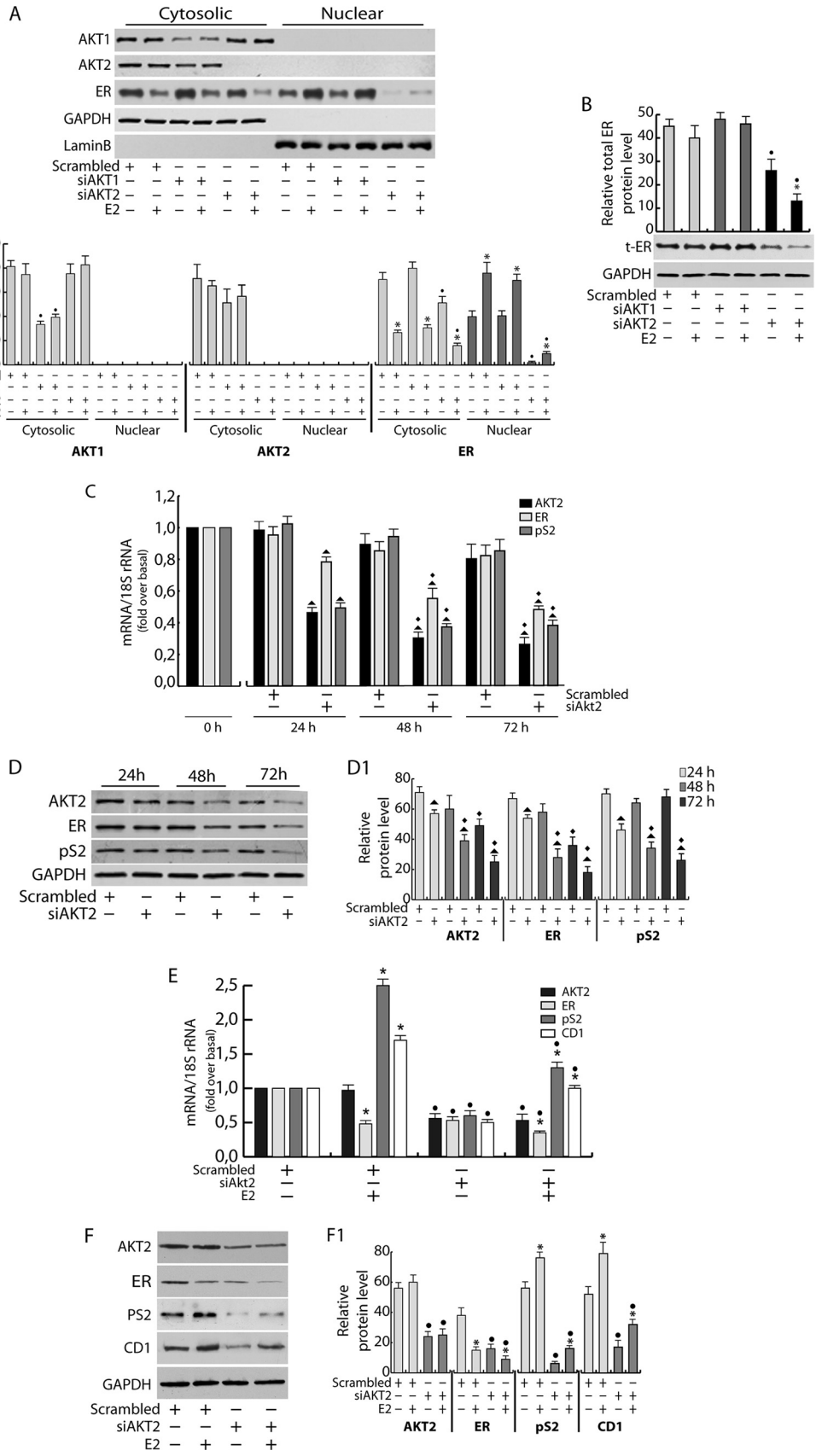

blotting [WB]) or 45 min (for chromatin immunoprecipitation [ChIP] and DNA affinity precipitation assays) and 16 h (gene reporter assay and reverse transcription [RT]-PCR).

Plasmids, transfections, and ERE-luciferase assay. The following plasmids were used: the reporter plasmid XETL, driving the expression of firefly luciferase by an ERE from the *Xenopus* vitellogenin promoter (9); pS2/*TFF-1*-ERE (pS2-ERE) containing a 1,050-bp fragment of the pS2 promoter preceding the luciferase reporter of pGL3 (5); pSG5-HeG0, a simian virus 40 (SV40) promoter-based pSG5 vector encoding wild-type ER (HeG0) (56a); the *Renilla reniformis* luciferase expression vector pRL-Tk, used to assess transfection efficiency (Promega); and pECE-HA-FoxO3a (HA-FoxO3a) WT, encoding wild-type FoxO3a (Addgene plasmid 1787).

To monitor the effect of API-2 on ER transactivation, MCF-7, HeLa, and SKBR3 cells (density, 5×10^4) were plated on 24-well plates, grown in culture medium to an approximate confluence of 70 to 80%, and then switched to PRF-SFM and cotransfected with XETL and pRL-Tk (MCF-7) or XETL, pRL-Tk, and HeG0 (HeLa and SKBR3). All the transfections were carried out using Fugene 6 (Roche) (DNA/Fugene ratio, 3:1). After 6 h, the medium was replaced with fresh PRF-SFM, and the cells were pretreated for 1 h with 1 μM API-2 (triciribine; Calbiochem) and then treated for 16 h with 100 nM E2 (Sigma-Aldrich, United Kingdom).

To evaluate the effect of FoxO3a on ER transactivation, FoxO3a was either silenced for 24 h with FoxO3a small interfering RNA (siRNA) (Invitrogen) or overexpressed using hemagglutinin (HA)-FoxO3a WT and then cotransfected with pRL-Tk and XETL or pRL-Tk and pS2-ERE and exposed to 100 nM E2 for 16 h. Luciferase activity was measured using the dual-luciferase assay system (Promega), normalized to pRL-Tk activity, and expressed as fold induction over the control. Cell extracts were also processed by Western blot analysis and/or RT-PCR. Similar experiments were conducted to evaluate the effect of FoxO3a on ER gene transcription, using a pGL3 plasmid bearing the full ER promoter (fragment E, containing both promoters A and B), pGL3-ERprom(E), mapping from −4,100 to +212 bp from the first transcription start site (15).

Real-time reverse transcription-PCR. Before the experiments, cells were serum starved for 24 h and then treated for the indicated times. Total RNA was isolated using TRIzol reagent (Invitrogen) according to the manufacturer's instructions and treated with DNase I (Ambion). Two μg of total RNA was reverse transcribed with the ImProm-II reverse transcription system kit (Promega) using random primers; cDNA was diluted 1:3 in nuclease-free water, and 5 μl was analyzed in triplicate by real-time PCR in an iCycler iQ Detection System (Bio-Rad) using SYBR green Universal PCR Master Mix (Bio-Rad) with 0.1 μmol/liter of each primer in a total volume of 30 μl of reaction mixture. The primers used for the amplification were based on published sequences for human Akt 2, ER, FoxO3a, cyclin D1 (CD1), and pS2 (data available on request). The PCR conditions were 95°C for 3 min and 40 cycles of 95°C for 30 s, T_a (data available on request) for 30 s, and 72°C for 30 s; negative controls contained water instead of first-strand cDNA. Each sample was normalized on its 18S rRNA content. The 18S quantification was done using a TaqMan rRNA reagent kit (Applied Biosystems) following the manufacturer's instructions. The relative gene expression levels were normalized to a calibrator that was chosen to be the basal, untreated sample. The final results were expressed as *n*-fold differences in gene expression relative to 18S rRNA and the calibrator, calculated using the $\Delta\Delta C_T$ method as follows: $n\text{-fold} = 2^{-(\Delta C_T\text{sample} - \Delta C_T\text{calibrator})}$, where the ΔC_T values of the sample and calibrator were determined by subtracting the average C_T value of the 18S rRNA reference gene from the average C_T value of the different genes analyzed.

Chromatin immunoprecipitation. MCF-7 cells were grown in 100-mm plates. Subconfluent cultures (70%) were shifted to PRF-SFM for 24 h, pretreated with API-2 for 1 h, and then treated with 100 nM E2 or left untreated for 45 min. Alternatively, growing cells were switched to PRF-SFM, transfected with HA-FoxO3a using Fugene 6 (Fugene 6/plasmid ratio, 3:1), and treated the following day with E2 for 45 min. ChIP methodology was performed as described previously (37). The precleared chromatin was precipitated for 16 h with anti-ER monoclonal antibody (MAb) (Santa Cruz) for ER, anti-FoxO3a polyclonal antibody (PAb) (Cell Signaling) for FoxO3a, and anti-polymerase II PAb (Santa Cruz) for Pol II. Normal rabbit IgG and normal mouse IgG (Santa Cruz) were used instead of primary Abs as negative controls. Immunoprecipitated DNA was analyzed in triplicate by real-time PCR using 5 μl of the diluted (1:3) template DNA as described above, and the the pS2 promoter region (pS2-prom) was amplified using specific primers (data available on request).

Real-time PCR data were normalized with respect to unprocessed lysates (input DNA). Input DNA quantification was performed by using 5 μl of the diluted (1/50) template DNA. The relative antibody-bound fractions were normalized to a calibrator that was chosen to be the basal, untreated sample. The final results were expressed as fold differences with respect to the relative inputs.

Immunoprecipitation and Western blotting. Protein expression and complex formation were assessed by Western blotting (WB) or immunoprecipitation (IP), followed by WB using total protein lysates, cytoplasmic protein lysates, or fractionated proteins, where appropriate. MCF-7 cells were serum starved for 24 h and treated with 100 nM E2 and/or the Akt inhibitor API-2 (1 μM) for different times, depending on the experiment. Cytoplasmic proteins were obtained using lysis buffer containing 50 mmol/liter HEPES (pH 7.5), 150 mmol/liter NaCl, 1% Triton X-100, 1.5 mmol/liter $MgCl_2$, 10 mmol/liter EGTA (pH 7.5), 10% glycerol, and inhibitors (0.1 mmol/liter Na_3VO_4, 1% phenylmethylsulfonyl fluoride, and 20 mg/ml aprotinin). After the collection of cytoplasmic proteins, the nuclei were lysed with nuclear buffer containing 20 mmol/liter HEPES (pH 8), 0.1 mmol/liter EDTA, 5 mmol/liter $MgCl_2$, 0.5 mol/liter NaCl, 20% glycerol, 1% NP-40, and inhibitors (as described above). For total protein extracts, RIPA buffer was used (50 mM Tris-HCl, pH 7.4, 150 mM NaCl, 1% NP-40, 0.25% Na deoxycholate, plus inhibitors). The protein content was determined using Bradford dye reagent (Bio-Rad). For WB, 50 μg of lysates was separated on an 11% polyacrylamide denaturing gel (SDS-PAGE) and transferred to nitrocellulose membranes. Proteins of interest were detected with specific Abs, recognized by peroxidase-coupled secondary Abs, and developed using the ECL Plus Western Blotting detection system (Amersham Pharmacia Biotech, United Kingdom). For IP, 500 μg of protein lysates was precleared for 1 h with protein A/G-agarose (Santa Cruz) for either MAb or PAbs, incubated with primary Abs at 4°C for 18 h in HNTG buffer (20 mmol/liter HEPES, pH 7.5, 150 mmol/liter NaCl, 0.1% Triton X-100, 10% glycerol, and 0.1 mmol/liter Na_3VO_4), and then the antigen-Ab complexes were precipitated with protein A/G agarose for 2 h in HNTG buffer. In control samples, the primary immunoprecipitating Abs were replaced with normal rabbit IgG (Santa Cruz Biotechnology). The immunoprecipitated proteins were washed three times with HNTG buffer, separated on SDS-PAGE, and processed by WB. The images were acquired by using an Epson Perfection scanner (Epson, Japan) using Photoshop software (Adobe). The optical densities of the spots were analyzed by using ImageJ software (NIH; http://rsb.info.nih.gov/IJ).

Antibodies for Western blotting and immunoprecipitation. Total and phosphorylated Akt isoforms were detected by WB with specific Abs: anti-Akt1/2 (H-136) PAb, anti-Akt1 (G5) MAb, anti p-Akt1/2/3 (Ser473)-R (Santa Cruz), and anti-Akt2 (5B5) MAb (Cell Signaling). ER and FoxO3a were assessed by WB and IP with anti-ER F-10 MAb (Santa Cruz) and anti-FoxO3a PAb (Cell Signaling). pS2 was probed with anti-pS2 PAb (Santa Cruz), phosphorylated GSK-3β with anti-GSK-3β (Ser9) PAb (Cell Signaling), total GSK-3β with anti-GSK-3β MAb (Cell Signaling), CD1 with anti-cyclin D1 PAb (Santa Cruz), and

FIG. 3. Akt2 regulates ER expression. (A and B) MCF-7 cells were transfected in suspension with 100 pmol siRNAs/35-mm well (siAkt1, siAkt2, or scrambled siRNA for control samples), plated, starved for 48 h, and treated with 100 nM E2 for 6 h. Cytosolic and nuclear proteins (A) or total extracts (B) (50 μg/lane) were analyzed by WB using appropriate antibodies. The relative protein levels (A1 and B) were analyzed, and the optical density is reported. (C and D) AKT2 was silenced for 24, 48, and 72 h, as described previously. (C) Two μg RNA was reverse transcribed and subjected to real-time PCR analysis. Each sample was normalized to its 18S rRNA content and reported as fold increase over the control (0 h). (D) Fifty micrograms of cytosolic proteins was subjected to WB analysis. (D1) The relative protein levels were analyzed, and the optical density is shown. (E and F) MCF-7 cells were transfected, as described above, with siAkt2 or scrambled siRNA, starved for 24 h, and treated with 100 nM E2 for an additional 24 h. (E) Two μg RNA was reverse transcribed and subjected to real-time PCR. (F) Fifty micrograms of total proteins was processed by WB analysis, and the relative densitometric analysis is reported (F1). All data were normalized over GAPDH (cytosolic or total proteins) or lamin B (nuclear proteins). In all experiments, significance values were as follows: ∗, $P < 0.05$ versus non-E2-treated samples; ●, $P < 0.05$ versus the corresponding treatment in scrambled siRNA; ▲, $P < 0.05$ versus scrambled siRNA; ·, $P < 0.05$ versus the corresponding sample at 24 h. The error bars indicate SD.

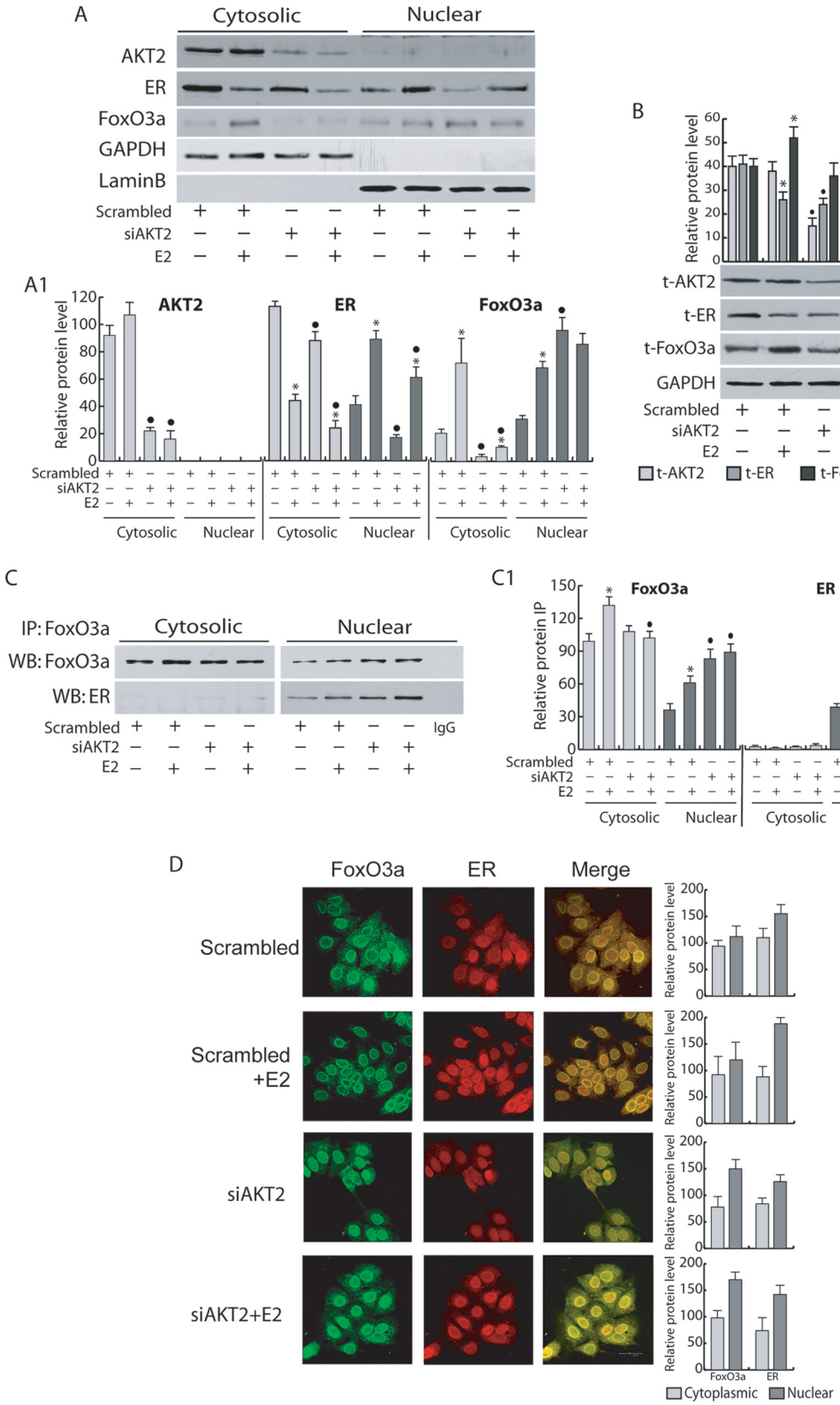

FIG. 4. FoxO3a coprecipitates and colocalizes with ER in the nucleus. AKT2 silencing was carried out for 48 h, as described in Materials and Methods, followed by 100 nM E2 treatment for 6 h. Protein expression and complex formation were assessed by WB (A and B) and IP analysis (C), respectively, using fractionated protein lysates (A and C) or whole-cell lysates (B). (C) Five hundred micrograms of protein lysates was immunoprecipitated with anti-FoxO3a Ab and blotted for both FoxO3a and ER. Normal rabbit IgG was used as a negative control to precipitate

glyceraldehyde-3-phosphate dehydrogenase (GAPDH) and lamin B were assessed by WB as controls for loading and purity of lysates with the anti-GAPDH (FL-335) PAb and the anti-lamin B (C-20) PAb (Santa Cruz), respectively. Normal rabbit IgG and normal mouse IgG (Santa Cruz) were used instead of primary Abs for IP negative controls. All Abs were used at concentrations recommended by the manufacturers.

siRNA-mediated RNA interference. Custom-synthesized siRNA (Invitrogen)-annealed duplexes (25-bp double-stranded RNA [dsRNA]) were used for effective depletion of Akt1, Akt2, and FoxO3a genes. A scrambled siRNA (Invitrogen) that lacked identity with known gene targets was used as a control for non-sequence-specific effects. Cells were trypsinized; transfected in suspension with Lipofectamine 2000 (Invitrogen), as suggested by the manufacturer; and then plated in six-well plates (3.5×10^5 cells per well). Briefly, the cells were transfected with 100 pmol siRNAs (siAkt1, siAkt2, siFoxO3a, or nonspecific siRNA) in 3 ml total growing medium. The siRNAs were diluted in 500 μl of PRF-SFM without antibiotic; after 5 min, Lipofectamine 2000 was added to the mixture and incubated at room temperature for 20 min. The siRNA-Lipofectamine 2000 complex was then added to the cells and incubated at 37°C for 6 h, switched to PRF-SFM, and further incubated for an additional 18 h. Then, the cells were treated with E2 (100 nM) for 6 h or 24 h before analysis, depending on the experiment. For time course purposes, cells were harvested after 24 h, 48 h, or 72 h.

Confocal laser scanning microscopy (CLSM). MCF-7 cells were transfected in suspension with Akt2 siRNA as described previously, plated on coverslips, serum starved, and then treated with 100 nM E2 for 6 h. After incubation, the cells were fixed with 3% paraformaldehyde and permeabilized with 0.2% Triton X-100, and nonspecific sites were blocked with bovine serum albumin (BSA) (3% for 30 min). The blocked samples were incubated for 1 h with a mixture of primary antibodies (2 mg/ml each) recognizing ER (MAb; Santa Cruz) and FoxO3a (PAb; Cell Signaling), washed with phosphate-buffered saline (PBS) (Gibco), and incubated with a mixture of fluorescein-conjugated goat anti-rabbit IgG and rhodamine-conjugated goat anti-mouse IgG (Santa Cruz) secondary Abs. The cellular localization of the two proteins was examined under a Leica TCS SP2 confocal laser scanning microscope at ×400 magnification. The optical sections were taken at the central plane. The fluorophores were imaged separately to ensure there was no excitation/emission wavelength overlap. The optical densities of stained proteins were analyzed by ImageJ software.

DAPA. The binding of nuclear FoxO3a to Forkhead-responsive elements on the pS2 promoter was assessed *in vitro* using a modified version of the DNA affinity precipitation assay (DAPA) protocol of Zhu et al. (63). Briefly, nuclear-protein extracts were obtained from starved cells pretreated with API-2 (1 μM) for 1 h and stimulated with E2 (100 nM) for 45 min. One hundred μg of nuclear proteins was mixed with 2 μg of specific biotinylated DNA probes (see below) in 400 μl of buffer D (20 mM HEPES, pH 7.9, 10% glycerol, 50 mM KCl, 0.2 mM EDTA, 1.5 mM $MgCl_2$, 10 μM $ZnCl_2$, 1 mM dithiothreitol, and 0.25% Triton X-100) and then incubated on ice for 45 min. After that, 20 μl of streptavidin-agarose beads (Promega) was added, and the samples were incubated under rotation for 2 h at 4°C. Next, the agarose bead-protein complexes were collected by brief centrifugation and washed twice in buffer D. Proteins were uncoupled from DNA probes by the addition of 40 μl of 2× Laemmli's sample buffer and by heating them at 96°C for 10 min. The beads were removed by centrifugation, and the supernatants were analyzed by WB for the presence of FoxO3a. The DNA motif probes (pS2/FKH) were prepared by annealing a 5′-biotinylated sense oligonucleotide bearing a Forkhead consensus sequence (5′-Bio-ACGCT CTTTAAGCAAACAGAGCCTGCCCTA-3′) with a nonbiotinylated antisense oligonucleotide (5′-TAGGGCAGGCTCTGTTTGCTTAAAGAGCGT-3′). A labeled probe with the consensus sequence [pS2/FKH(−)], underlined above, deleted was used as a negative control (forward, 5′-Bio-ACGCTCTTTAAACA GAGCCTGCCCTA-3′; reverse, 5′-TAGGGCAGGCTCTGTTTAAAGAGCG T-3′). The optical densities of the spots were analyzed by ImageJ software.

Proliferation assay. MCF-7 cells were transfected in suspension with either HA-FoxO3a or siFoxO3a (the empty vector or scrambled siRNA, respectively, was used as a control) in growth medium without antibiotic and plated in 12-well plates at a concentration of 10^5 cells/plate. After 6 h, the cells were starved for 18 h (day zero) and then treated or not with E2 (100 nM) for 1, 2, and 3 days (the hormone was refreshed every day to maintain constant levels in the medium). At each time point, the cells were harvested by trypsinization and counted in a hemocytometer using the trypan blue exclusion assay.

Statistical analysis. All data were expressed as the means ± standard deviations (SD) of at least three independent experiments. Statistical significances were tested using Student's *t* test.

RESULTS

Akt inhibition decreases ER transcriptional activity. It has been well established that Akt is involved in the control of cell survival and that its inhibition is responsible for growth retardation; in MCF-7 cells, this effect is paralleled by a decrease of ER transcriptional activity (32, 53). This assumption was confirmed through transactivation experiments using an ER-responsive 1× ERE-Luc construct (XETL). In our experimental system, E2 treatment, as expected, determined a 4-fold induction of luciferase activity (Fig. 1A). The inhibition of Akt kinase function by API-2 pretreatment completely abrogated ER transcriptional activity in response to E2 administration (Fig. 1A). Similar results were obtained in two additional ER-positive cell lines, T47D and ZR75 (data not shown). Hormone treatment caused an increase of Akt phosphorylation in either untreated or API-2-treated samples (Fig. 1B). Interestingly, API-2 treatment resulted in pSer-Akt accumulation, while Akt kinase activity was dramatically reduced, since its downstream target, GSK-3β, was no longer phosphorylated (Fig. 1B). Notably, the inhibition of ER transactivation is consistent with a reduction of the ER-mediated transcription, since, under the same experimental conditions, a dramatic decrease in mRNA levels of the ER target gene pS2 was observed both under basal conditions and after E2 treatment (Fig. 1C). This event was paralleled by a significant decrease in ER protein and mRNA levels (Fig. 1B and C). Interestingly, the inhibition of Akt kinase function did not alter either Akt or GSK-3β protein expression (Fig. 1B), while it did induce a 40% reduction of ER protein and mRNA levels in untreated samples, as well as further emphasizing the ligand-induced downregulation of the receptor (Fig. 1B and C).

To assess cell specificity, a gene reporter assay was conducted in two ER-negative cell lines, HeLa and SKBR3, ectopically expressing ER. In both cell systems, ER presence was responsible for E2-dependent transactivation (Fig. 1D and E). Interestingly, in HeLa cells, no significant difference in luciferase induction was observed in API-2-treated samples compared to nontreated samples, while in SKBR3 cells, the re-

E2-treated samples. (A1, B, and C1) The relative protein levels were analyzed, and the optical density is reported. Samples were normalized over GAPDH (A, cytosolic, or B, total proteins) and lamin B (A, nuclear proteins). In all experiments, significance values were as follows: ∗, $P < 0.05$ versus non-E2 treated; ●, $P < 0.05$ versus the corresponding treatment in scrambled siRNA. (D) Cytoplasmic and nuclear distribution of ER and FoxO3a in response to AKT2 knockdown was also evaluated by confocal microscopy. To avoid fluorescence overlapping, a rabbit PAb for FoxO3a and a mouse MAb for ER were used. A mixture of fluorescein-conjugated goat anti-rabbit IgG (green) and rhodamine-conjugated goat anti-mouse IgG (red) secondary Abs was used to detect primary immune complexes of FoxO3a and ER, respectively. The merged images show FoxO3a-ER colocalization (yellow). The optical sections were taken at the central plane at ×400 magnification. The fluorophores were imaged separately to ensure there was no excitation/emission wavelength overlap. The histograms on the right show the corresponding means and SD of the densitometric analysis performed in three independent experiments.

sponse to the same treatment paralleled that observed in MCF-7 cells (Fig. 1D and E). In both cell lines, API-2 did not affect the ER protein content (Fig. 1, D1 and D2).

To clarify the role of Akt in ER transcriptional activity, chromatin-bound ER and Pol II were precipitated from MCF-7 cell nuclear extracts. As shown in Fig. 2A, strong inhibition of ER and Pol II recruitment on the estrogen-responsive sequence of the pS2 promoter was observed in cells pretreated with API-2 for 1 h and exposed to E2 for 45 min. The reduced occupancy of ER on the pS2 promoter was related to a decrease in ER nuclear content. Indeed, 1 h of exposure to API-2 was able to interfere with ligand-dependent retention of ER in the nucleus (Fig. 2B) without affecting total ER and GSK-3β protein amounts (Fig. 2C).

In our system, E2 induced phosphorylation of Akt and, as a consequence, GSK-3β phosphorylation after 5 min of treatment (Fig. 2B). The efficacy of API-2 pretreatment was evidenced by the clear inhibition of GSK-3β phosphorylation while, as expected, at this time point, API-2 did not alter Akt expression or its phosphorylation on Ser473 in either the presence or absence of E2 (Fig. 2B).

Akt2 silencing reduces ER expression and function. Since API-2 is not able to discriminate between the Akt isoforms, Akt1 and Akt2 mRNA transcripts (Akt3 is not expressed in MCF-7 cells [reference 21 and data not shown]) were silenced by siRNA. A strong reduction of ER total expression was observed in Akt2, but not in Akt1, silenced samples (Fig. 3A and B). Time course experiments (24 to 72 h) showed that a significant decrease in ER expression also occurs at the transcriptional level following Akt2 silencing (Fig. 3C and D). This event was reflected by a strong reduction in pS2 mRNA (Fig. 3C) and protein (Fig. 3D) expression at all investigated time points. The reduction of Akt2 and ER cytosolic content observed after 72 h in scrambled-siRNA samples (Fig. 3D) could simply be ascribed to a general phenomenon in response to the prolonged starvation. As mentioned above, siAkt1 did not alter either ER (Fig. 3A and B) or pS2 (data not shown) expression, supporting the hypothesis that ER functional disruption specifically depends on Akt2 inhibition. A comparable trend was maintained in the presence of E2 in Akt2 silenced samples. In fact, E2 treatment did not alter the inhibitory effect of silenced Akt2 on the mRNA and protein levels of ER and pS2, as well as an additional ER-regulated gene, CD1 (Fig. 3E and F). Similar experiments were conducted in T47D and ZR75 cells (data not shown). In both cell lines, Akt2 inhibition led to a dramatic reduction of ER, and consequently pS2, mRNA and protein levels.

FoxO3a coprecipitates and colocalizes with ER in the nucleus. To elucidate the mechanism underlying the involvement of Akt2 on the regulation of both ER expression and function, we focused our attention on one of its downstream effectors, FoxO3a, a member of the Forkhead transcription factor family. FoxO3a is well expressed in MCF-7 cells and has been reported to functionally interact with ER (17, 62). As shown in Fig. 4A and B, an increase in total FoxO3a protein levels was observed in response to E2 stimulation. siAkt2 caused a drastic reduction of FoxO3a cytosolic content in MCF-7 cells in either the presence or absence of E2 (Fig. 4A). The latter effect was paralleled by a marked increase in FoxO3a nuclear content (Fig. 4A and D), even though it is worth noting that E2 treatment did not significantly affect siAkt2-induced FoxO3a nuclear translocation. Interestingly, Akt2 knockdown did not affect total expression of FoxO3a, while it counteracted E2-induced FoxO3a upregulation, since, as previously described, total ER expression was significantly reduced (Fig. 4B).

Immunoprecipitation experiments and confocal microscopy confirmed the existence of a physical interaction (Fig. 4C) and colocalization (Fig. 4D) between ER and FoxO3a. In accordance with previously reported data in cell-free systems (49), the ER/FoxO3a interaction occurred mainly at the nuclear and perinuclear levels, where it was enhanced by E2, and became more evident in Akt2 silenced samples (Fig. 4C and D).

FoxO3a binds Forkhead-responsive elements on the pS2 promoter. Some recently published reports evidenced an overrepresentation of TA-rich motifs, particularly Forkhead binding sites (AAG[A]TAAA[G]C[T]A), in several ER-bound regions (30–31), including the pS2 promoter (4, 11). To investigate if ER/FoxO3a interaction does exert a functional role in ER-mediated transcription, chromatin-bound FoxO3a was immunoprecipitated with a specific antibody. The presence of FoxO3a on the pS2 promoter was detected targeting the Forkhead DNA binding site close to the TATAA box (4). As shown in Fig. 5A, a constitutive association of FoxO3a with the pS2 promoter was observed, which was increased by E2 stimulation. As expected, the inhibition of Akt kinase activity by API-2 treatment increased the promoter occupancy by FoxO3a, consistent with the induced FoxO3a translocation into the nucleus (Fig. 4A). Additionally, to investigate if FoxO3a binding occurs on the Forkhead-responsive element of the pS2 promoter (pS2/FKH), a DAPA assay was conducted on nuclear extracts from MCF-7 cells. The results obtained showed that nuclear FoxO3a binds with high affinity to the pS2/FKH sequence but not to the same region partially deleted in the Forkhead-responsive element [pS2/FKH(−)] used as a negative control (Fig. 5B). These data support the hypothesis that this region is involved in pS2 regulation by the Forkhead transcription factor.

To evaluate the effects of FoxO3a recruitment to Forkhead-responsive sites on the binding of ER to ERE-containing promoters, we performed a ChIP assay transiently overexpressing FoxO3a. As shown in Fig. 5C, a significant decrease of both basal and E2-induced recruitment of ER on the pS2 promoter was observed in FoxO3a-overexpressing samples, corroborating our hypothesis of the negative role of FoxO3a in ER function.

FoxO3a inhibits ER expression and functional activity. To further understand the role of FoxO3a in inhibiting ER transcription, we both overexpressed and silenced FoxO3a and performed gene reporter experiments using either XETL (Fig. 6A) or a full-length pS2 promoter construct (Fig. 6B). Our results showed that FoxO3a overexpression caused a significant decrease of ER-dependent transcription in response to E2 stimulation, while FoxO3a knockdown led to the opposite effect (Fig. 6A and B). Comparable results were obtained in T47D and ZR75 (data not shown) cell lines transfected with XETL.

Moreover FoxO3a overexpression determined strong downregulation in ER mRNA and protein levels, both in controls and in E2-treated samples, which most likely is responsible for decreased pS2 and CD1 transcription (Fig. 6C and D). The

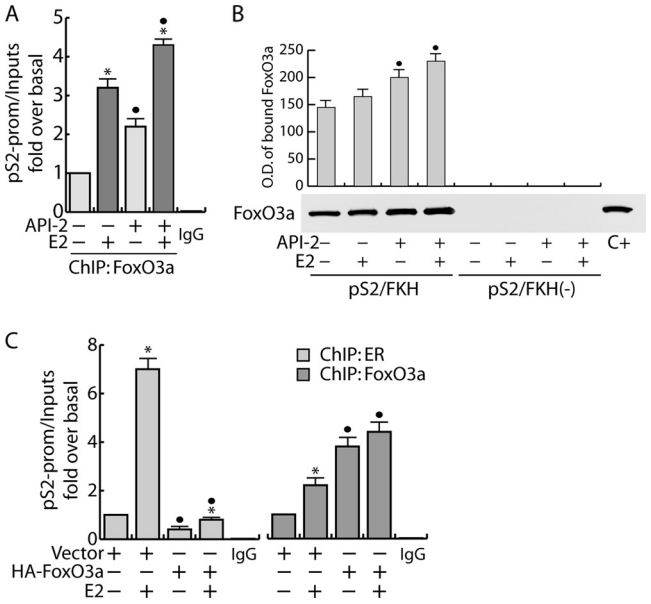

FIG. 5. FoxO3a binds Forkhead-responsive elements on the pS2 promoter. (A) ChIP assay. Starved MCF-7 cells were pretreated with 1 μM API-2 for 1 h and then treated with 100 nM E2 or left untreated for 45 min. FoxO3a was immunoprecipitated from the precleared chromatin. Samples were analyzed through real-time PCR targeting a Forkhead-containing pS2 promoter region (see Materials and Methods). Normal rabbit IgG was used in place of the primary Ab as a negative control to precipitate E2-treated samples. Each sample was normalized to its input (*, $P < 0.05$ versus each non-E2-treated sample; ●, $P < 0.05$ versus the corresponding treatment in non-API-2-treated samples). (B) DAPA assay. Cells were treated as for panel A, and FoxO3a was isolated from 100 μg of nuclear proteins using specific biotinylated DNA probes (pS2/FKH) as described in Materials and Methods and pulled down by streptavidin-agarose beads. The proteins recovered after removal of the beads were analyzed by WB for the presence of FoxO3a. Labeled probes with the consensus sequence [pS2/FKH(−)] deleted were used as negative controls. Fifty μg of cytosolic lysate (C+) was used as a positive control. The relative protein levels were analyzed, and the optical density (O.D.) is reported (●, $P < 0.05$ versus the corresponding treatment in non-API-2-treated samples). (C) ChIP analysis was performed on subconfluent MCF-7 cells transfected for 48 h with either HA-FoxO3a or empty vector (10 μg/100-mm petri dish). Twenty-four hours after transfection, the cells were synchronized in PRF-SFM for an additional 24 h and then treated with 100 nM E2 for 45 min or left untreated. The ERE- and FKH-containing pS2 promoter regions, precipitated with anti-ER and anti-FoxO3a Abs, respectively, were amplified using a specific pair of primers (data available on request). A mixture of normal rabbit IgG and normal mouse IgG was used as a negative control for both primary Abs to precipitate the E2-treated samples. Each sample was normalized to its input. In all experiments significance values were as follows: *, $P < 0.05$ versus each non-E2-treated sample; ●, $P < 0.05$ versus the corresponding treatment in vector-transfected samples. The error bars indicate SD.

same experiments were conducted in T47D and ZR75 (data not shown) cell lines, leading to similar results. On the other hand, a slight upregulation in ER mRNA and protein levels was observed in FoxO3a silenced samples (Fig. 6E and F), paralleled by an increase in pS2 and CD1 transcription and expression.

Preliminary data showing an ~2.5-fold reduction in pGL3-ERprom(E) luciferase activity in FoxO3a-overexpressiong cells, as well as an ~1.5-fold increase in FoxO3a silenced samples (Fig. 6G), confirmed these observations, leading us to hypothesize that the inhibition of ER expression exerted by FoxO3a could occur at the genomic level.

Interestingly, FoxO3a mRNA and protein were upregulated by E2 (Fig. 6C to F and 4A and B), suggesting a potential involvement of FoxO3a in a negative feedback loop aimed at downregulating ER and therefore attenuating ER function. This assumption was confirmed by proliferation assays, by either overexpressing or knocking down FoxO3a in MCF-7 cells (Fig. 7A and B). The results evidenced a dramatic inhibition of both basal and E2-stimulated cell growth in MCF-7 cells overexpressing FoxO3a (Fig. 7A), while both basal and E2-induced proliferation increased in FoxO3a-silenced cells (Fig. 7B).

DISCUSSION

In the last 2 decades a great amount of data confirmed the existence of a functional cross talk between estrogens and growth factors and its essential role in breast cancer development and progression (51). Specifically, growth factors are known to influence the expression and activity of ER, as well as its transcriptional cofactors; conversely, ER regulates the expression of growth factor receptors and their ligands and signaling intermediates (28). For instance, several authors reported that MAPK/ERK and Akt can be activated following estrogen stimulation, independently of growth factors (12, 18, 53). The results presented here partially confirm these findings, since in MCF-7 breast cancer cells, E2 treatment increased Akt phosphorylation within 5 min, while at that time point it had no effect on MAPK/ERK activation (data not shown). Moreover, inhibition of the PI3-K/Akt pathway, either following prolonged exposure to a specific inhibitor of Akt kinase activity, API-2, or knocking down Akt2, led to a decrease in ER mRNA and protein expression, both in the presence and in the absence of ligand. Such a decrease was paralleled by a dramatic reduction of ER-regulated transcription. Our observations are in contrast to previously reported results showing ER upregulation in response to the expression of an Akt dominant negative, despite a reduction in ER-mediated transcription (53).

In particular, we observed a dual effect on ER regulation, depending on the persistence of Akt inhibition. While long-term treatment (~16 h) with API-2 led to a decrease in both ER mRNA and protein levels, as well as in ER-mediated transcription, 1 h of treatment was not sufficient to alter ER levels but only interfered with E2-dependent ER nuclear retention, evidencing an important role for Akt in mediating the cytoplasmic-nuclear shuttling of the receptor. Ligand-induced full activation of ER seems to depend on Akt, and this event can occur, since Akt itself, in turn, undergoes phosphorylation within minutes of E2 treatment. In fact, ER can be phosphorylated on serine 167 by Akt in either an E2-dependent (12, 53, 55) or -independent manner (10, 55). Since our experiments were conducted in PRF-SFM and in the total absence of growth factors, it can be reasonably speculated that ER phosphorylation by Akt is solely dependent on E2. These observations could explain the reduced recruitment of ER and, consequently, of Pol II on the pS2 promoter following 1 h of API-2 pretreatment.

API-2 was used as an Akt inhibitor rather than the commonly used PI-3K inhibitors (i.e., wortmannin or LY294002)

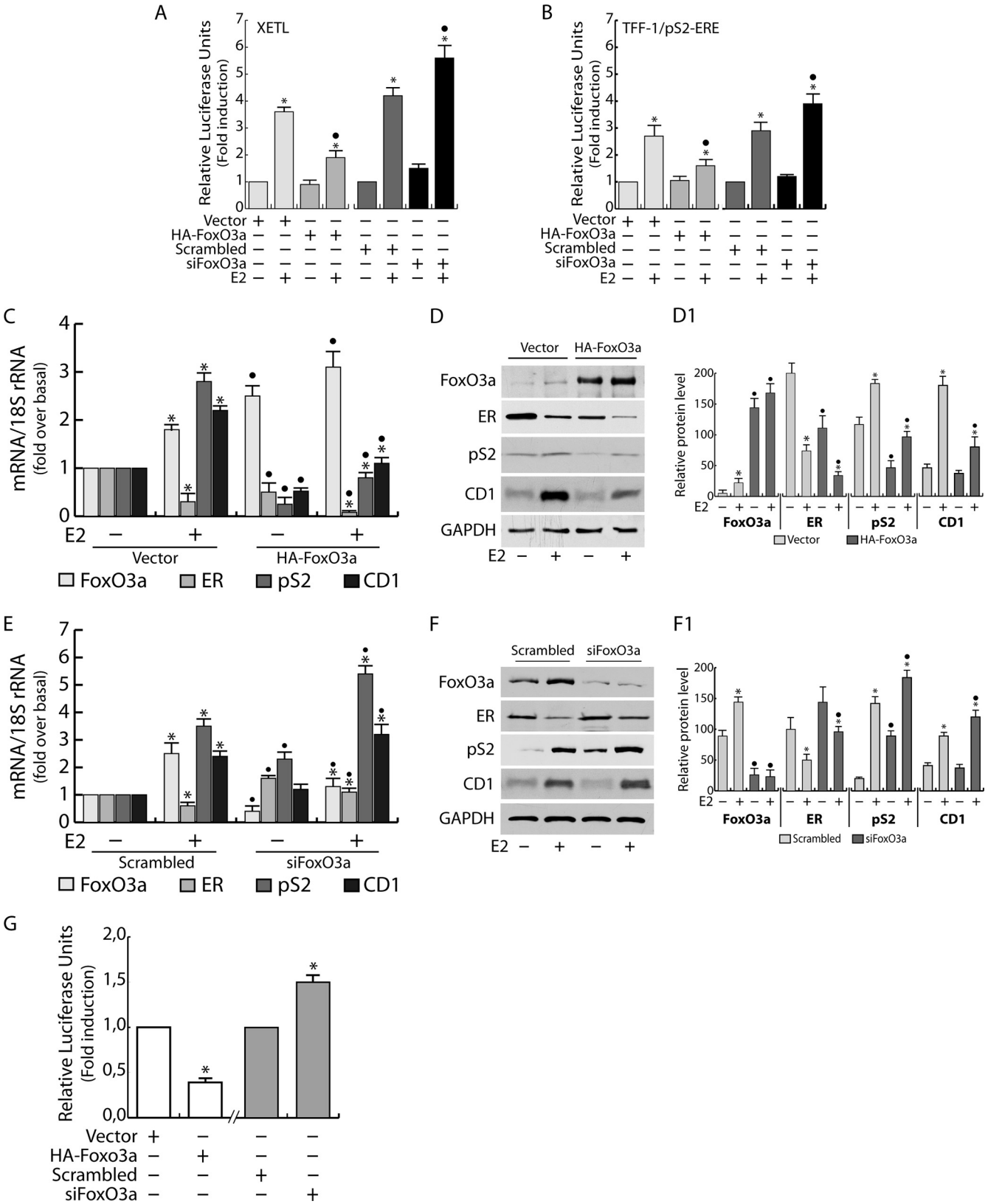

FIG. 6. FoxO3a modulates ER expression and functional activity. FoxO3a was either overexpressed or silenced in MCF-7 cells, cotransfected the day after with the XETL (A) or pS2 (B) promoter, and exposed to 100 nM E2 for 16 h (see Materials and Methods). Luciferase activity was normalized to pRL-Tk activity and expressed as relative luciferase units. (C) MCF-7 cells were transfected for 48 h in 35-mm dishes with HA-FoxO3a (1 μg) or empty vector (1 μg) and then treated for 24 h with E2 (100 nM). RNA was then extracted and reverse transcribed, and

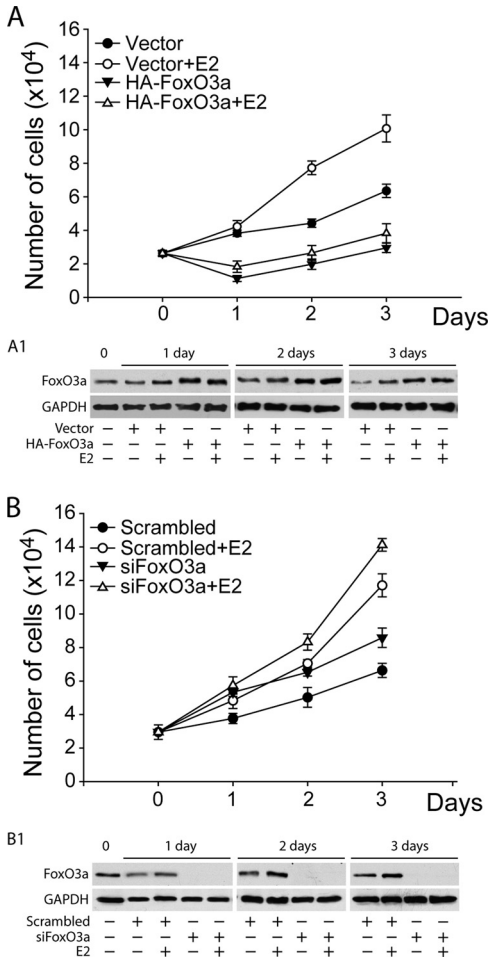

FIG. 7. FoxO3a inhibits cell proliferation. MCF-7 cells were transfected with either HA-FoxO3a (A) or siFoxO3a (B) and treated as described in Materials and Methods. The cells were counted in a hemocytometer at 50% confluence (day 0) and 1, 2, and 3 days later. The results represent the means ± SD of three independent experiments. (A1 and B1) The FoxO3a content was analyzed by WB at each time point.

for several reasons: (i) we were interested in focusing on Akt's role in ER signaling and not the PI-3K/Akt axis in general; (ii) wortmannin, used at suggested concentrations, never inhibited ER function as API-2 did; and (iii) LY294002 has been suspected of having antiestrogenic properties (43), which clearly could have interfered with our experiments. However, since API-2 is unable to discriminate among Akt isoforms, small interfering RNAs were used to silence either Akt1 or Akt2.

Interestingly, only Akt2 knockdown produced effects on both ER expression and function comparable to those observed after a prolonged exposure to API-2. Indeed, an evident decrease in ER protein content and in mRNA levels, followed by a predictable decrease in estrogen-dependent pS2 expression, was evidenced. As mentioned above, these effects were obtained only by Akt2 and not by Akt1 knockdown, suggesting a pivotal role of Akt2 in both the regulation of ER function and its expression.

Although there are reports of Akt1 presence at the nuclear level, e.g., in thyroid cancer specimens and cultures (58) or in IGF-1-stimulated human embryonic kidney cells (3), in our cellular model and under our experimental conditions we never observed either Akt1 or Akt2 in the nucleus. Therefore, the genomic events deriving from Akt2 knockdown can be assumed to be mediated by one of its downstream nuclear effectors, such as the Forkhead winged-helix transcription factor FoxO3a, the most highly expressed in MCF-7 cells among the four known members of the box O family.

Forkhead members were found to bind ER in a cell-free system in the presence of ER ligand (49, 62, 65). Our data, for the first time, demonstrate that the interaction between ER and FoxO3a occurs in a whole-cell system. Indeed, ER was found to colocalize with FoxO3a at the perinuclear and nuclear levels and to coprecipitate from MCF-7 nuclear-protein extracts. E2 stimulation enhanced the binding between the two proteins, most likely as a consequence of the increased ER nuclear retention, as well as of the E2-induced FoxO3a overexpression. This ER/FoxO3a interaction became much more evident in Akt2 silenced samples, probably for a more sustained FoxO3a translocation into the nucleus. More interestingly, we found that FoxO3a was recruited to the pS2 promoter in an E2-dependent manner and that Akt2 inhibition emphasized this phenomenon. FoxO3a binding to DNA occurred on the Forkhead-responsive sequence close to the TATAA box (Fig. 5). The current literature reports controversial data regarding the Forkhead box O function on ER target promoters. Some authors state that these transcriptional factors can act as coactivators (49), while others found that they can have a bifunctional role, behaving as ER coactivators or corepressors, depending on the cellular model (62, 65). In our MCF-7 clone, FoxO3a overexpression inhibited ER-mediated transcription of E2-regulated genes, such as pS2 and CD1. This effect could most likely be ascribable to reduced recruitment of ER to ERE sites on the pS2 promoter, due to both reduced ER expression

FoxO3a, ER, pS2, and CD1 transcripts were analyzed by real-time PCR. Each sample was normalized to its 18S rRNA content. (D) Fifty μg of whole-cell extracts from a duplicate set of cells treated as described above was subjected to WB analysis. (D1) The relative protein levels, normalized over GAPDH, are reported. (E) RNA extracted from FoxO3a-silenced MCF-7 cells, treated with E2 (100 nM) for 24 h, was reverse transcribed, and FoxO3a, ER, pS2, and CD1 transcripts were analyzed by real-time PCR. Each sample was normalized to its 18S rRNA content. (F) A duplicate set of cells, treated as described above, was lysed, and 50 μg of whole-cell lysates was loaded for protein expression. (F1) The relative protein levels, normalized versus GAPDH, were analyzed, and the optical density is reported. (G) MCF-7 cells were transfected with HA-FoxO3a or control vector (white bars) or FoxO3a siRNA or scrambled siRNA (gray bars) and cotransfected the day after with pGL3-ERprom(E). As described above, luciferase activity was normalized to pRL-Tk activity and expressed as relative luciferase units. In all experiments, significance values were as follows: ∗, $P < 0.05$ versus each non-E2-treated sample; ●, $P < 0.05$ versus the corresponding treatment in scrambled siRNA or vector-transfected samples. The error bars indicate SD.

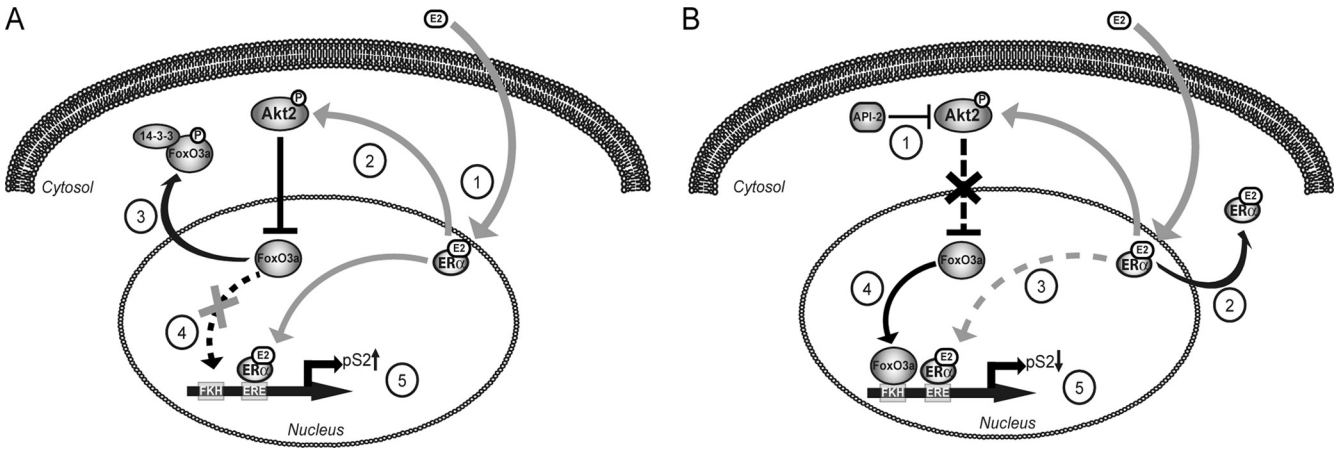

FIG. 8. Suggested mechanism through which the Akt2/FoxO3a axis modulates ER expression and activity. (A) Liganded ER (1) activates Akt2 (2), which in turn phosphorylates, and thus inhibits, the FoxO3a transcription factor, promoting its nuclear exclusion and retention in the cytoplasm, where it binds to 14-3-3 proteins (3). FoxO3a is no longer recruited on the pS2 promoter (4), leading to enhanced ER transactivation and pS2 transcription (5). (B) Akt2 inhibition (1) leads to ER transcriptional repression, acting at different levels: reduction of liganded-ER retention in the nucleus (2) and, consequently, of ER recruitment on the pS2 promoter (3); activation and subsequent recruitment of FoxO3a on the pS2 promoter (4), leading to pS2 downregulation (5).

and the increased recruitment of the overexpressed negative modulator FoxO3a on its own binding motif, while FoxO3a silencing led to the opposite effect. It is worthwhile to emphasize that, unlike pS2, we cannot state at the moment whether CD1 is directly regulated by FoxO3a through its binding to Forkhead-responsive elements, though they are present on the CD1 promoter, or whether this effect is due to a reduced general ER content. In fact, as mentioned above, a strong decrease in ER expression, at both the RNA and protein levels, was observed in FoxO3a-overexpressing samples. Although our preliminary results suggest possible regulation of the ER promoter by FoxO3a, further investigations are needed to elucidate if this effect really depends on the loss of FoxO3a as a repressive element for ER gene transcription or if it is due to prolonged ER mRNA stability. Indeed, at least two functional Forkhead binding sites were identified on ER promoter B (17), but the authors demonstrateed an activating effect of constitutively active FoxO3a at this level in mouse mammary tumor-derived NF639 cells paralleled by an increase in ER protein in cells transiently overexpressing FoxO3a. These data do not support our hypothesis, nor are they in agreement with recent observations by Zou et al., who did not find significant differences in ER expression in FoxO3a-overexpressing MCF-7 stable clones (65). Furthermore, our findings also contrast with the reported decrease in ER levels in MCF-7 cells infected with dominant-negative FoxO3a-expressing adenovirus (17). The incongruence of these data could be partially explained by the different cell systems, culture conditions, and experimental procedures used, but this cannot replace further study of the possible mechanism through which FoxO3a regulates ER expression and/or stability. However, our findings were further corroborated by the growth inhibition observed in FoxO3a-overexpressing cells, as well as by the proliferative rate increase in FoxO3a silenced samples, evidencing the physiological relevance of this transcription factor in regulating the ER mitogenic signal. Moreover, we reproduced the main experiments in two additional ER-positive cell lines, T47D and ZR75, where Akt inhibition, as well as FoxO3a overexpression, led to ER downregulation and impaired transcriptional activity, suggesting how the Akt2/FoxO3a axis has a pivotal role in modulating ER function in ER-expressing breast cancer cells.

In fact, in two ER-negative cell lines, HeLa and SKBR3, that ectopically express ER, Akt inhibition did not lead to ER loss (protein and mRNA), supporting our hypothesis that the Akt pathway might control ER expression at a genomic level. Notably SKBR3 showed a significant decrease of ER transcriptional activity in response to API-2, mimicking MCF-7 behavior, while in HeLa cells, API-2 did not significantly affect ER transactivaton. The latter result could be explained by considering the different expression levels of Akt2 and Foxo3a in the two cell lines: in fact, HeLa cells express negligible amounts of both proteins, while their levels in SKBR3 cells are comparable to those found in MCF-7 cells, underlining the fact that the molecular machinery introduced here might work properly in cells expressing both Akt2 and FoxO3a.

Finally, as already mentioned, E2 stimulation induced FoxO3a transcription and protein expression, which leads us to hypothesize the presence of estrogen target sequences on the FoxO3a promoter region. This observation could suggest a homeostatic control mechanism through which E2-induced FoxO3a upregulation is a required event to ensure liganded ER inactivation. The molecular basis on which E2 activates FoxO3a expression is currently under investigation in our laboratory. In conclusion, in our model, FoxO3a, transcriptionally activated by Akt inhibition, might behave as a repressor for ER-mediated transcription (i) directly, by binding to Forkhead-responsive elements on ER target gene promoters; (ii) indirectly, by the recruitment on ERE sequences of the FoxO3a/ER complex; and (iii) by inhibiting ER expression.

Taken together, the results presented here show that, among PKB members, only Akt2 seems to modulate ER activity at multiple levels, having a key role in the regulation of (i) the retention of ER in the nucleus, (ii) ER expression, and (iii) FoxO3a activation. A schematic summary of our findings is

shown in Fig. 8. Our data point out the importance of the Akt/FoxO axis in E2-induced ER activation and signaling, evidencing additional mechanisms that could represent novel targets in ER-positive breast cancer therapy.

ACKNOWLEDGMENTS

We thank B. Van der Burg (Utrecht, the Netherlands) for providing MCF-7 cells, V. Giguère (McGill University, Quebec City, Canada) for the pS2/*TFF-1*-ERE (pS2-ERE) plasmid, and S. A. W. Fuqua (Baylor College of Medicine, Breast Center, Houston, TX) for the pGL3-ERprom(E).

Financial support for this work was received from AIRC, MIUR Ex 60%, and Regione Calabria.

We declare that there is no conflict of interest that would prejudice the impartiality of this scientific work.

REFERENCES

1. **Alvarez, B., A. C. Martinez, B. M. Burgering, and A. C. Carrera.** 2001. Forkhead transcription factors contribute to execution of the mitotic programme in mammals. Nature **413:**744–747.
2. **Anderson, E., R. B. Clarke, and A. Howell.** 1998. Estrogen responsiveness and control of normal human breast proliferation. J. Mammary Gland Biol. Neoplasia **3:**23–35.
3. **Andjelkovic, M., D. R. Alessi, R. Meier, A. Fernandez, N. J. Lamb, M. Frech, P. Cron, P. Cohen, J. M. Lucocq, and B. A. Hemmings.** 1997. Role of translocation in the activation and function of protein kinase B. J. Biol. Chem. **272:**31515–31524.
4. **Beck, S., P. Sommer, E. dos Santos Silva, N. Blin, and P. Gott.** 1999. Hepatocyte nuclear factor 3 (winged helix domain) activates trefoil factor gene TFF1 through a binding motif adjacent to the TATAA box. DNA Cell Biol. **18:**157–164.
5. **Berry, M., A. M. Nunez, and P. Chambon.** 1989. Estrogen-responsive element of the human pS2 gene is an imperfectly palindromic sequence. Proc. Natl. Acad. Sci. U. S. A. **86:**1218–1222.
6. **Biswas, D. K., A. P. Cruz, E. Gansberger, and A. B. Pardee.** 2000. Epidermal growth factor-induced nuclear factor kappa B activation: a major pathway of cell-cycle progression in estrogen-receptor negative breast cancer cells. Proc. Natl. Acad. Sci. U. S. A. **97:**8542–8547.
7. **Brader, S., and S. A. Eccles.** 2004. Phosphoinositide 3-kinase signalling pathways in tumor progression, invasion and angiogenesis. Tumori **90:**2–8.
8. **Brunet, A., A. Bonni, M. J. Zigmond, M. Z. Lin, P. Juo, L. S. Hu, M. J. Anderson, K. C. Arden, J. Blenis, and M. E. Greenberg.** 1999. Akt promotes cell survival by phosphorylating and inhibiting a Forkhead transcription factor. Cell **96:**857–868.
9. **Bunone, G., P. A. Briand, R. J. Miksicek, and D. Picard.** 1996. Activation of the unliganded estrogen receptor by EGF involves the MAP kinase pathway and direct phosphorylation. EMBO J. **15:**2174–2183.
10. **Campbell, R. A., P. Bhat-Nakshatri, N. M. Patel, D. Constantinidou, S. Ali, and H. Nakshatri.** 2001. Phosphatidylinositol 3-kinase/AKT-mediated activation of estrogen receptor alpha: a new model for anti-estrogen resistance. J. Biol. Chem. **276:**9817–9824.
11. **Carroll, J. S., X. S. Liu, A. S. Brodsky, W. Li, C. A. Meyer, A. J. Szary, J. Eeckhoute, W. Shao, E. V. Hestermann, T. R. Geistlinger, E. A. Fox, P. A. Silver, and M. Brown.** 2005. Chromosome-wide mapping of estrogen receptor binding reveals long-range regulation requiring the Forkhead protein FoxA1. Cell **122:**33–43.
12. **Castoria, G., A. Migliaccio, A. Bilancio, M. Di Domenico, A. de Falco, M. Lombardi, R. Fiorentino, L. Varricchio, M. V. Barone, and F. Auricchio.** 2001. PI3-kinase in concert with Src promotes the S-phase entry of oestradiol-stimulated MCF-7 cells. EMBO J. **20:**6050–6059.
13. **Clark, G. M., C. K. Osborne, and W. L. McGuire.** 1984. Correlations between estrogen receptor, progesterone receptor, and patient characteristics in human breast cancer. J. Clin. Oncol. **2:**1102–1109.
14. **Couse, J. F., and K. S. Korach.** 1999. Estrogen receptor null mice: what have we learned and where will they lead us? Endocr. Rev. **20:**358–417.
15. **deGraffenried, L. A., S. G. Hilsenbeck, and S. A. Fuqua.** 2002. Sp1 is essential for estrogen receptor alpha gene transcription. J. Steroid Biochem. Mol. Biol. **82:**7–18.
16. **Dowsett, M.** 2001. Overexpression of HER-2 as a resistance mechanism to hormonal therapy for breast cancer. Endocr. Relat. Cancer **8:**191–195.
17. **Guo, S., and G. E. Sonenshein.** 2004. Forkhead box transcription factor FOXO3a regulates estrogen receptor alpha expression and is repressed by the Her-2/neu/phosphatidylinositol 3-kinase/Akt signaling pathway. Mol. Cell. Biol. **24:**8681–8690.
18. **Improta-Brears, T., A. R. Whorton, F. Codazzi, J. D. York, T. Meyer, and D. P. McDonnell.** 1999. Estrogen-induced activation of mitogen-activated protein kinase requires mobilization of intracellular calcium. Proc. Natl. Acad. Sci. U. S. A. **96:**4686–4691.
19. **Jackson, J. G., J. I. Kreisberg, A. P. Koterba, D. Yee, and M. G. Brattain.** 2000. Phosphorylation and nuclear exclusion of the forkhead transcription factor FKHR after epidermal growth factor treatment in human breast cancer cells. Oncogene **19:**4574–4581.
20. **Jacobs, F. M., L. P. van der Heide, P. J. Wijchers, J. P. Burbach, M. F. Hoekman, and M. P. Smidt.** 2003. FoxO6, a novel member of the FoxO class of transcription factors with distinct shuttling dynamics. J. Biol. Chem. **278:**35959–35967.
21. **Jordan, N. J., J. M. Gee, D. Barrow, A. E. Wakeling, and R. I. Nicholson.** 2004. Increased constitutive activity of PKB/Akt in tamoxifen resistant breast cancer MCF-7 cells. Breast Cancer Res. Treat. **87:**167–180.
22. **Kandel, E. S., and N. Hay.** 1999. The regulation and activities of the multifunctional serine/threonine kinase Akt/PKB. Exp. Cell Res. **253:**210–229.
23. **Kato, S., H. Endoh, Y. Masuhiro, T. Kitamoto, S. Uchiyama, H. Sasaki, S. Masushige, Y. Gotoh, E. Nishida, H. Kawashima, D. Metzger, and P. Chambon.** 1995. Activation of the estrogen receptor through phosphorylation by mitogen-activated protein kinase. Science **270:**1491–1494.
24. **Katzenellenbogen, B. S., K. L. Kendra, M. J. Norman, and Y. Berthois.** 1987. Proliferation, hormonal responsiveness, and estrogen receptor content of MCF-7 human breast cancer cells grown in the short-term and long-term absence of estrogens. Cancer Res. **47:**4355–4360.
25. **Keen, J. C., and N. E. Davidson.** 2003. The biology of breast carcinoma. Cancer **97:**825–833.
26. **Knuefermann, C., Y. Lu, B. Liu, W. Jin, K. Liang, L. Wu, M. Schmidt, G. B. Mills, J. Mendelsohn, and Z. Fan.** 2003. HER2/PI-3K/Akt activation leads to a multidrug resistance in human breast adenocarcinoma cells. Oncogene **22:**3205–3212.
27. **Konecny, G., G. Pauletti, M. Pegram, M. Untch, S. Dandekar, Z. Aguilar, C. Wilson, H. M. Rong, I. Bauerfeind, M. Felber, H. J. Wang, M. Beryt, R. Seshadri, H. Hepp, and D. J. Slamon.** 2003. Quantitative association between HER-2/neu and steroid hormone receptors in hormone receptor-positive primary breast cancer. J. Natl. Cancer Inst. **95:**142–153.
28. **Lanzino, M., C. Morelli, C. Garofalo, M. L. Panno, L. Mauro, S. Ando, and D. Sisci.** 2008. Interaction between estrogen receptor alpha and insulin/IGF signaling in breast cancer. Curr. Cancer Drug Targets **8:**597–610.
29. **Lee, C. S., A. deFazio, C. J. Ormandy, and R. L. Sutherland.** 1996. Inverse regulation of oestrogen receptor and epidermal growth factor receptor gene expression in MCF-7 breast cancer cells treated with phorbol ester. J. Steroid Biochem. Mol. Biol. **58:**267–275.
30. **Lin, C. Y., V. B. Vega, J. S. Thomsen, T. Zhang, S. L. Kong, M. Xie, K. P. Chiu, L. Lipovich, D. H. Barnett, F. Stossi, A. Yeo, J. George, V. A. Kuznetsov, Y. K. Lee, T. H. Charn, N. Palanisamy, L. D. Miller, E. Cheung, B. S. Katzenellenbogen, Y. Ruan, G. Bourque, C. L. Wei, and E. T. Liu.** 2007. Whole-genome cartography of estrogen receptor alpha binding sites. PLoS Genet. **3:**e87.
31. **Liu, Y., H. Gao, T. T. Marstrand, A. Strom, E. Valen, A. Sandelin, J. A. Gustafsson, and K. Dahlman-Wright.** 2008. The genome landscape of ER-alpha- and ERbeta-binding DNA regions. Proc. Natl. Acad. Sci. U. S. A. **105:**2604–2609.
32. **Lobenhofer, E. K., G. Huper, J. D. Iglehart, and J. R. Marks.** 2000. Inhibition of mitogen-activated protein kinase and phosphatidylinositol 3-kinase activity in MCF-7 cells prevents estrogen-induced mitogenesis. Cell Growth Differ. **11:**99–110.
33. **Lombardi, M., G. Castoria, A. Migliaccio, M. V. Barone, R. Di Stasio, A. Ciociola, D. Bottero, H. Yamaguchi, E. Appella, and F. Auricchio.** 2008. Hormone-dependent nuclear export of estradiol receptor and DNA synthesis in breast cancer cells. J. Cell Biol. **182:**327–340.
34. **Mazumdar, A., and R. Kumar.** 2003. Estrogen regulation of Pak1 and FKHR pathways in breast cancer cells. FEBS Lett. **535:**6–10.
35. **McCarty, K. S., Jr., T. K. Barton, B. F. Fetter, B. H. Woodard, J. A. Mossler, W. Reeves, J. Daly, W. E. Wilkinson, and K. S. McCarty, Sr.** 1980. Correlation of estrogen and progesterone receptors with histologic differentiation in mammary carcinoma. Cancer **46:**2851–2858.
36. **Medema, R. H., G. J. Kops, J. L. Bos, and B. M. Burgering.** 2000. AFX-like Forkhead transcription factors mediate cell-cycle regulation by Ras and PKB through p27kip1. Nature **404:**782–787.
37. **Morelli, C., C. Garofalo, D. Sisci, S. del Rincon, S. Cascio, X. Tu, A. Vecchione, E. R. Sauter, W. H. Miller, Jr., and E. Surmacz.** 2004. Nuclear insulin receptor substrate 1 interacts with estrogen receptor alpha at ERE promoters. Oncogene **23:**7517–7526.
38. **Mossler, J. A., K. S. McCarty, Jr., and W. W. Johnston.** 1981. The correlation of cytologic grade and steroid receptor content in effusions of metastatic breast carcinoma. Acta Cytol. **25:**653–658.
39. **Nakamura, N., S. Ramaswamy, F. Vazquez, S. Signoretti, M. Loda, and W. R. Sellers.** 2000. Forkhead transcription factors are critical effectors of cell death and cell cycle arrest downstream of PTEN. Mol. Cell. Biol. **20:**8969–8982.
40. **Nakatani, K., D. A. Thompson, A. Barthel, H. Sakaue, W. Liu, R. J. Weigel, and R. A. Roth.** 1999. Up-regulation of Akt3 in estrogen receptor-deficient breast cancers and androgen-independent prostate cancer lines. J. Biol. Chem. **274:**21528–21532.

41. **Osborne, C. K.** 1998. Steroid hormone receptors in breast cancer management. Breast Cancer Res. Treat. **51:**227–238.
42. **Osborne, C. K., K. Hobbs, and G. M. Clark.** 1985. Effect of estrogens and antiestrogens on growth of human breast cancer cells in athymic nude mice. Cancer Res. **45:**584–590.
43. **Pasapera Limon, A. M., J. Herrera-Munoz, R. Gutierrez-Sagal, and A. Ulloa-Aguirre.** 2003. The phosphatidylinositol 3-kinase inhibitor LY294002 binds the estrogen receptor and inhibits 17beta-estradiol-induced transcriptional activity of an estrogen sensitive reporter gene. Mol. Cell Endocrinol. **200:**199–202.
44. **Perou, C. M., T. Sorlie, M. B. Eisen, M. van de Rijn, S. S. Jeffrey, C. A. Rees, J. R. Pollack, D. T. Ross, H. Johnsen, L. A. Akslen, O. Fluge, A. Pergamenschikov, C. Williams, S. X. Zhu, P. E. Lonning, A. L. Borresen-Dale, P. O. Brown, and D. Botstein.** 2000. Molecular portraits of human breast tumours. Nature **406:**747–752.
45. **Reagan-Shaw, S., and N. Ahmad.** 2006. RNA interference-mediated depletion of phosphoinositide 3-kinase activates forkhead box class O transcription factors and induces cell cycle arrest and apoptosis in breast carcinoma cells. Cancer Res. **66:**1062–1069.
46. **Rena, G., S. Guo, S. C. Cichy, T. G. Unterman, and P. Cohen.** 1999. Phosphorylation of the transcription factor forkhead family member FKHR by protein kinase B. J. Biol. Chem. **274:**17179–17183.
47. **Samatar, A. A., L. Wang, A. Mirza, S. Koseoglu, S. Liu, and C. C. Kumar.** 2002. Transforming growth factor-beta 2 is a transcriptional target for Akt/protein kinase B via forkhead transcription factor. J. Biol. Chem. **277:**28118–28126.
48. **Santini, D., C. Ceccarelli, M. Taffurelli, S. Pileri, and D. Marrano.** 1996. Differentiation pathways in primary invasive breast carcinoma as suggested by intermediate filament and biopathological marker expression. J. Pathol. **179:**386–391.
49. **Schuur, E. R., A. V. Loktev, M. Sharma, Z. Sun, R. A. Roth, and R. J. Weigel.** 2001. Ligand-dependent interaction of estrogen receptor-alpha with members of the forkhead transcription factor family. J. Biol. Chem. **276:**33554–33560.
50. **Sisci, D., C. Morelli, C. Garofalo, F. Romeo, L. Morabito, F. Casaburi, E. Middea, S. Cascio, E. Brunelli, S. Ando, and E. Surmacz.** 2007. Expression of nuclear insulin receptor substrate 1 in breast cancer. J. Clin. Pathol. **60:**633–641.
51. **Sisci, D., and E. Surmacz.** 2007. Crosstalk between IGF signaling and steroid hormone receptors in breast cancer. Curr. Pharm. Des. **13:**705–717.
52. **Stal, O., G. Perez-Tenorio, L. Akerberg, B. Olsson, B. Nordenskjold, L. Skoog, and L. E. Rutqvist.** 2003. Akt kinases in breast cancer and the results of adjuvant therapy. Breast Cancer Res. **5:**R37–R44.
53. **Stoica, G. E., T. F. Franke, M. Moroni, S. Mueller, E. Morgan, M. C. Iann, A. D. Winder, R. Reiter, A. Wellstein, M. B. Martin, and A. Stoica.** 2003. Effect of estradiol on estrogen receptor-alpha gene expression and activity can be modulated by the ErbB2/PI 3-K/Akt pathway. Oncogene **22:**7998–8011.
54. **Suhara, T., H. S. Kim, L. A. Kirshenbaum, and K. Walsh.** 2002. Suppression of Akt signaling induces Fas ligand expression: involvement of caspase and Jun kinase activation in Akt-mediated Fas ligand regulation. Mol. Cell. Biol. **22:**680–691.
55. **Sun, M., J. E. Paciga, R. I. Feldman, Z. Yuan, D. Coppola, Y. Y. Lu, S. A. Shelley, S. V. Nicosia, and J. Q. Cheng.** 2001. Phosphatidylinositol-3-OH kinase (PI3K)/AKT2, activated in breast cancer, regulates and is induced by estrogen receptor alpha (ERalpha) via interaction between ERalpha and PI3K. Cancer Res. **61:**5985–5991.
56. **Sun, M., G. Wang, J. E. Paciga, R. I. Feldman, Z. Q. Yuan, X. L. Ma, S. A. Shelley, R. Jove, P. N. Tsichlis, S. V. Nicosia, and J. Q. Cheng.** 2001. AKT1/PKBalpha kinase is frequently elevated in human cancers and its constitutive activation is required for oncogenic transformation in NIH3T3 cells. Am. J. Pathol. **159:**431–437.
56a. **Tora, L., A. Mullick, D. Metzger, M. Ponglikitmongkol, I. Park, and P. Chambon.** 1989. The cloned human oestrogen receptor contains a mutation which alters its hormone binding properties. EMBO J. **8:**1981–1986.
57. **Tsai, E. M., S. C. Wang, J. N. Lee, and M. C. Hung.** 2001. Akt activation by estrogen in estrogen receptor-negative breast cancer cells. Cancer Res. **61:**8390–8392.
58. **Vasko, V., M. Saji, E. Hardy, M. Kruhlak, A. Larin, V. Savchenko, M. Miyakawa, O. Isozaki, H. Murakami, T. Tsushima, K. D. Burman, C. De Micco, and M. D. Ringel.** 2004. Akt activation and localisation correlate with tumour invasion and oncogene expression in thyroid cancer. J. Med. Genet. **41:**161–170.
59. **Witton, C. J., J. R. Reeves, J. J. Going, T. G. Cooke, and J. M. Bartlett.** 2003. Expression of the HER1-4 family of receptor tyrosine kinases in breast cancer. J. Pathol. **200:**290–297.
60. **Yu, X., R. V. Rajala, J. F. McGinnis, F. Li, R. E. Anderson, X. Yan, S. Li, R. V. Elias, R. R. Knapp, X. Zhou, and W. Cao.** 2004. Involvement of insulin/phosphoinositide 3-kinase/Akt signal pathway in 17 beta-estradiol-mediated neuroprotection. J. Biol. Chem. **279:**13086–13094.
61. **Yuan, Z. Q., M. Sun, R. I. Feldman, G. Wang, X. Ma, C. Jiang, D. Coppola, S. V. Nicosia, and J. Q. Cheng.** 2000. Frequent activation of AKT2 and induction of apoptosis by inhibition of phosphoinositide-3-OH kinase/Akt pathway in human ovarian cancer. Oncogene **19:**2324–2330.
62. **Zhao, H. H., R. E. Herrera, E. Coronado-Heinsohn, M. C. Yang, J. H. Ludes-Meyers, K. J. Seybold-Tilson, Z. Nawaz, D. Yee, F. G. Barr, S. G. Diab, P. H. Brown, S. A. Fuqua, and C. K. Osborne.** 2001. Forkhead homologue in rhabdomyosarcoma functions as a bifunctional nuclear receptor-interacting protein with both coactivator and corepressor functions. J. Biol. Chem. **276:**27907–27912.
63. **Zhu, Y., M. A. Saunders, H. Yeh, W. G. Deng, and K. K. Wu.** 2002. Dynamic regulation of cyclooxygenase-2 promoter activity by isoforms of CCAAT/enhancer-binding proteins. J. Biol. Chem. **277:**6923–6928.
64. **Zinda, M. J., M. A. Johnson, J. D. Paul, C. Horn, B. W. Konicek, Z. H. Lu, G. Sandusky, J. E. Thomas, B. L. Neubauer, M. T. Lai, and J. R. Graff.** 2001. AKT-1, -2, and -3 are expressed in both normal and tumor tissues of the lung, breast, prostate, and colon. Clin. Cancer Res. **7:**2475–2479.
65. **Zou, Y., W. B. Tsai, C. J. Cheng, C. Hsu, Y. M. Chung, P. C. Li, S. H. Lin, and M. C. Hu.** 2008. Forkhead box transcription factor FOXO3a suppresses estrogen-dependent breast cancer cell proliferation and tumorigenesis. Breast Cancer Res. **10:**R21.